AIR INFILTRATION AND HEAT EXCHANGE PERFORMANCE OF THE BUILDING ENVELOPE

Kai Qiu

A Thesis

in

The department

of

Building, Civil and Environmental Engineering

Presented in Partial Fulfillment of the Requirements for the

Degree of Doctor of Philosophy (Building studies)

at

Concordia University

Montreal, Quebec, Canada

May 2006

Your file Votre référence
ISBN: 978-0-494-23839-4
Our file Notre référence
ISBN: 978-0-494-23839-4

Abstract

Air Infiltration and Heat Exchange Performance of the Building Envelope

Kai Qiu, Ph.D.

Concordia University, 2006

Air infiltration has an important impact on the energy consumption of buildings. Influenced by the heat exchange in it, the temperature profile in the building envelope deviates from that of conduction. Therefore, energy analysis of a building needs to consider the coupled process of conduction and infiltration.

A numerical model is presented to study the heat exchange performance of the building envelope, based on air flow and heat transfer through porous media. The governing equations are derived using the volume average method, and one-medium treatment is adopted for the description of heat transfer in the porous insulation. Computational fluid dynamics approach is used to solve the equations. As Darcy's term is the dominant factor in the momentum equation, an easily-implemented pressure correction method is presented. The model has been applied to an exterior wall, under four infiltration path conditions. Factors influencing the heat exchange performance have been discussed. The presented model has been verified by comparing its results with the experimental data.

Investigation is also conducted for the dynamic insulation, which is a potential implementation of the heat exchange process in the building envelope. Numerical

simulation is first performed to study the heat transfer in dynamic insulation, under both transient and steady-state boundary conditions. The results show that the steady-state analysis is a good approximation for the estimation of heat loss through the dynamic insulation. A steady-state analytical model is hence derived for the thermal performance of a dynamic insulated wall. An analytical model is also presented for the heat exchange performance of air infiltration in a conventional wall, by dividing the wall into ventilated and non-ventilated area, and treating the ventilated area as the dynamic insulated wall.

The results in the study show that the heat exchange performance in the building envelope is first determined by the air flow rate, with the secondary impact from the air flow path. The influence of permeability of the material is also important as it is related to the air flow rate. However, influence of porosity of the material, and indoor-outdoor temperature gradient, is not significant.

Acknowledgement

I would like to express my sincere gratitude to my supervisor, Dr. Fariborz Haghighat, for his thorough guidance, constant support and encouragement throughout this research.

I would also like to express my sincere thanks to Dr. Wahid S. Ghaly, for his suggestions and guidance in the research process.

I also like to appreciate the help of Ms Guylaine Desmarias, who supplied the experimental data obtained from the environmental chamber of Concordia University, and Mr. Brian Coffey, who helped me to conduct the simulation using TRNSYS.

Many thanks are also due to my colleagues and friend for their helpful advice in my study and research period.

Finally, I would like to express appreciate to my wife Jing Wang, my son Leo, and my parents, for their love, patience, understanding, and expectation.

Table of Contents

List of Figures

List of Tables

Nomenclature

A - The area of the building envelope (m^2)

A_{fs} - The area of the fluid-solid phase interface

A_{inf} - The ventilated area (m^2)

A_m – The amplitude of temperature variation (K)

A_{nf} – Non-ventilated area (m^2)

C_{pa} - The heat capacity of air (J/kg K)

d_p - The particle diameter of the porous media (m)

D_h - The hydraulic diameter (m)

G_0 - The coolant mass velocity ($kg/s \cdot m^2$)

h - The convective heat transfer coefficient (W/m^2K), the width of the ventilated area (m)

h_c - The convective heat transfer coefficient of cold side (W/m^2K)

h_{cout} - The convective heat transfer coefficient at outdoor side (W/m^2K)

h_{crack} – The width of the crack (m)

h_h - The convective heat transfer coefficient of hot side (W/m^2K)

h_{in} - The convective heat transfer coefficient inside the room (W/m^2K)

h_r - The radiative heat transfer coefficient (W/m^2K)

h_{sf} - The fluid to solid heat transfer coefficient (W/m^2 K)

H - The height of the wall (m)

I_t - The solar radiation flux normal to the surface (W/m^2)

k - The thermal conductivity of the wall material (W/m K)

k_a - The thermal conductivity of the air (W/m K)

k_d - The thermal dispersion coefficient (W/m K)

k_e - The effective conductivity (W/m K)

k_{feff} - The effective heat conductivity of fluid phase (W/m K)

k_s - The conductivity of solid matrix (W/m K)

k_{seff} - The effective heat conductivity of solid phase (W/m K)

K – The permeability (m^2)

L_c - The length of the cavity (m)

L_{eff} The effective thickness of the ventilated area (m)

L_v - The water evaporation energy (J/kg)

$\dot{m}$ - The mass flow rate through the envelope (kg/s)

m_v - The moisture flux (kg s/m^2)

n – The ventilated area coefficient (-)

$\vec{n}_{fs}$ - The outwardly oriented unit vector normal to A_{fs}

p – The pressure (pa)

Q_{cond} - The heat loss through the envelope by conduction (W)

Q_{conv} - The heat loss through the envelope because of air flow (W)

$Q_{\inf}$ - The actual heat load due to infiltration (W)

$Q_{\inf C}$ - The infiltration heat load calculated by conventional method (W)

Q_T - The total heat loss through the building envelope (W)

Q_0 - The conduction heat load without infiltration (W)

R – The thermal resistance of the envelope (m^2K/W)

R_i- The local thermal resistance of inner air film (m^2K/W)

R_0- The local thermal resistance of outer air film (m^2K/W)

t - The time(s)

T- Temperature (K)

T_{bo} - The outdoor surface temperature (K)

T_c - The temperature of the cold surface (K)

T_f - The volume average temperature of fluid phase (K)

T_h - The temperature of the hot surface (K)

T_i - The indoor bulk temperature (K)

T_m - The average temperature (K)

T_o - The temperature at outdoor side (K)

T_s - The volume average temperature of solid phase (K)

T_{si}- The temperature of inner surface of dynamic wall (K)

T_{wi} - The inside surface temperature (K)

u - The air velocity (m/s)

u_{in}- Average velocity in the crack area (m/s)

U - The U-vale of the envelope (W/m^2K)

U_{dyn} - The dynamic U-value of the dynamic insulation (W/m^2K)

U_T - The total heat loss coefficient through dynamic insulated wall (W/m^2K)

V- The volume of the representative elementary volume (m^3)

V_i – The inlet velocity (m/s)

w - The width of the wall (m)

x,y,z- The Cartesian Coordinates (m)

α_f - The thermal diffusivity of fluid phase (m^2/s)

α_s - The thermal diffusivity of the solid phase (m^2/s)

a_{sf} - The specific surface area of the packed bed (m^2)

α_{sol} - The surface solar-absorption coefficient (-)

β Expansion coefficient (1/K)

γ - The ratio of dynamic insulation to the whole wall (-)

ε- Porosity of the material (-)

ε' - The phase change rate (-)

ε_c - The effective porosity (-)

ε_s - The surface emissivity (-)

η - The infiltration heat exchange efficiency (-)

θ – Non-dimensional temperature (-)

μ - The dynamic viscosity of the fluid (kg/m s)

μ^t - The effective viscosity of the medium (kg/m s)

ν- The kinematic viscosity of the air (m^2/s)

ρ - The density (kg/m^3)

ρ_a - The density of the air (kg/m^3)

ρ_m - The density of the dry material (kg/m^3)

ρ_0 The density of air at reference temperature (kg/m^3)

σ_s - The Stephan-Boltzman constant 5.67×10^{-8}

Φ - The heat flux density (W/m^2)

ω_n - The frequency (1/s)

Da - The Darcy number $Da = K / L^2$

Nu - The Nusselt number (W/m^{2}K)

Pe - The Peclet number $Pe = \frac{V_i L}{\alpha}$

Pr - The Prandtl number $\mathrm{Pr} = \frac{\nu}{\alpha}$

Ra - The Raleigh number $Ra = \frac{g\beta\Delta T L^3}{\alpha\nu}$

Re - The Reynolds number $\mathrm{Re} = \frac{V_i L}{\nu}$

σ - The Heat capacity ratio $\sigma = [(1-\varepsilon)(\rho C_p)_s + \varepsilon(\rho C_p)_a]/(\rho C_p)_a$

Chapter 1 Introduction

1.1 Heat loss through the building envelope: conventional analytical methods and their shortcomings

The building envelope is one of the most important systems affecting energy efficiency of a building. Comprehensive analyses of heat loss through the envelope are needed in order to design energy-efficient buildings. Generally, it is regarded that heat is mainly lost by conduction. Treating the building envelope as a multilayer system, the steady-state conduction heat loss can be calculated by using the U-value of the envelope, i.e.:

$$Q_{cond} = UA\Delta T \tag{1.1}$$

Q_{cond} - The heat loss through the envelope by conduction (W)

A - The surface area of the envelope (m^2)

U - The overall heat transmission coefficient (W/m^2K)

ΔT - The indoor and outdoor temperature difference (K)

Heat loss through the building envelope also occurs due to infiltration/exfiltration. It is the uncontrolled leakage of air, moisture and other substances, through cracks and gaps in the building envelope, and through pores of the building materials. The infiltration/exfiltration heat loss generally accounts for about 15-20% of the overall heat loss through the building envelope (Caffey, 1979). It is conventionally estimated by the following equation:

$$Q_{\inf C} = \dot{m}C_{pa}\Delta T \tag{1.2}$$

$Q_{\inf C}$ - The infiltration heat load calculated by conventional method (W)

$\dot{m}$ - The infiltration mass flow rate (kg/s)

C_{pa} - The heat capacity of air (J/kg K)

Assuming that the processes of conduction and infiltration do not interact with each other, the total heat loss through the envelope can be obtained by adding conduction heat loss and infiltration loss estimated (equation (1.2))

$$Q_T = Q_{cond} + Q_{\inf C} \tag{1.3}$$

Q_T - The total heat loss through the envelope (W)

However, Bhattacharyya and Claridge (1995) experimentally showed that this method over-estimates the actual infiltration heat loss. If we use equation (1.1) to account for the conduction heat loss, then the real infiltration heat loss is only a fraction of the result calculated by the conventional approach. The infiltration heat exchange efficiency (IHEE), η, was defined to reflect this effect:

$$Q_{\inf} = (1-\eta)Q_{\inf C} \tag{1.4}$$

η - The infiltration heat exchange efficiency (-)

$Q_{\inf}$ - The actual heat load due to infiltration (W)

Therefore the simple summation of conduction and infiltration heat loss following the conventional way using equation (1.3) is not suitable to calculate the real energy demand for the building. To reflect the combined influence of conduction and infiltration, a new approach should be investigated.

1.2 New concepts in building envelope design

The building envelope, including the exterior walls and the roof, is a means of protecting people in the building from the outside environment, such as bad weather conditions, pollution and noise. Due to this, and the concept of energy saving, the building enveloped is usually designed to be airtight, using an air and vapor barrier. Because of this kind of design, the building envelope acts as the barrier between the indoor and outdoor environment, resulting in small indoor temperature swing in spite of the fluctuation of outdoor temperature.

However, the design of a better-insulated and more airtight building envelope not only has the positive aspects of energy saving, but also unfortunately results in an increase of sick building syndrome (SBS). Building occupants often complain of symptoms such as headache; eye, nose, or throat irritation; dizziness and nausea; and difficulty in concentrating. These symptoms of poor indoor air quality (IAQ) influence people's attitude towards building design, as they spend much of their time in buildings and increasingly pay more and more attention on their health and comfort.

Therefore building users are becoming more concerned about pleasant working and living environments, healthy indoor conditions and thermal comfort. Thus only considering the energy efficiency aspect of the building does not guarantee buildings of high quality. It is now thought that the building envelope should work in a way that the optimal parameters for the indoor environment are achieved in relationship with the external environment, while keeping the energy consumption of the building as low as

possible (Gratia and De Herde, 2004). With these demands comes the development of advanced building envelopes, which try to integrate aspects of building performance, such as weather protection, thermal insulation and ventilation. One important concept among advanced envelopes is the active envelope. Its typical structure consists of an air cavity between two panes. The airflow can work in three ways: acting as an air curtain, in which the air leaves the cavity at the same side as it comes in; supplying fresh air from outside to the inside of the building; or exhausting air from inside to the outside of the building (Baker et al, 2000).

Regarding energy efficiency, two operational modes of active envelopes have been developed. The first is to have active envelopes work as heat exchangers. Dynamic insulation (Taylor and Imbabi, 1998) is an example of this mode. The dynamic insulated wall uses the concept of "breathing construction". It allows the movement of air through the external walls. The second mode is that active envelopes work as solar collectors. In this mode, one noticeable technology is the double-skin façade, which consists of outer and inner façade layer, with a cavity between them (Oesterle, 2001). Taking advantage of the solar energy, ventilation air in the cavity is preheated to save energy.

Besides the potential energy savings, advanced building envelopes have other advantages. For example, the fibrous structure of dynamic insulation can filter the air and capture pollution particles within the depth of the insulation. Thus dynamic insulation might have the potential of approaching effective air filters with a considerably lower

pressure drop, and could be an ideal choice for naturally ventilated buildings (Taylor et al, 1999).

The development of advanced building envelopes also brings the challenge of development of the calculation method for heat loss through such envelopes. The building envelope is traditionally treated as a solid multilayer system without cracks. In this approach, only conduction heat loss is accounted for while convection heat loss is neglected. However, convection heat transfer is obviously very important for the active envelopes, which integrate the airflow in the envelopes. Therefore the traditional simulation method of heat loss through the building envelope should be modified to include the influence of convective flow in the envelope.

1.3 Research objectives

The fact that the conventional approach to calculate the infiltration/exfiltration heat loss over-estimates the real heat loss can be explained from the following point of view: the building envelope can work as a heat exchanger. The building envelope contains gaps and cracks, and the interaction between these gaps or cracks and the solid wall can work as a heat exchanger. Besides, the more important reason is that building materials are porous media. The interaction between the fluid phase and solid matrix in the porous media can also act as a heat exchanger. Due to the recovered heat in the air infiltration process, the actual heating load is not as high as that calculated by equation (1.3).

Thus the specific research objectives of this study are:

1. To develop a systematic approach of analyzing the heat exchange performance of the building envelope based on the simulation of heat and mass transfer in porous media. By performing a systematic study of air flow and heat transfer in the porous media and analyzing their characters in the building envelope, the governing equations for the description of the conduction-infiltration coupled process in the building envelope will be derived.
2. To find out the key parameters influencing heat exchange in the building envelope. Factors affecting the heat exchange performance, such as air flow rate, buoyancy, and properties of the building material (porosity and permeability), will be investigated.
3. To discuss the impact of air infiltration on the energy consumption of the building. Generally speaking, air infiltration has a negative effect on the energy consumption of the building. However, the heat exchange phenomenon in the building envelope decreases this negative effect to some extent. This effect will be analyzed in detail in this study.
4. To explore the feasibility of implementing this heat exchange phenomenon in the building envelope. Specific application of advanced building envelopes, especially dynamic insulation will be investigated in order to supply guideline of these technologies in the building design.

1.4 Organization of the thesis

This thesis is organized as follows:

- Chapter 2 conducts a comprehensive review on the current work relating to heat exchange phenomenon in the building envelope, as well as the fundamentals of fluid transport and heat transfer in porous media;
- Chapter 3 presents the numerical model, adopting the approach of heat transfer and air flow through porous media. The derivation of the conservation equations is described in detail. Boundary conditions are analyzed and determined as well. The solution method of the numerical model is also presented.
- Chapter 4 illustrates and analyzes the simulation results. Model verification is also presented in this chapter. Data from the literature, as well as from recent experiments are compared with the simulation results, to demonstrate the suitability of the approach and the accuracy of the model.
- Chapter 5 discusses the potential implementation of the model and approach. First, the current-state-of-the-art of dynamic insulation is reviewed to demonstrate its advantages and disadvantages. Then the numerical and analytical modelings are carried out concerning the thermal performance of dynamic insulation. Finally, an analytical model for the heat exchange in the conventional wall is presented based on the previous numerical simulation, aiming to set up a more suitable model for the application.
- Chapter 6 presents the conclusions obtained from the study, and provides suggestions for the work of future research.

Chapter 2 Literature Review

2.1 Air cavity models treating the wall as a heat exchanger

Bhattacharyya and Claridge (1995) are among the earliest researchers to investigate the heat exchange performance in insulated walls. They developed a simplified 1-D model to examine the general features of the dependence of infiltration heat exchange on air flow path and rate, using the measured quantities as key parameters. In their model for a single stud-cavity specimen, airflow is through a crack which follows a straight line between the inlet at the bottom of the stud cavity and the outlet at a certain height of the specimen (Fig 2.1). Thus the energy equation can be expressed as

$$\dot{m}c_p\frac{dT_f}{dx}+U_{left}w(T_f-T_c) = U_{right}w(T_h-T_f) \qquad (2.1)$$

where $U_{left}=\frac{U_{wall}h_cL}{U_{wall}L+h_cy}$

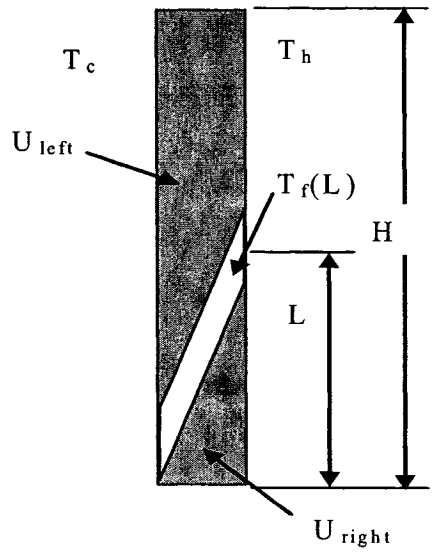

T_c - The cool side (outdoor) temperature

T_h - The hot side (indoor) temperature

T_f - The Air temperature

H - The height of the wall

U_{left} - The U value of the left side of the wall

U_{right} - The U value of the right side of the wall

L - The length of the infiltration path

Fig 2.1: Model by Bhattacharyya and Claridge (1995)

$$U_{right} = \frac{U_{wall} h_h L}{U_{wall} L + h_h (L - y)}$$

w - The width of the wall (m)

h_h - The convective heat transfer coefficient of hot side (W/m^2K)

h_c - The convective heat transfer coefficient of cold side (W/m^2K)

y- The wall height direction coordinate (m)

The equation to calculate infiltration heat exchange efficiency (IHEE), η, was derived, by performing an energy balance on the whole building considering infiltration/exfiltration at the same time,

Corresponding to this model, Claridge et al (1995) performed a systematic investigation using a number of experimental setups. To consider different infiltration paths, they adopted the concept of concentrated-flow (CF) and diffuse-flow (DF). CF was defined as a short pass flow, such as airflow through doors, windows, and large cracks or holes. DF was defined as long pass flow in which the air travels some distance before leaving the wall.

The above work by Claridge et al. (1995), including measurement and modeling, has important impacts on our understanding of the heat exchange phenomenon in the building envelope. However, in their simulation model, they did not take into account the properties of the building materials. The 1-D air cavity model straight through the wall is not suitable to reflect the complex condition of air infiltration. Meanwhile, to use their model, the length of infiltration path L should be measured or assumed in advance.

One obvious advantage of air cavity heat exchanger model is that it is possible to derive an analytical solution. The recent work of Barhoun and Guarracino (2004) follows this idea. Starting from the model of Bhattacharyya and Claridge (1995), which states that the heat transfer coefficient for the left side of the wall, U_{left}, and for the right side of the wall, U_{right}, changes with the outlet position in the y-direction, they assumed that the air flows vertically throughout the wall from the bottom to the top, and the channel is in the middle of the wall. Therefore, U_{left} and U_{right} are constants and were expressed as:

$$U_{left} = (\frac{1}{h_c} + \frac{L}{2k})^{-1}$$

$$U_{right} = (\frac{1}{h_h} + \frac{L}{2k})^{-1} \tag{2.2}$$

Based on this, by solving the linear differential equation, an analytical solution of infiltration temperature, T_{inf}, as a function of the vertical coordinate y was derived as follows:

$$T_f(y) = (T_c - \frac{b}{a})\exp(-ay) + \frac{b}{a} \tag{2.3}$$

$$a = \frac{w}{\dot{m}c_p}(U_{left} + U_{right})$$

$$b = \frac{w}{\dot{m}c_p}(T_c U_{left} + T_h U_{right})$$

It is clear that some important factors, such as the airflow rate and convective boundary condition, have been included in this analytical solution. Thus it is very helpful to understand the complex heat exchange phenomenon in the wall.

The air cavity approach was also adopted by Chebil et al (2003) to simulate the transient 3-D heat and air transfer phenomena to evaluate air leakage effects on typical multilayer wall structures. Instead of solving complex fluid flow equations, the airflow in each cavity was considered as one-dimensional and correlations of the Nusselt number (Nu_f) from the literature were used to determine the heat exchange between air cavities and solid parts. In the case of air infiltration, the following Nusselt number corrections for forced convection (Kohonen et al, 1987) were used:

$$Nu_f = 1.85(\mathrm{Re}\cdot\mathrm{Pr}\cdot D_h / H)^{1/3} \qquad \mathrm{Re}\cdot\mathrm{Pr}\cdot D_h > 70$$

$$Nu_f = 7.54 \qquad \mathrm{Re}\cdot\mathrm{Pr}\cdot D_h < 70 \qquad (2.4)$$

D_h - The hydraulic diameter (m)

H - The height of the wall (m)

Meanwhile, radiation heat transfer was also included in the total heat transfer coefficient in the cavity. Several scenarios were used to represent the variation of the airflow path. Overall heat loss was evaluated depending on the airflow rates in each scenario. Their simulation results show that the scenario having the longest airflow path has the most obvious overall heat load reduction effect.

2.2 Research on convection in wall elements

The above models deal with the heat exchange performance of the whole wall. Considering the wall structure, cavities may exist in the wall elements. Heat exchange phenomenon might take place due to the convection in these wall elements.

Research of convection in the exterior wall elements first comes from the study of heat transfer in hollow bricks, which is a frequently used component of exterior walls in Asian and European countries. Batchelor (1954) pointed out that in a differentially heated closed cavity, there exist two transfer regimes: the boundary layer and conduction zone. Therefore heat losses through hollow bricks may be due to natural convection heat transfer inside the cavity.

Natural convection is due to the buoyancy force resulting from the temperature difference between cold and hot surfaces, may be the most important from of heat transfer in closed cavities. Its fundamentals have been well summarized by Bejan (1995). Theoretical and numerical studies show that the solution of natural convection in an enclosure is a function of three non-dimensional parameters: the aspect ratio of the cavity; the Prandtl number of the fluid, *Pr*; and the Rayleigh number, *Ra*.

For air (Pr about 0.7) and cavity of aspect ratio of 40, Lorente (2002) carried out a numerical study and measurement using particle image velocimetry (PIV) to determine the local Nusselt number, which is the ratio of convective heat transfer over conductive heat transfer, and is expressed as:

$$Nu(z) = \frac{h(z)x}{k_a(T)} \tag{2.5}$$

where $$h(z) = \frac{\Phi(z)}{T_h - T_c}$$

$k_a(T)$ - The thermal conductivity of the air (W/m K)

x, z - The Cartesian Coordinates (m)

$\Phi(z)$ - The wall heat flux calculated on the hot surface in the viscous boundary layer (W/m^2)

T_h, T_c - The temperature of hot and cold surface (K)

The results show that if *Ra* is below 6000, then the energy transfer from hot surface to the cold surface is carried out directly by conduction. When *Ra* increases above 6000, heat transfer is mostly by natural convection. Thus for typical bricks made of horizontal cavities, the influence of convection can be ignored. However, in the case of vertical hollow bricks, where less material is necessary to achieve the same mechanical resistance, an important part of heat transfer is due to natural convection. The actual heat transfer for buildings with vertical hollow bricks might be quite different from the conventional thinking: i.e., air is a no-motion fluid and heat transfer is dominated by conduction because of the small dimensions of cavities.

Following a similar procedures to study the heat transfer in a wall of vertically perforated bricks, Lacarriere et al (2003) suggested that it is possible to determine an equivalent thermal conductivity, which represents both conduction and convection heat transfer:

$$k_e = \frac{\Phi_m L_c}{T_h - T_c} \tag{2.6}$$

L_c - The length of the cavity (m)

Φ_m - The mean flux density, obtained by integration of the local heat flux along the cavity height (W/m^2)

2.3 Research on double-skin facade

In modern building design, air cavities are used for ventilation purposes. As airflow is intensively incorporated in the design, the influence of convection is more obvious compared with a wall made of hollow bricks. Double-skin façades are typical of this kind of ventilated wall.

The airflow in a double-skin façade can be the result of wind and/or buoyancy effect. Thus, compared with the condition in a closed cavity, heat transfer in a double-skin façade is more complicated. For flow which is only induced by solar radiation, Zoller et al (2002) pointed out that the flow regime in the box-window may be divided into natural convection with a channel formed by two vertical plates or forced convection in a rectangular duct, depending on the dimension of the gap and solar radiation. Their experimental results show that for the case of a distance between outer and inner layers less than 0.6m, the mixed convection in the air gap should be analyzed using a "channel

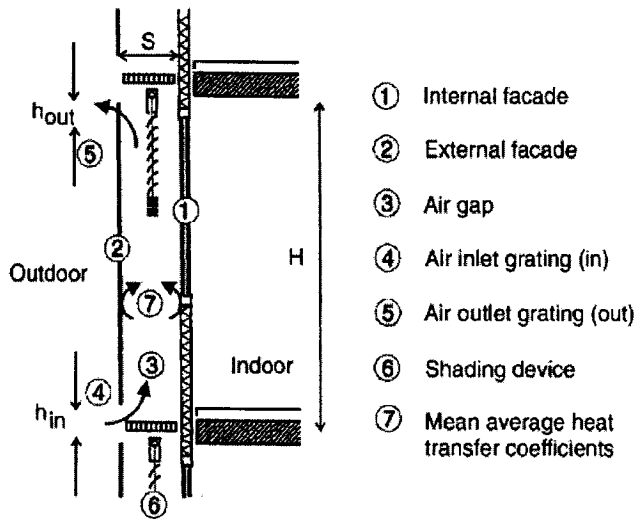

Fig 2.2: Schematic diagram of double-skin façade (Zoller et al, 2002)

model", whereas for the situation of outer and inner layer distance greater than 0.6m, the "plate model" should be employed.

Because of the complexity of convective heat transfer in a double-skin façade, computer modeling is necessary for the real application and research on this topic has been performed by many researchers. Manz (2003) adopted a CFD approach to study the heat transfer by natural convection of air layers in vertical, rectangular cavities, which is related to the element of double-skin façade. With aspect ratios of 20, 40 and 80, and *Ra* between 1000 and 10^6, the flow was either laminar or turbulent. Conduction, transition, and boundary layer regimes were discussed. The resulting average Nusselt numbers were compared with corrections mainly from experimental data and found they are generally in good agreement.

Though CFD is a powerful tool to study airflow and heat transfer in double-skin façade construction, there are problems in application. Hensen et al (2002) discussed the advantages and disadvantages of the CFD approach and of the mass balance network method (multizone model). They pointed out that the CFD approach is less appropriate in the real application of systems of double-skin façade since it is necessary to take into account a large part of the building with dynamic interactions between several zones and ambient conditions. However, the network method could be improved through separate CFD studies. For example, the CFD results could be used to verify and/or improve the network pressure-flow relations and local loss factors for airflow conditions typical of natural and hybrid ventilation systems.

Due to this, researchers have been working on simplified models to simulate the temperature behavior and flow characteristics of double-skin facades. For example, von Grabe (2002) presented a one-dimensional flow model, starting from the energy transport and the Bernoulli equation, while introducing a resistance factor to represent frictional loss.

2.4 Models based on heat and airflow through porous media

Because building materials are porous media, air can flow through the building envelope. This is especially obvious for the insulation which has a high porosity. In the infiltration process, air becomes warmer if the outside temperature is cooler than room temperature, and gradually becomes closer to the room air temperature because of the heat exchange with the solid matrix. This heat exchange phenomenon has been studied by several researchers. Krarti (1994) presented a one-dimensional model, assuming air transfer through the wall with a constant speed. An analytical solution was derived by adopting convective boundary conditions on both surfaces inside and outside the room, and regarding that the outdoor and indoor temperature follows a sinusoid, i.e.:

$$T = T_m + A_m \mathrm{Re}(e^{j\omega_n t}) \tag{2.7}$$

T_m - The average temperature (K)

A_m – The amplitude of temperature variation (K)

ω_n - The frequency (1/s)

An investigation was conducted based on the analytical solution of equation (2.7) to evaluate the thermal performance of dynamic insulation system integrated with a whole building. The criteria "wall efficiency" was defined using the ratio of conductive heat

loss at the internal surface of insulation without and with ventilation. The change of wall efficiency in a day was presented. The results show that the wall efficiency changes from 15% to 45% over a day, with an average of 22%, under the most ideal condition.

To better reflect the fundamental physics of the infiltration heat recovery process, Buchanan and Sherman (2000) implemented CFD simulations. The calculation model for the whole building is illustrated in Fig 2.3. In this model, flow and energy transport in the room are determined by the Navier-Stokes and energy equations, considering the flow as laminar. The plywood sheathing is represented as an impermeable, solid material and energy transport is calculated by the conduction equation. Insulation is represented as porous media and airflow through it is calculated using Darcy's law. To represent the heat transfer in the porous media, the following effective conductivity was used in the energy equation:

$$k_e = \varepsilon k_a + (1-\varepsilon)k_s \tag{2.8}$$

k_e - The effective conductivity (W/m K)

k_a - The conductivity of air (W/m K)

k_s - The conductivity of solid matrix (W/m K)

ε- The porosity of the material (-)

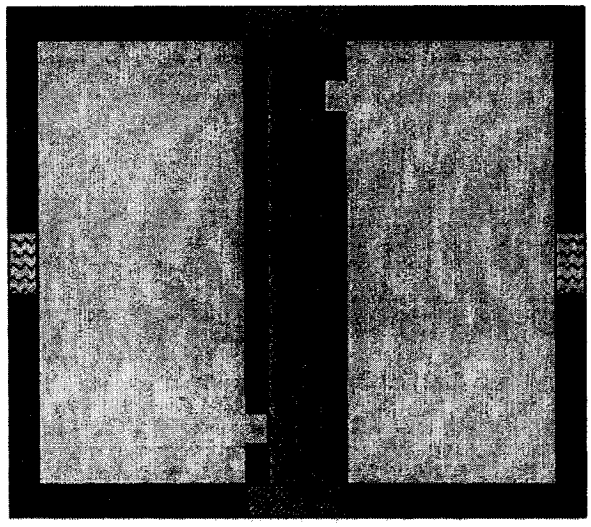

Wall 1 b.c.'s (U=0, T=T1)

Wall 2 b.c.'s (U=0, T=T2)

Inlet or outlet b.c.'s (U, P, T)

Adiabatic wall

Air (Navier–Stokes & energy eqns.)

Wall sheathing (conduction eqn.)

Insulation (Darcy's Law & energy eqn.)

b.c: boundary condition

Fig 2.3: Buchanan and Sherman's calculation model (2000)

To investigate the influence of the airflow path, several kinds of configuration of walls, in which air enters and leaves the insulation at different positions, are used in the simulations.

Their simulation results show that the infiltration heat recovery process mainly occurs within the wall structure and in the vicinity of the wall structures. Therefore, it is not necessary to study in detail the building interior for the heat exchange phenomenon in the wall. Corresponding to this, Abadie et al (2002) only considered the boundary layer flow near the wall rather than the flow in the whole room in their model. To do this, they added an air cavity on both the inner and outer side of the wall to extend the computational domain. These additional spaces are large enough that the boundary layer flows on the wall surface are largely unaffected by the CFD computational space boundaries, and small enough that the increase in CFD computational time is acceptable.

A model containing the flow in the air gap and flow through porous media is also presented by Chen and Liu (2004) to study the heat transfer and airflow in a composite-wall solar-collector system, which consists of a glass cover, a porous absorber, an air gap and a massive thermal storage wall. Their work is to show that heat can be stored in the porous absorber by the incident solar radiation, and thus the porous absorber can work as a good thermal insulator when sunlight is not available. However, heat exchange performance is not addressed in the model.

The model by Buchanan and Sherman (2000) does not focus on the wall. As the simulation in the wall is coupled with the indoor airflow, it took too long for the authors to obtain converging solutions using small time-steps which assure convergence at each time-step. The technique of variable time-step is therefore needed to speed up the solution for real application.

2.5 Research on mechanism of air flow through air permeable materials in buildings

Miguel et al (2001a, 2001b) studied in detail the mechanism of airflow through permeable materials which contain either pores or apertures, by dividing the material into a medium with poor fluid transmissivity, (i.e. a medium containing pores), and a medium with high transmissivity, (which is a medium containing an aperture). They established a theoretical model, discussed the approach's range of validity, and presented a correct interpretation of the equation terms. The model presented is based on the momentum conservation equation and is developed in terms of volume average method. Each term in the equation is interpreted so as to set up a basic understanding of airflow through permeable materials. The non-linear differential equation they obtained was shown to be valid to describe airflow through materials with pores up to large apertures.

As the mathematical equation is difficult and usually impractical, even by numerical methods, a one-dimensional process was regarded to air infiltration. Thus a simplified form of the approach was also presented, which is an ordinary differential equation as follows:

$$(\rho/\varepsilon)\frac{du}{dt} + (\mu/K)u + \rho Y K^{-1/2}|u|u + \Omega u = -\frac{dp}{dx} \tag{2.9}$$

with

$$\Omega = 0.5\rho C_c^{-2}|u|H$$

$$Y = 4.30\times10^{-2}\varepsilon^{-2.13}$$

ε- The porosity of the material (-)

ρ - The density (kg/m^3)

K – The permeability (m^2)

p – The pressure (pa)

H – Characteristic length of the medium (m)

C_c - Coefficient accounting for the convective inertia and viscous effect

For filters and porous screen, the permeability is:

$$K = 3.44 \times 10^{-9} \varepsilon^{1.6} \qquad (2.10)$$

An experiment was also carried out by them to determine the coefficient C_c.

The investigation was focused on the transient response of infiltration air velocity in the porous screen. The air velocity across the screen is assumed to be uniform because of the very small thickness of the material. As a matter of fact, in this case, the air infiltration path is too short to allow heat exchange process occur. Therefore the relation (equation (2.10)) obtained from the experiment is not suitable for the analysis of heat transfer in the thick material like thermal insulation.

2.6 Analytical model for dynamic insulation

Dynamic insulation is considered as a potential technology to feasibly implement the heat exchange phenomenon in the building envelope. Unlike conventional construction, where ventilation air enters the building through a designated air inlet, the concept of dynamic insulation is to draw air from the outside into the building through a kind of "breathing envelope", i.e. an air permeable insulation. Structures with dynamic insulation

incorporate the air passing through porous material and heat exchange in the building envelope. According to the relation of direction of airflow and that of heat flow through the wall, dynamic insulation construction can be classified into the contra-flux mode and the pro-flux mode. In the contra-flux dynamic insulation, air moves through the wall in the opposite direction of the heat flow, while in the pro-flux insulation, air flows in the same direction as the heat flow (Fig 2.4). The insulation is expected to act as a contra-flow heat exchanger as airflows through it. However, the condition may change into the pro-flux mode in real operation (Dimouli, 2004).

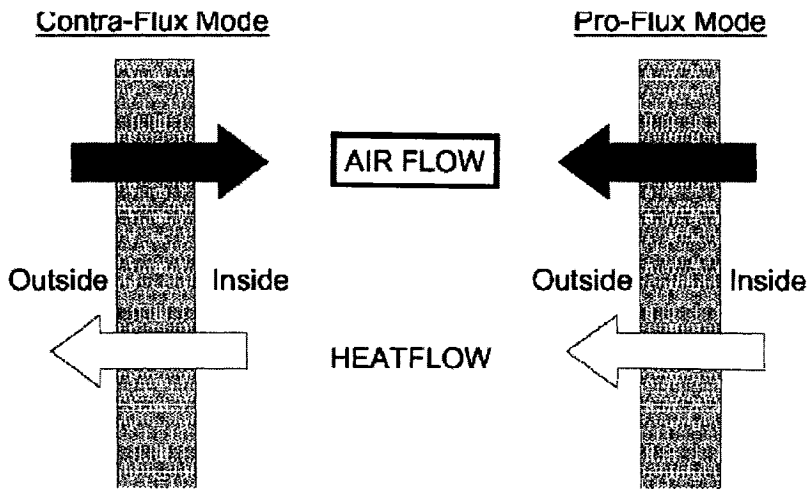

Fig 2.4: Contra-flux and pro-flux heat mode of dynamic insulation (Baker, 2003)

Theoretical analysis has been performed for a dynamic insulated wall, especially on its thermal performance. A steady-state one-dimensional model is presented by Taylor et al (1996) as follows:

$$k\frac{d^2T(x)}{dx^2} - u\rho C_{pa}\frac{dT(x)}{dx} = 0 \tag{2.11}$$

k - The thermal conductivity of the wall material (W/m K)

T - The temperature (K)

ρ - The density of the air (kg/m^3)

u - The air velocity (m/s)

C_{pa} - The heat capacity of air (J/kg K)

By setting the temperature at two boundaries being the outdoor and indoor temperature, and assuming the air velocity in the wall is constant, analytical solution can be obtained as follows:

$$\frac{T - T_o}{T_i - T_o} = \frac{\exp(\frac{u\rho c_p x}{k}) - 1}{\exp(\frac{u\rho c_p L}{k}) - 1} \tag{2.12}$$

T_i - The temperature at indoor side (K)

T_o - The temperature at outdoor side (K)

L - The thickness of the dynamic insulation (m)

The model has been extended to a three layer wall system and assumed that the heat flux in each layer of the wall is constant and equals to the heat flux at the outer surface of the wall, i.e.:

$$\Phi = \frac{\ln G}{G-1}\frac{T_i - T_o}{R} \tag{2.13}$$

$R = \sum_{i=1}^{3}\frac{L_i - L_{i-1}}{k_i}$ Total thermal resistance for the envelope (m^{2}K/W)

$G = \exp(u\rho c_p R)$ Dimensionless parameter

According to this one-dimensional steady-state model, the dynamic *U*-value was derived as follows (Taylor and Imbabi , 1998):

$$U_{dyn} = \frac{u\rho_a c_p}{R(e^{u\rho_a c_p L/k} - 1)} \tag{2.14}$$

It is clear that this dynamic *U*-value is a function of the air velocity. It is regarded as a character of the performance of dynamic insulation (Baker, 2003). However, a simple calculation using equation (2.14) shows that U_{dyn} decreases with the increase of the velocity. This conclusion is contradicted to the common observation. This is because the equation is derived from the heat transfer performance in the air inlet position. With the increase of the air flow, the temperature gradient near the air inlet decreases, resulting a smaller U_{dyn}. However, if the incoming air is not pre-heated before it enters the dynamic insulation, and its temperature is equal to the outdoor temperature, then the convective heat loss will increase with airflow rate. Thus the overall heat loss will increase with airflow rate. Therefore a comprehensive analysis is needed for the thermal performance of dynamic insulation.

Meanwhile, it is noticed that U_{dyn} in equation (2.14) is a non-dimensional parameter, thus it represents the ratio of *U*-value influenced by the air flow, with the steady-state *U*-value. This is not mentioned in the literature.

In the derivation of equation (2.14), the boundary conditions are set up such that the temperature at the outside and inside nodes of the walls are constant and equal to that of outdoor and indoor temperature. However, influenced by the air film near the wall, the temperature at the boundaries may be different from that, especially for the indoor side of the wall. As the air flow velocity is very slow in the dynamic insulation wall, the more suitable boundary condition for the analysis is as follows (Taylor and Imbabi, 1997):.

$$-k\left.\frac{dT}{dx}\right|_{x=L} = h(T_i - T_{wi})$$

T_i - The indoor temperature (K)

T_{wi} - The inside surface temperature (K)

h - The convective heat transfer coefficient (W/m^{2}K)

Under steady-state conditions, if considering the influence of thermal resistance of inside and outside air films, the temperature of internal surface of dynamic insulated wall can be calculated as (Taylor and Imbabi, 1997, Gan, 2000):

$$\frac{T_i - T_{si}}{T_i - T_0} = \frac{R_i \exp(Pe)}{R_i \exp(Pe) + \dfrac{\exp(Pe) - 1}{kPe/L} + R_0} \tag{2.15}$$

T_{si}- The temperature of inner surface of dynamic wall (K)

R_i- The thermal resistance of inner air film (m^{2}K/W)

R_0- The thermal resistance of outer air film (m^{2}K/W)

Therefore the inner surface temperature decreases with the airflow rate.

Corresponding with this theory, results obtained in the above investigations concerning the performance of dynamic insulation wall include:

1. When calculating the inner or outer surface temperature, the suitable boundary condition is that the conductive heat flux at the wall surface, rather than the net heat flux, is equal to the flux incident on the wall from the environment;
2. In the assessment of heat loss through dynamic insulation over the static equivalent, the influence of both inner and outer surface air films can be neglected;
3. The air film influences the inner and outer surface temperatures, so it will impact the thermal comfort of occupants in the room.

The actual structure of a dynamic insulated wall is complicated, though the most designs try to assure one-dimensional flow thorough the wall, by using an air gap in front of the insulation. For example, in the schematic of dynamic insulation presented by Gan (2000) and prototype dynamic insulated wall by Baker (2003), air comes into and exits from the wall at different heights, hence the incoming air velocity to the insulation is not uniform. Thus a 1-D analytical model is not able to reflect the complete situation of heat transfer in the dynamic insulated wall. To fully investigate the heat exchange performance in the wall, 2-D or 3-D numerical models may be needed.

2.7 Combined heat, air and moisture transfer models

As moisture in the air can penetrate into the porous building materials, moisture transfer will have a significant influence on the performance of the building envelope, including

heat transfer and exchange performance. Heat and moisture transfer in porous material has been investigated since the pioneering work of Philip and Devries (1957) and Luikov (1966). A general description of heat and moisture transfer in porous media was presented by them. The energy equation is incorporated with vapor and liquid transport caused by capillary forces. The capillary force is represented in terms of gradients of the moisture content and temperature. After that, Whitaker (1977) averaged the transport equations on a representative elementary volume (REV) at the continuum level and obtained the governing equations in a higher level. Based on these fundamental approaches, research on combined heat and moisture transfer is very active in building science. Corresponding with theoretical works, several software packages have been developed, such as 1D-HAM, WUFI and MATCH. The model used in the package 1D-HAM (Hagentoft and Blomberg) is a basic model that includes heat, air and moisture transfer in a multi-layer porous envelope in one direction, and based on a finite difference method with explicit forward differences in time. In the simulation model, the airflow rate through the envelope is assumed the same everywhere, determined by the constant flow resistance and pressure difference over the structure. Moisture is transferred by diffusion and convection in the vapor phase and heat is transferred by conduction, convection and latent heat. To simplify the problem, water transport is not included in their model. However, surface absorption of solar radiation is accounted for in the program.

Up to now, investigations relating to moisture in building materials have focused on mass transfer effect and most of them assume an isothermal condition for moisture transfer,

only considering the influence of phase change for heat transfer. To overcome this shortcoming, Vasile et al (1998) developed a model concentrating on heat transfer, by attempting to describe the influence of the moisture level on heat transfer occurring through hollow vertical terra-cotta bricks. According to them, the 1-D energy conservation equation including the effects of phase change by condensation/evaporation is as follows:

$$\rho_m c_p \frac{\partial T}{\partial t} = \frac{\partial}{\partial x}(k\frac{\partial T}{\partial x}) - L_v \varepsilon' \frac{\partial \dot{m}}{\partial x} \tag{2.16}$$

t - The time(s)

ρ_m - The density of the dry material (kg/m^3)

T - The temperature (K)

ϕ - The heat flux density (W/m^2)

L_v - The water evaporation energy (J/kg)

m - The total mass flux (kg s/m^2)

ε' - The phase change rate (-)

However, it is clear that only conduction heat transfer and phase change is considered, while influence of air infiltration is neglected in this model.

2.8 Limitations of the existing models

Table 2.1 is a summary of models related to heat exchange phenomenon in the building envelope. We can see that limitations exist in these models:

1. The air cavity models do not consider the characteristics of heat and mass transfer in porous media, instead, they adopt an assumed infiltration path for the airflow in the wall, such as the flow path considered by Bhattacharyya and Claridge (1995) and Chebil (2003). However, the direct path corresponds more with the situation of air infiltration through cracks around doors or windows, for the infiltration with inlet and outlet at different vertical position, this kind of assumption cannot reflect the actual situation. This shortcoming limits the adaptability of this kind of models.
2. In the models based on heat and air transfer flow through porous media developed so far, such as the work of Buchanan and Sherman (2000), only macroscopic effects are considered, which means that the interaction of different phases, for example, between solid matrix and gas phase, are not taken into account. The research also lacks of the deep analysis of air flow and temperature profile in the wall. Though an analytical model is presented, it does not connect with the numerical simulation to determine the infiltration-affected area. Meanwhile, equations for the wall are coupled with those for indoor airflows in the model. A great amount of computational resources are needed to obtain the converged solution in the simulation.
3. Dynamic insulation is a kind of technology for the implementation the heat exchange phenomenon in the building envelope. However, only steady-state heat transfer models have been reported until now and these models do not discuss the influence of property of the porous media. Considering the principle of heat exchange in the building envelope, which comes from the interaction between the air and solid matrix in the porous media, this model needs to be further developed.

4. In models based on combined heat and mass transfer in porous media, convection is either not considered for the heat transfer effect (Vasile et al, 1998), or it is only represented using a one directional constant airflow rate (1D-HAM). Thus these models need to be further developed.

Table 2.1 Summary of main models

Source	Type	Solution	Advantage	Disadvantage
Bhattacharyya and Claridge (1995)	1-D air cavity	Numerical	Easy to solve	Based on an assumed infiltration path
Barhoun and Guarracino (2004)	1-D air cavity	Analytical		
Chebil et al (2003)	3-D air cavity	Numerical		
Buchanan and Sherman (2000)	Heat and air transfer in porous media	Numerical	Reflect the real properties of building material	Only considers the macroscopic effect, does not focus on the heat exchange in the wall
Abadie et al. (2002)				
Chen and Liu (2004)				
Migeul et al (2001a, 2001b)	Heat and mass transfer in porous media	Numerical with experimental determination of key factor	Describe the fundamental mechanism	Specified for air flow in thin porous screen
Vasile et al (1998)	Heat transfer containing the influence of moisture	Numerical	Considering the heat exchange of phase change	Not focus on the heat exchange in air infiltration

2.9 Research on heat and mass transfer in porous media

The heat exchange performance of building envelope is mainly due to the convective flow in the porous material. For convective heat transfer in porous media, numerous studies have been performed so far and the state of art has been summarized by Bear (1972), Kaviany (1995, 1999), and Hsu (2003). According to Alazami and Vafai (2000), work on this topic can be classified into four categories, namely constant porosity, variable porosity, thermal dispersion, and local thermal nonequilibrium (LTNE).

Generally, research on transport phenomenon in porous media is based on the assumption of constant porosity. However, the porosity of this kind of model is an average value. Thus researchers have been trying to set up the model using a more accurate porosity value. A frequently used variable porosity model regards that porosity is higher at zones near the boundaries and the distribution of porosity follows the following law (Fu and Huang, 1999):

$$\varepsilon = \varepsilon_c[1 + r_1 e^{-r_2 \Delta s / d_p}] \tag{2.17}$$

Δs - The shortest distance from the calculated point to the boundary (m)

r_1, r_2 - The empirical constants (-)

ε_c - The effective porosity (-)

d_p - The particle diameter of the porous media (m)

Compared with research work considering the influence of constant and variable porosity, the concept of LTNE and thermal dispersion is more difficult to deal with and attracts more attention now.

For porous media consisting of a solid matrix and a fluid phase and without phase change, from the point of the view of heat transfer, it is pointed out that even for a steady-state problem, the solid matrix and the fluid phase cannot be in absolute thermal equilibrium when there is flow in porous media (Moyne et al, 2000). Therefore intrinsic phase average temperature is an important concept to set up the heat transfer equation. If the difference of volume averaged temperature distribution of solid and fluid phase is not negligible, i.e. the material is in local thermal nonequilibrium (LTNE), then the energy equation must be set up for solid phase and fluid phase separately. This is called a two media treatment. For a packed bed, if local thermal nonequilibrium is considered, then for the solid phase, the energy equation is (Alazami and Vafai, 2000):

$$\nabla \cdot (k_{seff} \cdot \nabla T_s) - h_{sf} A_{fs} (T_s - T_f) = 0 \tag{2.18}$$

And fluid-phase energy equation is:

$$(\rho C_p)_f \mathbf{u} \cdot \nabla T_f = \nabla \cdot (k_{feff} \cdot \nabla T_f) + h_{sf} A_{fs} (T_s - T_f) \tag{2.19}$$

T_s - The volume average temperature of solid phase (K)

T_f - The volume average temperature of fluid phase (K)

k_{seff} - The effective heat conductivity of solid phase (W/m K)

k_{feff} - The effective heat conductivity of fluid phase (W/m K)

h_{sf} - The fluid to solid heat transfer coefficient (W/m^2 K)

A_{fs} - The specific surface area of the packed bed (m^2)

It is generally regarded that A_{fs} is related to the porosity and the particle diameter of porous media while h_{sf} is related to Re number of the flow. Several models for h_{sf} and A_{fs} have been summarized by Alazami and Vafai (2000). According to their reviews, there are significant differences in the results obtained using different models. Thus much work is needed in this area.

The two media model is widely used to analyze the performance of a compact heat exchanger made of porous media. In this kind of heat exchangers, one important variable is the surface-area-to-volume ratio β of the porous media (Kim, et al, 2000). Adopting two media analysis, Wirtz (1997) presented a semi-empirical 1-D model for porous media heat exchanger. According to this model, for a porous wall with uniform thickness and composition, the porous matrix heat exchange effectiveness is derived as:

$$\eta_p = \frac{F}{mH}\tanh[mHF] \tag{2.20}$$

where $$mH = \sqrt{\frac{c_p G_0 H^2}{k_e L}}$$

G_0 - The coolant mass velocity (kg/s m^2)

H - The porous wall height (m)

L- The porous wall thickness (m)

k_e - The effective conductivity of porous media (W/m K)

$$F = \begin{cases} \sqrt{\dfrac{2+ntu}{2ntu}} & ntu < 2 \\ 1 & ntu \geq 2 \end{cases}$$

$ntu = St \cdot \beta t$ Local number of heat transfer units of the porous matrix

$St = h_{sf} c_p / G_0$ Particle Stanton number

The semi-empirical model is derived based on the assumption that temperature distribution along the flow direction is linear. However, generally this temperature distribution has a logarithmic profile. Therefore the validity of this model needs to be further examined.

In Equation (2.20), we can see that when $ntu \geq 2$, the heat transfer coefficient h_{sf} will not influence η_p. Actually, in this thermodynamic-limit solution, the coolant is heated to the porous media temperature before exiting the matrix. That is to say, the difference of volume averaged temperature distribution of solid and fluid phase can be ignored, and it is in local thermal equilibrium (LTE).

For the problem in local thermal equilibrium, one medium treatment is valid, i.e., heat transfer in the medium is represented by one equation. In this treatment, if we consider the influence of the heat transfer by local velocity nonuniformity in the representative elementary volume (REV), the concept of thermal dispersion is introduced. Research on this category is very active and several models have been developed, such as the model by Cheng and Hsu (1986), Moyne et al (2000) and Du et al (2003). Jiang et al (1999) pointed out by comparing numerical simulations results and experimental data that the thermal dispersion effect plays an important role in forced and mixed convection heat transfer in porous media, and must be included in the mathematical model for the case of

one medium treatment. Meanwhile, their discussion shows that the influence of thermal dispersion is obvious for the fluid phase being either gas (air) or liquid (water).

For the one medium treatment, it is generally assumed that the fluid and the solid phase are both at same intrinsic average temperature, and equals to the average of the medium. However, Monye et al (2000) argued that the temperature is an intensive property from thermodynamic point of view, thus it is justifiable to average enthalpy, which is an extensive property of the medium, rather than the temperature. They presented a new definition of average temperature of the medium according to the enthalpy of the unit mass, and derived a new effective thermal dispersion tensor.

One medium treatment is widely adopted in the investigation of forced convection or natural convection in porous media. Based on this method, recently investigations have been conducted on the topic of double diffusion convection in the fluid-porous layer, or multilayer system, and on forced or mixed convection in porous media. These works are related to the heat transfer problems in the building envelope, considering the air flow by the wind effect or buoyancy, and the influence of potential moisture transfer.

Double diffusion convection, where the buoyancy arises not only from density differences due to variations in temperature but also from those due to variations in solute concentration, is closely connected with heat transfer and moisture migration in fibrous insulation. As a rich variety of phenomena can occur on account of the combined effect of heat and mass transfer, research on this topic attracts many interests, especially on

fluid-porous layer structure, or multilayer system. Typical works include uniform equations for both the porous layer and the fluid area, and analytical expressions for the one dimensional velocity and temperature distribution (Mercier et al, 2002); relation of rate of heat and mass transfer on Darcy number and permeability in anisotropic porous layers symmetrically located in an enclosure filled with air (Merrikh and Mohamad, 2002); and boundary conditions at the interface between two porous layers, such as continuity of pressure, temperature and conservation of stress (Bannacer et al, 2003).

While double diffusion natural convection is important when considering moist migration and heat transfer in the building envelope, research on forced and mixed convection in porous media is necessary if we focus on the effect of air flow in the envelope. Chang and Chang (1997) studied the mixed convection in a vertical parallel-plate channel partially filled with porous media. The velocity and temperature distribution and local Nusselt number are obtained under various parameters, such as different thickness of porous medium, Darcy number (*Da*) and Grashof number (*Gr*). Numerical approach, i.e., SIMPLEC algorithm combining with the techniques of ADI (Alternative Direction Implicit) and SOR (Successive Over-Relaxation) was used in the study. These are closely related to the study of heat exchange phenomenon in this study, and some methods will be adopted.

2.10 Summary

Considering the thermal performance, the building envelope can behave as a heat exchanger. This literature survey summarizes the work related to this concept and achievements achieved so far. Investigations in this area have been performed both by theoretical approach and experimental measurement. Models based on heat and mass transfer in porous media are more suitable to reflect the real air flow situation in the envelope than the air cavity models. Meanwhile, the CFD approach shows its advantages in getting more accurate and detailed results. However, models based on heat and mass transfer in porous media presented up to now do not consider the interaction of the different phases in the porous media, and thus cannot reflect all the information of thermal performance. Furthermore, the link between the study on heat exchange in the building envelope and its potential implementation has not been addressed. Concerning these limitations, more detailed work is needed in order to better understand this thermal phenomenon and have it implemented in building design.

Chapter 3 Numerical model

3.1 Assumptions

Air infiltration and heat exchange phenomenon in the building envelope are complicated processes. This first comes from the fact that infiltration air usually contains water vapor. When this humid air flows through the envelope, condensation may occur under certain conditions. The moisture transfer and phase change will influence the heat exchange performance in the envelope. Besides, the temperature in the environment around the building may change from time to time. This means that the outdoor boundary condition is dynamic. Meanwhile, other effects, such as the wind direction, and variation of solar radiation, will affect the heat and mass transfer in the envelope. A comprehensive analysis of heat transfer in the building envelope should consider all these factors and this will definitely be the final goal of research on this topic. But if the simulation model includes all these variables that influence each other, the coupled equations will be very difficult to solve. At present, the study of exchange phenomenon will focus on the fundamental mechanism of heat transfer in the building envelope. Thus the research will be performed step by step and the following assumptions are made in the current study.

1. To make the problem simpler and concentrate on heat transfer through porous media, only dry air transfer through porous media is considered for the first step and the porous media is assumed to have uniform porosity and isotropic properties.
2. Although heat and mass flows in the building envelope are actually three dimensional, a two dimensional model is adopted in this study for simplicity. This

two dimensional approach offers significant advantages by simplifying CFD programming and reducing computation time.

3. Both indoor and outdoor temperature are assumed constant, which means the influence of weather variation is ignored, and simulation is carried under steady-state condition.

3.2 Airflow model

3.2.1 Darcy and Forchheimer flow

For low porosity and steady flow rates of incompressible fluids, Darcy's work sets up the basis in the research. This formula is expressed as:

$$\frac{\Delta p}{\Delta x} = \frac{\mu}{K} u \tag{3.1}$$

p - The pressure (Pa)

u - The average velocity in the flow direction (m/s)

K - The permeability of the porous medium (m^2)

μ - The dynamic viscosity of the fluid (kg/m s)

x- The Cartesian coordinate (m)

The permeability K takes the well-accepted form of:

$$K = \frac{\varepsilon^3 d_p^2}{a(1-\varepsilon)^2}$$

ε - The porosity of porous media (-)

d_p - The particle diameter of the porous media (m)

a - Constant depending on the microscopic geometry of the porous media (-)

For packed beds, $a = 180$, according to generally adopted Carmen-Kozeny theory (Kaviany, 1995).

As this equation is valid strictly for very low velocity flows, it was suggested to be corrected with the quadratic drag form:

$$\frac{\Delta p}{\Delta x} = Au^2 + Bu \tag{3.2}$$

A and B - Dimensional constants

This is known as the Forchheimer law, and it usually uses the following expression:

$$\frac{dp}{dx} = \frac{\mu u}{K} + \frac{c\rho u^2}{\sqrt{K}} \tag{3.3}$$

c - Dimensionless constant (-)

To account for the viscous shearing effect, the following form of Brinkman law is used to modify Darcy law:

$$\nabla p = -\frac{\mu}{K}u + \mu' \nabla^2 u \tag{3.4}$$

μ' - Effective viscosity of the medium (kg/m s)

3.2.2 Volume average method

In order to set up a general model for flow in porous media, just as Navier-Stokes equation for the pure fluid flow, a volume average method is widely used. In this method, for any quantity associated with the fluid in a representative elementary volume (REV), the volume average value is defined as (Kaviany, 1999):

$$\langle \psi \rangle = \frac{1}{V} \int_{V_f} \psi dV \tag{3.5}$$

where subscript *f* represents fluid.

A second average is the intrinsic phase average which is computed by finding the integral only over the volume V_f of the fluid phase contained in the representative elementary volume V:

$$\langle \psi \rangle^f = \frac{1}{V_f} \int_{V_f} \psi dV \tag{3.6}$$

The two averages are related by:

$$\langle \psi \rangle = \varepsilon \langle \psi \rangle^f \tag{3.7}$$

ε - The porosity of the material

Another important relationship is the theorem that relates the average of a derivative to the derivative of an average:

$$\langle \nabla \psi \rangle = \nabla \langle \psi \rangle + \frac{1}{V} \int_{A_{fs}} \psi \vec{n}_{fs} dA \tag{3.8}$$

A_{fs} - The area of the fluid-solid phase interface

$\vec{n}_{fs}$ - The outwardly oriented unit vector normal to A_{fs}

Based on the above relations, the semiheuristic volume average equation was derived by Vafai and Tien (1981) as follows (< > is dropped off for simplicity):

$$\frac{\rho_f}{\varepsilon^2}(\varepsilon \frac{\partial \mathbf{u}}{\partial t} + (\mathbf{u} \cdot \nabla)\mathbf{u}) = -\nabla p - \frac{\mu_f}{K}\mathbf{u} - \rho_f \frac{C_F}{\sqrt{K}}|\mathbf{u}|\mathbf{u} + \mu_f \nabla \mathbf{u} \tag{3.9}$$

The second, third and fourth terms in the right side of equation (3.9) are Darcy term, Forchheimer term and Brinkman term, respectively. Several models have been developed on both Darcy and non-Darcy effects and have been summarized by Alazmi and Vafai (2000) in table 3.1.

Table 3.1 Different models on Darcy and non-Darcy effect (Alazmi and Vafai, 2000)

Model	Darcy	Forchheimer	Brinkman
Vafai and Tien (1981)	$\frac{\mu}{K}u$	$\rho\frac{F\varepsilon}{\sqrt{K}}u^2$	$\frac{\varepsilon}{\mu}\nabla^2 u$
Kim et al (1994)	$\frac{\mu}{K}u$	$\rho\frac{F}{\sqrt{K}}u^2$	$\frac{\varepsilon}{\mu}\nabla^2 u$
Hadim (1994)	$\frac{\mu}{K}u$	$\rho\frac{F}{\sqrt{K}}u^2$	$\varepsilon\nabla^2 u$

There are slight differences between the expressions of these models. However, a comprehensive comparative study by Alazmi and Vafai (2000) shows that the calculated results are about the same.

For air permeable building materials, Miguel et al (2001a) derived the following momentum equation base on the volume average method:

$$(\rho/\varepsilon)\frac{\partial \mathbf{u}}{\partial t}+(\rho/\varepsilon^2)\mathbf{u}\cdot\nabla\mathbf{u}=-\nabla p+\mu\mathbf{u}\cdot\left[(1/\varepsilon)(V_f^{-1}\int\mathbf{n}\cdot\nabla\Gamma dA-V_f^{-1}\int\mathbf{n}\cdot\Phi dA)\right]$$
$$-\rho\mathbf{u}\cdot\mathbf{u}\left[(1/\varepsilon^2)(V_f^{-1}\int\mathbf{n}\Gamma dA)\right]+\mu\nabla\mathbf{u}\cdot\left[(1/\varepsilon)V_f^{-1}\int\mathbf{n}\Gamma dA\right]+(\mu/\varepsilon^2)\nabla^2\mathbf{u}$$

A- The interfacial area contained within the averaging volume

n- The unit vector

Γ - Quantity relating the intrinsic phase average velocity to the spatial deviation of the velocity

Φ - Quantity relating the intrinsic phase average velocity to the spatial deviation of the pressure

This equation is similar to equation (3.9), except that it includes the viscous resistance of fluid flow $(\mu/\varepsilon^2)\nabla^2\mathbf{u}$, the other three terms in the right hand of this equation corresponds with the Darcy's term, Forchheimer term and Brinkman term. However, it is demonstrated from this equation that permeability of the medium is associated with the viscous resistance due to the momentum transfer at the matrix-fluid interface, which is:

$$(1/\varepsilon)(V_f^{-1}\int \mathbf{n}\cdot\nabla\Gamma dA - V_f^{-1}\int \mathbf{n}\cdot\Phi dA) = -K^{-1}$$

Therefore permeability represents the ability of the medium to transmit the fluid through itself. In accordance to kinetic gas theory, it is related to the reciprocal of the collision frequency of diffusing particles against the solid matrix and the kinematic fluid viscosity. It can be a vector to represent the non-isotropic property of the material, for example, the different value of permeability in two directions has been adopted by Bankvall et al (2004) in their simulation of air transport in and through the building envelope.

The same relation can be arrived to the Forchheimer term as:

$$\left|(1/\varepsilon^2)(V_f^{-1}\int \mathbf{n}\Gamma dA)\right| = C_F K^{-1/2}$$

3.2.3 Selection of the model

The Darcy model is valid for slow flows through porous media with low permeability. However, as the velocity increases, deviations from Darcy's law are observed (Kaviany, 1999). For Darcy or creeping flow regime, the pore Reynolds number Re_p should be less than 1 (Pedras and de Lemos, 2001). When it comes to the airflow in the building envelope, it is pointed out that typical indoor and outdoor pressure differences for residential buildings are within the range of 0.1Pa to 10Pa (Abadie et al, 2002). As the viscosity of air is about 1.8×10^{-5}kg/ (m·s) and the permeability of air is less than $10^{-8}m^2$, the infiltration air velocity will be less than 0.5m/s, even for the condition of a pressure difference of 50Pa, an airflow rate of 10 to 30 times of typical infiltration rate (Chan et al, 2003). Because the pore diameter is generally less than 10^{-5}m for porous media used in building insulation, we can say that Re_p is less than 1 and the Darcy's law is valid in this condition.

3.2.4 Governing equations

Therefore conservation equations representing airflow in the building envelope are as follows:

The continuum equation is:

$$\nabla \cdot \mathbf{u} = 0 \tag{3.10}$$

where $\mathbf{u}$ is the velocity vector

The momentum equation, which includes inertial, gravity and buoyancy terms, is as follows:

$$\frac{\rho_a}{\varepsilon^2}(\varepsilon\frac{\partial \mathbf{u}}{\partial t}+\mathbf{u}\cdot\nabla\mathbf{u})=-\nabla p-\frac{\mu_f}{K}\mathbf{u}-\rho_a\mathbf{g} \tag{3.11}$$

For the buoyancy term, which comes from density variation, Boussinesq approximation is used, i.e.:

$$\rho_a=\rho_0[1-\beta(T-T_0)] \tag{3.12}$$

β Expansion coefficient (1/K)

ρ_0 Density of air at reference temperature (kg/m^3)

This is different from the model by Buchanan and Sherman (2000) with respect to: (1) the initial term is included in the current model; (2) Boussinesq approximation is adopted to simplify the treatment of the variation of density. In the work by Buchanan and Sherman (2000), the equation was expressed as that for compressible flow; however, it was mentioned that a temperature-dependent empirical relation was used for the density, thus it was also treated as incompressible flow.

3.3 Heat transfer model

3.3.1 One-medium treatment

To set up the energy equation, the first thing to determine is whether one medium model or two media model should be applied. When it comes to the situation in building science, Buchanan and Sherman (2000) performed an analysis to determine if the air/insulation system is in thermal equilibrium. For a flow velocity of 0.08m/s, and an outside bulk air and glass fiber temperature 274K and 298K respectively, the calculation

result shows that as the air flows deeper into the insulation, its temperature increases rapidly and eventually reaches the temperature of the solid matrix at a distance of about 5×10^{-5}m, which is a negligible distance. For the entire depth of the envelope, the temperatures of air and insulation fiber are nearly equal, meaning that the assumption of local thermal equilibrium between air and glass fiber is valid.

3.3.2 Derivation of the governing equation

In the one-medium treatment of heat transfer in porous media, from a microscopic point of view, interaction between solid matrix and fluid phase exists, thus the energy conservation equation should be set up for solid matrix and fluid phase in the REV, separately. The final macroscopic governing equation is derived on the basis of the microscopic equations.

The solid phase energy equation is:

$$\frac{\partial T_s}{\partial t} = \alpha_s \nabla^2 T_s \tag{3.13}$$

where α_s is the thermal diffusivity of the solid phase (m^2/s)

The fluid phase energy equation is:

$$\frac{\partial T_f}{\partial t} + (\nabla \cdot \mathbf{u}T)_f = \alpha_f (\nabla \cdot \nabla T)_f \tag{3.14}$$

where α_f is the thermal diffusivity of fluid phase (m^2/s)

The boundary conditions at the interface face A_{fs} are:

$$\mathbf{n}_{fs} \cdot k_f \nabla T_f = \mathbf{n}_{fs} \cdot k_s \nabla T_s \tag{3.15}$$

$$T_s = T_f \tag{3.16}$$

where $\mathbf{n}_{fs}$ Normal unit vector at the interface:

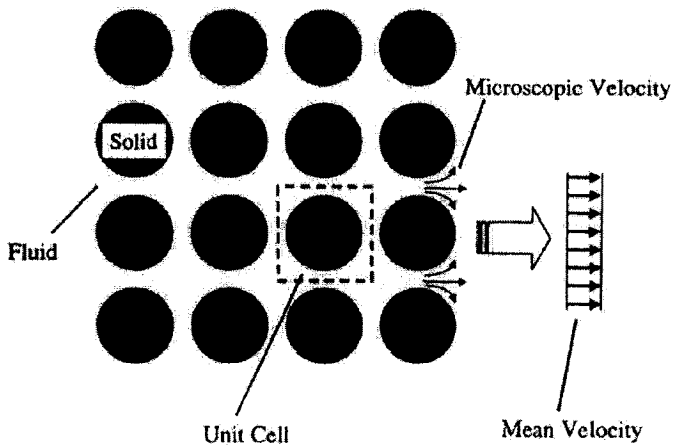

Fig 3.1: Microscopic velocity for periodic porous media (Hsiao and Advani, 2002)

Concerning the pore-level airflow, the fluctuation of velocity and temperature distribution from the volume average value exists (illustrated in Fig 3.1) because of the interaction of solid phase and liquid phase. To include this effect, we define:

$$T_f' = T_f - \langle T \rangle$$

$$\mathbf{u}' = \mathbf{u} - \langle \mathbf{u} \rangle \tag{3.17}$$

Using these definitions and considering the boundary conditions at the interface, the overall fluid-solid energy equation based on the volume average method can be derived as follows (Kaviany, 1999):

$$[\varepsilon(\rho c_p)_f + (1-\varepsilon)(\rho c_p)_s]\frac{\partial T}{\partial t} + (\rho c_p)_f \mathbf{u}\cdot\nabla T = [\varepsilon k_f + (1-\varepsilon)k_s]\nabla\cdot\nabla T$$
$$+\frac{k_f - k_s}{V}\int_{A_{fs}} T_f' \mathbf{n}_{fs} dA + (\rho c_p)_f \nabla\cdot\mathbf{u}' T_f' \tag{3.18}$$

Because the difference between thermal conductivity of solid phase and gas phase (air) in this study is not high, the second term on the right side, which is the influence of temperature deviation, can be omitted. However, the third term, which is the effect of the velocity nonuniformity, should be taken into account and it represents the microscopic effect in the overall macroscopic equation. In the product level, the concept of thermal dispersion is generally used and it is represented by a thermal dispersion coefficient k_d on the basis of the following relationship

$$\mathbf{u}' T_f' = k_d \nabla T \tag{3.19}$$

Thus the final governing equation is as follows

$$[\varepsilon(\rho c_p)_f + (1-\varepsilon)(\rho c_p)_s]\frac{\partial T}{\partial t} + (\rho c_p)_f \mathbf{u}\cdot\nabla T = [\varepsilon k_f + (1-\varepsilon)k_s]\nabla\cdot\nabla T + k_d \nabla T \tag{3.20}$$

Determining the thermal dispersion coefficient k_d, which includes the microscopic effect in the macroscopic equation, is an important topic in heat and mass transfer in porous media. Research on this topic is currently active. Considering that the turbulent flow is also due to the velocity nonuniformity, many researchers regard that thermal dispersion has similarity with turbulent flow. Based on this observation, various theoretical models have been developed. For example, to analyze the steep temperature gradient near the wall observed in the forced convection for a packed bed, Cheng and Hsu (1986)

introduced a dimensionless dispersion length represented by a wall function into the modeling of the thermal dispersion conductivity.

However, these theoretical models are still under development and need validation. Experimental relations are more frequently used. For fibrous material, Koch and Brady (1986) suggested that it can be represented as:

$$k_d = \frac{\lambda\sqrt{K}|\mathbf{u}|}{\ln(\frac{1}{1-\varepsilon})} \tag{3.21}$$

In which coefficient λ is:

$$\lambda_x = \frac{57\pi^3}{160} \qquad \lambda_y = \frac{3\pi^3}{320} \tag{3.22}$$

Equation (3.20) is different with the model by Buchanan and Sherman (2000): (1) the influence of dispersion is considered; (2) the influence of pressure variation on the heat transfer, which is generally not considered in heat transfer problem, is not included in the current model.

3.4 Solution method

3.4.1 Pressure correction in the simulation

As the Boussinesq approximation is assumed, the problem is treated as an incompressible flow. The solution method of incompressible flow can be either the vorticity-stream function method or the primitive-variable approach.

Compared with the primitive-variable method, the vorticity-stream function is easier to implement. In this approach, the stream function and vorticity are defined as follows:

$$u = \frac{\partial \psi}{\partial y} \qquad v = -\frac{\partial \psi}{\partial x} \qquad \omega = \frac{\partial u}{\partial y} - \frac{\partial v}{\partial x} \tag{3.23}$$

Using the stream function and vorticity, combining with the following transformation:

$$X = \frac{x}{L} \qquad Y = \frac{y}{L} \qquad \overline{u} = \frac{u}{V_i} \qquad \overline{v} = \frac{v}{V_i}$$

$$\overline{\psi} = \frac{\psi}{V_i L} \qquad \overline{\omega} = \frac{\omega L}{V_i} \qquad \tau = \frac{tV_i}{L} \qquad \theta = \frac{T - T_o}{T_i - T_o}$$

where V_i- Reference velocity at inlet (m/s)

L - The thickness of the building envelope (m)

T_i - The temperature at the indoor side (K)

T_o - The temperature at the outdoor side (K)

The control equations used in this study can be changed into non-dimensional form as follows:

$$\varepsilon \frac{\partial \overline{\omega}}{\partial \tau} + \overline{u} \frac{\partial \overline{\omega}}{\partial X} + \overline{v} \frac{\partial \overline{\omega}}{\partial Y} = \frac{\varepsilon^2 Ra}{Re^2 Pr} \frac{\partial \theta}{\partial X} - \frac{\varepsilon^2 \overline{\omega}}{DaRe} \tag{3.24}$$

$$\nabla^2 \overline{\psi} = -\overline{\omega} \tag{3.25}$$

$$\sigma\frac{\partial\theta}{\partial\tau}+\bar{u}\frac{\partial\theta}{\partial X}+\bar{v}\frac{\partial\theta}{\partial Y}=\frac{1}{Pe}\nabla\cdot(\frac{k_e}{k_f}+\varepsilon\frac{D_f^d}{\alpha_f})\cdot\nabla\theta \tag{3.26}$$

where Da - Darcy number $Da = K / L^2$

Ra - Raleigh number $Ra = \frac{g\beta\Delta TL^3}{\alpha\nu}$

Re - Reynolds number $\mathrm{Re} = \frac{V_i L}{\nu}$

Pr Prandtl number $\mathrm{Pr} = \frac{\nu}{\alpha}$

Pe - Peclet number $Pe = \frac{V_i L}{\alpha}$

σ - Heat capacity ratio $\sigma = [(1-\varepsilon)(\rho C_p)_s + \varepsilon(\rho C_p)_a]/(\rho C_p)_a$

These coupled non-dimensional equations can be solved simultaneously. The detailed procedure is as follows:

(1) Giving a time increment and assuming a temperature distribution. According to this assumed distribution, solve the vorticity equation (3.24) to get the values of vorticity ω.

(2) Based on this ω value, by solving the stream function equation (3.25), ψ value can be obtained and velocity can be determined.

(3) Using the known velocity, energy equation (3.26) is solved to get a new temperature distribution.

(4) Check convergence according to the difference of temperature between step (1) and that obtained in step (3). If convergence condition is satisfied, go to next time step, otherwise, go to step (1).

(5) Simulation continues until reaching to the steady state.

The vorticity-stream function approach is easy for the implementation, concerning its automatically satisfying the continuity condition. However, it is not easy to deal with the boundary conditions, as the physical meaning of stream function and vorticity is abstract, especially for vorticity. Approximate treatment is usually adopted in this approach, for example, for the points of non-slipping condition, such as on the bottom and the top, its vorticity is represented by:

$$\overline{\omega}_L = \frac{2*(\overline{\psi}_L - \overline{\psi}_{L\pm1})}{\Delta x^2} \tag{3.27}$$

There is an inconsistence of second and first order derivative in this equation and hence will induce additional error. However, it is pointed out that if higher order derivative is applied, the iteration process will be unstable.

Meanwhile, in the vorcitity-steam function approach, there is no direct relation between the pressure and velocity, thus it is not easy to include the influence of pressure. As the pressure gradient is the direct driving force for air flow in the current model, the limitation of this approach is obvious. Moreover, if the model is extended to the multiple layer structure, the boundary condition in the interface points is very difficult to deal with for the vorticy-stream function method. On account of these, the primitive-variable approach is adopted in the solution process.

In the primitive-variable approach, the SIMPLE (Patankar, 1980) family methods are generally used. In this kind of method, the procedure is based on a cyclic series of trail-

and-error operations to solve the governing equations. The velocity components are first calculated from the momentum equations by assuming a pressure field. The pressures and velocities are then corrected, so as to satisfy continuity equation. This procedure continues until the solution converges. SIMPLE and its families, i.e. modifications developed for SIMPLE method, are widely used in numerical simulation of heat and fluid flow. Currently, the SIMPLE family method has become the most common approach in computational fluid dynamics and numerical heat transfer. As a matter of fact, most of the commercial CFD software packages, such as FLUENT and STAR-CD, are developed on these methods. In the literature on heat and mass transfer in porous media, for example, Chen and Liu (2004), the SIMPLE family method is frequently seen.

Though most of the widely used CFD commercial software packages are based on the fundamental principle of the SIMPLE algorithm, it is not a good idea to treat them as black-box tools. On the contrary, it is necessary to study the detailed phenomena in the model used and discuss the more suitable approach. Actually, beside the SIMPLE family methods, other pressure-correction approaches are also adopted by investigators in the study of heat transfer phenomenon in porous media. For example, the MacCormack scheme (Merrikh and Mohamad 2002), uses a different procedure to achieve pressure and velocity corrections.

When it comes to the current model, by scaling analysis, we can find that the Darcy's item, which has a factor of $\frac{\mu}{K}$, takes a dominant role, because the viscosity is in the

magnitude of 10^{-5} and permeability is in the range of 10^{-8} or less, hence the magnitude of $\frac{\mu}{K}$ is 10^{3} or higher. This suggests adopting an easy implement approach.

The non-dimensional form of momentum equation in x- and y- direction according to equation (3.24) is as follows:

$$\varepsilon\frac{\partial\overline{u}}{\partial\tau}+\overline{u}\frac{\partial\overline{u}}{\partial X}+\overline{v}\frac{\partial\overline{u}}{\partial Y}=-\varepsilon\frac{\partial\overline{p}}{\partial X}-\frac{\varepsilon}{Da\,\mathrm{Re}}\overline{u} \tag{3.28}$$

$$\varepsilon\frac{\partial\overline{v}}{\partial\tau}+\overline{u}\frac{\partial\overline{v}}{\partial X}+\overline{v}\frac{\partial\overline{v}}{\partial Y}=-\varepsilon\frac{\partial\overline{p}}{\partial Y}-\frac{\varepsilon}{Da\,\mathrm{Re}}\overline{v}+\frac{\varepsilon Ra\,\mathrm{Pr}}{Pe^{2}}\theta \tag{3.29}$$

Rearrange these two equations in the following form:

$$\frac{\partial\overline{p}}{\partial X}=F(\overline{u},\overline{v}) \tag{3.30}$$

$$\frac{\partial\overline{p}}{\partial Y}=G(\overline{u},\overline{v}) \tag{3.31}$$

We can get the following Poisson equation:

$$\frac{\partial^{2}\overline{p}}{\partial X^{2}}+\frac{\partial^{2}\overline{P}}{\partial Y^{2}}=\frac{\partial F}{\partial X}+\frac{\partial G}{\partial Y} \tag{3.32}$$

That means assuming a pressure distribution, an estimated velocity at new time step can be obtained from the initial condition. After that, the correction of pressure can be carried out according to equation (3.22). This process continues until obtaining the convergence solution.

As the continuity equation is not directly solved by using the above method, it is found that the continuity condition is not satisfied in the solution process. In the actual

calculation, to assure the continuity condition, the following prediction-correction method is presented for unsteady flow in vertical channel (Saha, 2000):

$$\frac{\partial^2 \overline{p}'}{\partial X^2} + \frac{\partial^2 \overline{p}'}{\partial Y^2} = \frac{\partial \overline{u}^*}{\partial X} + \frac{\partial \overline{v}^*}{\partial Y} \tag{3.33}$$

In which u^* is the predicted velocity obtained by explicitly solving the following N-S equation:

$$\frac{\partial u_i}{\partial t} = G(u_i, u_j) - \frac{\partial p}{\partial x_i} \tag{3.34}$$

i, j- x, y directions.

The relation of pressure and velocity is given as:

$$\overline{p}^{n+1} = \overline{p}^n + \overline{p}' \tag{3.35}$$

$$\overline{u}_i^{n+1} = u_i^* + \frac{\delta t}{\delta X_i} \overline{p}' \tag{3.36}$$

In the current simulation, $\overline{u}^*$ and $\overline{v}^*$ are estimated velocity according to equation (3.28) and (3.29), using the following method:

$$\varepsilon \frac{\overline{u}^* - \overline{u}^n}{\Delta \tau} + \frac{\varepsilon}{Da\,\mathrm{Re}} \overline{u}^* = -\varepsilon \frac{\partial \overline{p}^n}{\partial X} - \overline{u}^n \frac{\Delta \overline{u}^n}{\Delta X} - \overline{v}^n \frac{\Delta \overline{u}^n}{\Delta Y} \tag{3.37}$$

$$\varepsilon \frac{\overline{v}^* - \overline{v}^n}{\Delta \tau} + \frac{\varepsilon}{Da\,\mathrm{Re}} \overline{v}^* = -\varepsilon \frac{\partial \overline{p}^n}{\partial Y} + \frac{\varepsilon Ra\,\mathrm{Pr}}{Pe^2} \theta^n - \overline{u}^n \frac{\Delta \overline{v}^n}{\Delta X} - \overline{v}^n \frac{\Delta \overline{v}^n}{\Delta Y} \tag{3.38}$$

The above equations can also be written as:

$$\left(\frac{1}{\Delta \tau} + \frac{1}{Da\,\mathrm{Re}}\right) \overline{u}^* - \frac{\overline{u}^n}{\Delta \tau} = F(\overline{u}^n, \overline{v}^n) - \frac{\partial \overline{p}^n}{\partial X} \tag{3.39}$$

$$\left(\frac{1}{\Delta \tau} + \frac{1}{Da\,\mathrm{Re}}\right) \overline{v}^* - \frac{\overline{v}^n}{\Delta \tau} = G(\overline{u}^n, \overline{v}^n) - \frac{\partial \overline{p}^n}{\partial Y} \tag{3.40}$$

Therefore relation in equation (3.33) is modified as follows in the numerical process of this study:

$$\frac{\partial^2 \overline{p}'}{\partial X^2} + \frac{\partial^2 \overline{p}'}{\partial Y^2} = \left(\frac{1}{\Delta \tau} + \frac{1}{Da\,\mathrm{Re}}\right)\frac{\partial \overline{u}^*}{\partial X} + \frac{\partial \overline{v}^*}{\partial Y} \tag{3.41}$$

3.4.2. Differencing scheme

The equations are solved using finite difference approach. To avoid the pressure oscillation in the simulation process, staggered grid is applied. A typical calculation element is shown in Fig 3.2. Velocity **u** and **v** are stored in the boundary nodes whereas pressure and temperature values are stored in the central nodes.

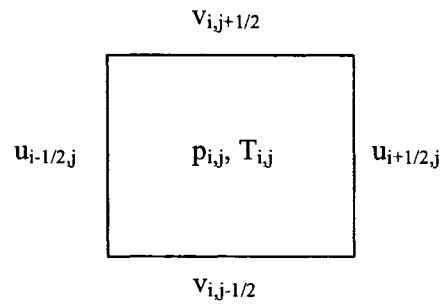

Fig 3.2: Calculation cell

In the simulation, a uniform mesh is applied on each coordination direction. For the diffusion term, central difference is used for variable ϕ as follows:

$$\frac{\partial^2 \phi}{\partial x^2} = \frac{\phi_{i+1,j} - 2\phi_{i,j} + \phi_{i-1,j}}{\Delta x^2} \qquad \frac{\partial^2 \phi}{\partial y^2} = \frac{\phi_{i,j+1} - 2\phi_{i,j} + \phi_{i,j-1}}{\Delta y^2} \tag{3.42}$$

For the convective term, upwind scheme is adopted for variable θ in equation (3.29) as follows (variable is also represented using ϕ):

$$\frac{\partial \phi}{\partial x} = \frac{\phi_{i,j} - \phi_{i-1,j}}{\Delta x} \quad if \quad u \succ 0 \qquad \frac{\partial \phi}{\partial x} = \frac{\phi_{i+1,j} - \phi_{i,j}}{\Delta x} \quad if \quad u \prec 0$$

$$\frac{\partial \phi}{\partial y} = \frac{\phi_{i,j} - \phi_{i,j-1}}{\Delta y} \quad if \quad v \succ 0 \qquad \frac{\partial \phi}{\partial y} = \frac{\phi_{i,j+1} - \phi_{i,j}}{\Delta y} \quad if \quad v \prec 0 \tag{3.43}$$

Whereas central difference is used for variable θ in left hand of equation (3.29):

$$\frac{\partial \theta}{\partial x} = \frac{\theta_{i+1,j} - \theta_{i-1,j}}{2\Delta x} \qquad \frac{\partial \theta}{\partial y} = \frac{\theta_{i,j+1} - \theta_{i,j-1}}{2\Delta y} \tag{3.44}$$

As Darcy's term dominates the momentum equation, explicit scheme is applied for the solution of momentum equation to assure higher accuracy. However, for the energy conservation equation, to avoid the oscillation in the solution process, an implicit scheme is employed. Therefore, the following equation of implicit scheme needs to be solved:

$$A\Phi = B_j \tag{3.45}$$

A- The coefficient matrix

B_j - The source term matrix

The variables of vector Φ are unknown and need to be solved simultaneously. To solve the equations, a direct method or an iteration method can be used. In the direct method, sweeping is performed to every column or row, or column and row alternatively, i.e. Alternative Direction Implicit (ADI) method. In each sweep, a TDMA algorithm is used to obtain the value for each node. Compared with this method, iteration method is easier to implement, and in the numerical simulation of natural convection in a rectangular cavity, the computing time needed is about the same order of magnitude (Wang and Rathby, 1979). Thus iteration method is adopted here using the normally used form of

Gauss-Seidel and successive over-relaxation (SOR). For each direction, the following discretization equation in point P can be obtained after rearrangement of variables

$$a_P\phi_P = a_E\phi_E + a_W\phi_W + a_N\phi_N + a_S\phi_S + b \tag{3.46}$$

By applying SOR method, n-th iteration is carried out as

$$\phi_P^{(n)} = \phi_P^{(n-1)} + \alpha[\frac{a_N\phi_N^{(n)} + a_S\phi_S^{(n)} + a_E\phi_E^{(n-1)} + a_W\phi_W^{(n)} + b}{a_P} - \phi_P^{(n-1)}] \tag{3.47}$$

α - Relaxation coefficient

b - Source term

Subscripts N, S, E, and W represent north, south, east and west points, respectively

3.5 Boundary conditions

Setting up the governing equations is only one step for the model. To obtain the meaningful solutions, boundary conditions are very important and must be determined in advance. As the model is a coupled problem of airflow and heat transfer, boundary conditions must be provided for the temperature, velocity and pressure.

3.5.1 Temperature boundary conditions

At the boundary inside the room, the temperature on the boundary is satisfied with the convective boundary condition:

$$-k\frac{\partial T}{\partial x} = h_{in}(T_{wi} - T_i) \tag{3.48}$$

T_{wi} - Temperature on the interior surface of the building envelope (K)

T_i - Bulk temperature inside the room (K)

h_{in} - Convective heat transfer coefficient inside the room (W/m^{2}K)

According to ASHRAE (1993), the convective coefficient is adopted as follow:

$$h_{in} = 1.87(\Delta T)^{0.32} H^{0.05} \tag{3.49}$$

H - The height of the wall (m)

ΔT - The indoor and outdoor temperature difference (K)

At the outside surface, the boundary condition is set up as:

$$-k\frac{\partial T}{\partial x} = \alpha_{sol} I_t + h_r (T_{air} - T_{bo}) + h_{cout} (T_o - T_{bo}) \tag{3.50}$$

α_{sol} - The surface solar-absorption coefficient (-)

I_t - The solar radiation flux normal to the surface (W/m^2)

T_o - The outdoor air temperature (K)

T_{bo} - The outdoor surface temperature (K)

h_r - The radiative heat transfer coefficient (W/m^{2}K):

$$h_r = \varepsilon_s \sigma_s (T_{air}^2 + T_{bo}^2)(T_{air} + T_{bo}) \tag{3.51}$$

ε_s - The surface emissivity (-)

σ_s - The Stephan-Boltzman constant 5.67×10^{-8}

h_{cout} - The convective heat transfer coefficient at outdoor side (W/m^{2}K)

Generally, h_{cout} is represented as a function of wind velocity. However, according to the measured data by Jayamaha et al (1996), it is about 6-10 W/m^{2}K.

The top and bottom are assumed to be adiabatic.

3.5.2 Velocity and pressure boundary condition

To determine the velocity boundary condition for the inlet and outlet, we need first to determine the location of the inlet and outlet. This configuration is important for the calculation because it will greatly affect the infiltration path, which is believed to have a significant influence on the heat exchange performance in the building envelope. However, considering air infiltration, there are great uncertainties in determining the position of the inlet and outlet. This problem brings the difficulty in dealing with the velocity boundary condition. However, the simulation results of Buchanan and Sherman (2000) and Abadie et al (2002) show that the phenomenon of heat exchange in the building envelope mainly happens in the area near the inlet and outlet. In other parts of the wall, its influence is negligible. Based on this, the whole envelope is divided into the area affected by leaking air and that not affected by leaking air in the simplified model developed by Buchanan and Sherman (2000). This means that heat exchange in the building envelope by air infiltration is a kind of local phenomenon. Thus we only need to focus on the zone of inlet and outlet in our simulation, and use different configurations to include the effect of uncertainties of the inlet and outlet locations. For example, in the

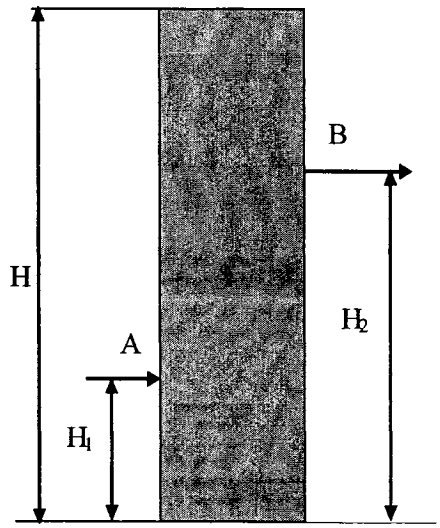

Fig 3.3: Boundary condition for calculation

model developed by Buchanan and Sherman (2000), several kinds of configurations for inlet and outlet are presented. Abadie et al (2002) considered three different configurations: straight through cracks (ST), low inlet/high outlet (LH) and high inlet/low outlet (HL). Following this approach, the influence of infiltration path can be included.

Upon the above analysis, the following boundary is used in the simulation model: air enters the building envelope at location A (Fig 3.3). The velocity of other points except the crack point at the left border is equal to zero. The bottom and top are assumed to be using an air barrier material and the non-slip boundary condition is valid. Similar to the inlet side, air is assumed to come into the room through location B. Velocity in this place is determined by mass conservation while velocity of other points on the right border is zero.

Corresponding with the above velocity, the following boundary conditions at the wall surface for p' is used in the simulation:

$$\frac{\partial \overline{p}'}{\partial n} = 0 \tag{3.52}$$

3.6 Summary

Based on the analysis of the specific condition in the building envelope, a numerical model is presented for the heat exchange phenomenon in the envelope. Details of the model include:

1. Darcy's model is adopted.

2. The influences of inertia, gravity and buoyancy are considered in the momentum equation.
3. By setting up the energy conservation for the solid matrix and gas phase, the one media macroscopic energy equation is derived from the microscopic point of view. The closure problem induced by volume average is solved by using a dispersion coefficient.
4. An easy to implement method is presented for the solution of the governing equations.
5. The velocity and pressure boundary is set up according to the flow condition.
6. A convective boundary condition is adopted for both the interior and the exterior side of the building envelope for the energy conservation equation.

Chapter 4 Simulation results and model verification

4.1 Simulation inputs and wall configurations

The developed numerical model is applied to study the heat exchange performance of a conventional exterior wall, to analyze the impact of heat exchange process in the building envelope to the energy consumption of buildings, and to find out the key influencing factors. A 0.2m thick and 2m high wall is considered in the study. Convergence criteria in the simulation are set to 10^{-6}. To obtain results that do not depend on the grid, several kinds of mesh were tried, i.e. 100×500, 100×1000, 200×500. According to the result, a 100×500 mesh is fine enough to get the grid-independent solution and is adopted in the simulation of all cases in this study.

The non-dimensional parameters in the control equation (3.24) to (3.26) are necessary for the solution. These parameters are determined by the properties of air and building materials. In the current simulation, these properties are assumed constant. Table 4.1 shows the values used in the simulation.

Table 4.1 Constant parameters in the simulation

Symbol	Meaning	Unit	Value
ρ_a	Density of the air	kg/m^3	1.0
C_{pa}	Heat capacity of the air	J/kg K	1000
k_a	Thermal conductivity of the air	W/m K	0.026
μ	Dynamic viscosity of the air	kg/m s	1.8×10^{-5}
ρ_s	Density of solid matrix	kg/m^3	70
C_{ps}	Heat capacity of solid matrix	J/kg K	1000
k_s	Thermal conductivity of solid matrix	W/m K	0.05
ε	Porosity	-	0.5, 0.8, 0.9
K	Permeability of the porous medium	m^2	1.0×10^{-9}
β	Expansion coefficient	1/K	3.95×10^{-3}

To discuss the influence of infiltration length, four kinds of infiltration configuration, i.e. different places of inlet and outlet arrangement, are adopted in the simulation. These configurations are illustrated in Fig 4.1.

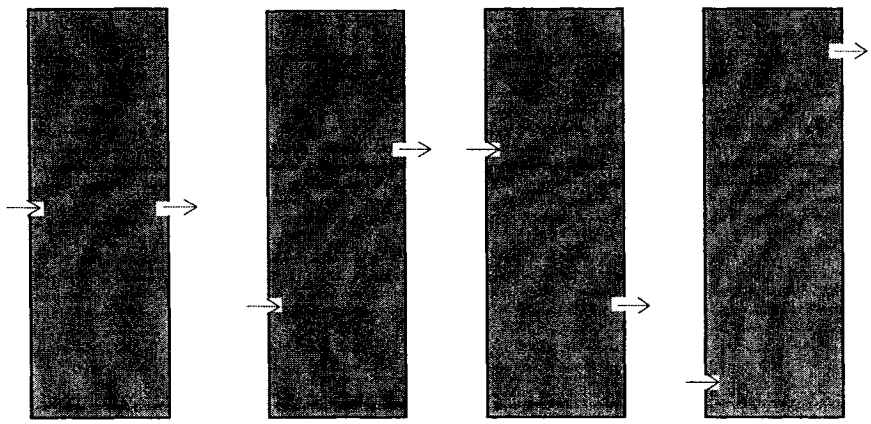

Fig 4.1: Four kinds of infiltration path configuration

4.2 Simulation results

4.2.1 Temperature and velocity distribution

Fig 4.2 and Fig 4.3 show the temperature distribution in the wall under the condition that inside and outside temperature is 20°C and 0°C respectively, and the inlet velocity is 0.1m/s. From the simulation result, for example, configuration A, it is found that without air infiltration, the average temperature outside and inside is 0.087°C and 19.65°C separately. Considering the influence of infiltration, the average temperatures change to 0.081°C and 19.62°C. From the temperature distribution, we can see that heat exchange in the exterior wall mainly occurs at the inlet and outlet vicinity area. In the area near the inlet and outlet locations, the temperature distribution changes from conduction, and has a "tilt" contour line. However, for most of the wall, the influence of heat exchange can be neglected. According to this observation, we can divide the whole wall into areas affected

and not affected by heat exchange phenomenon. The ratio of these areas will be an important factor to determine the heat exchange performance in the wall. Meanwhile, differences can be observed for straight through flow (configuration A) and configuration D. For the latter configuration, infiltration affected areas exist both near the inlet and outlet position, while the variation of temperature distribution is not as significant as that in configuration A. Besides, it can be seen that in this case, the influence of air infiltration to temperature in the wall in the vast area between inlet and outlet can be ignored. Therefore air flow in this configuration is called "diffused flow" (Claridge et al, 1995, Abadie et al 2002). It means that air vertically transfers from inlet to the outlet, with a slow and uniform velocity, induced by the pressure gradient between inlet and outlet.

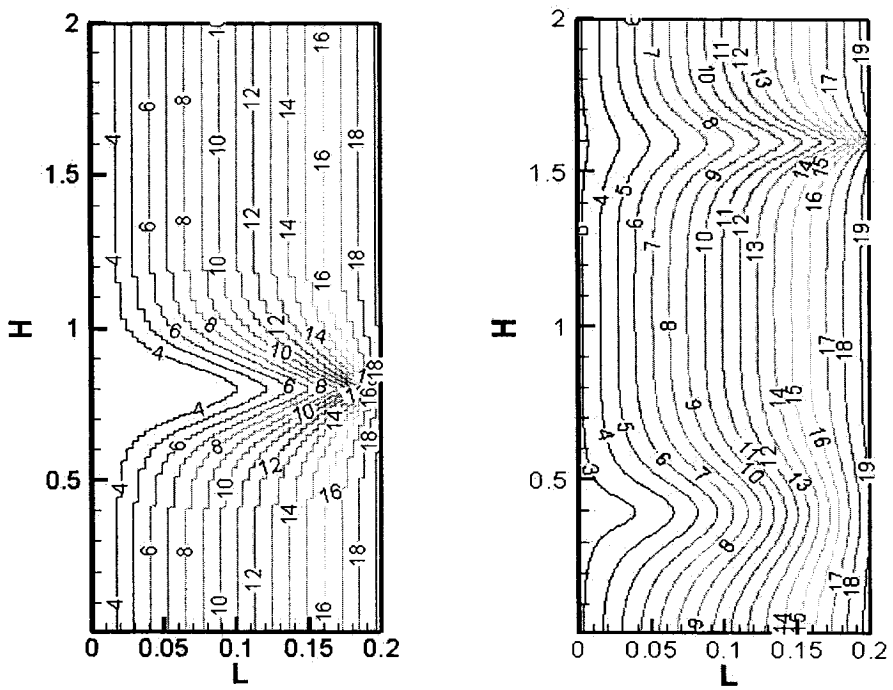

(a) Configuration A (b) Configuration D

Fig 4.2: Temperature distribution of configuration A and D

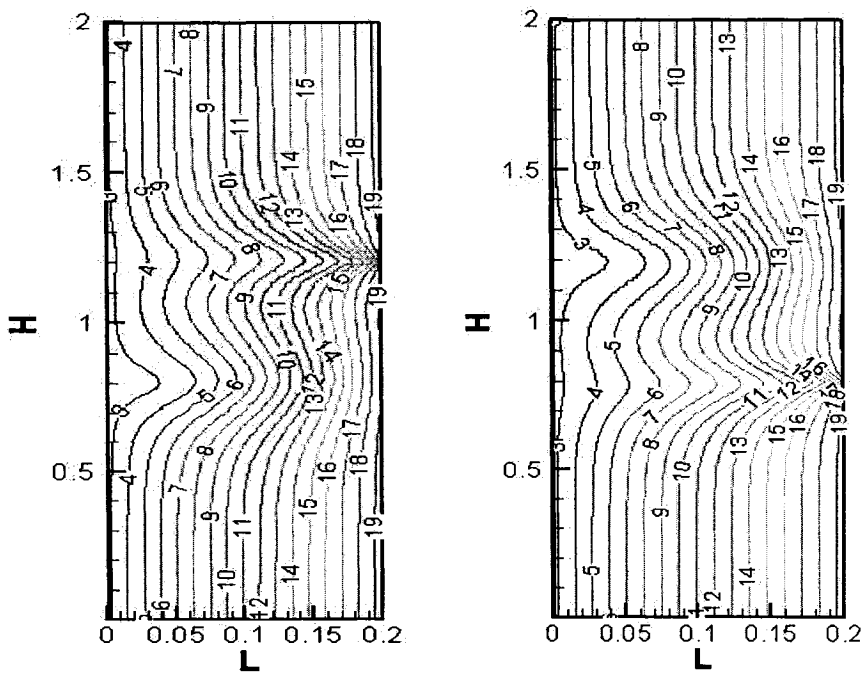

(a) Configuration B (b) Configuration C

Fig 4.3: Temperature distribution of configurations B and C

Fig 4.3 shows the temperature of configurations B and C to test the influence of low inlet/high outlet (LH) and high inlet/low outlet (HL) (Abadie et al, 2002). From the result, we can see that temperature distributions of these two conditions are almost symmetric except the differences at inlet and outlet positions. Thus whether it is low inlet/high outlet (LH) configuration, or high inlet/low outlet (HL) configuration, does not have significant influence on the heat exchange in the exterior building wall considered in this simulation. However, the influence of the vertical distance between inlet and outlet should be considered, as will be discussed later.

Fig 4.4 is the velocity vector corresponding with Fig 4.2. The figure also illustrates that in most parts of the wall, the air velocity is very slow. Therefore the heat exchange between the air and porous media is not significant. However, in the local zone near inlet and outlet locations, the influence of heat exchange process is obvious. At the same time, it can be found that though flow in the configuration D is called "diffused flow" in the literature, the similar condition exists in the configuration A. In this case, after a short distance from the inlet, the air flow in the infiltration area is slow and almost uniform, except in the places around the direct line connecting inlet and outlet.

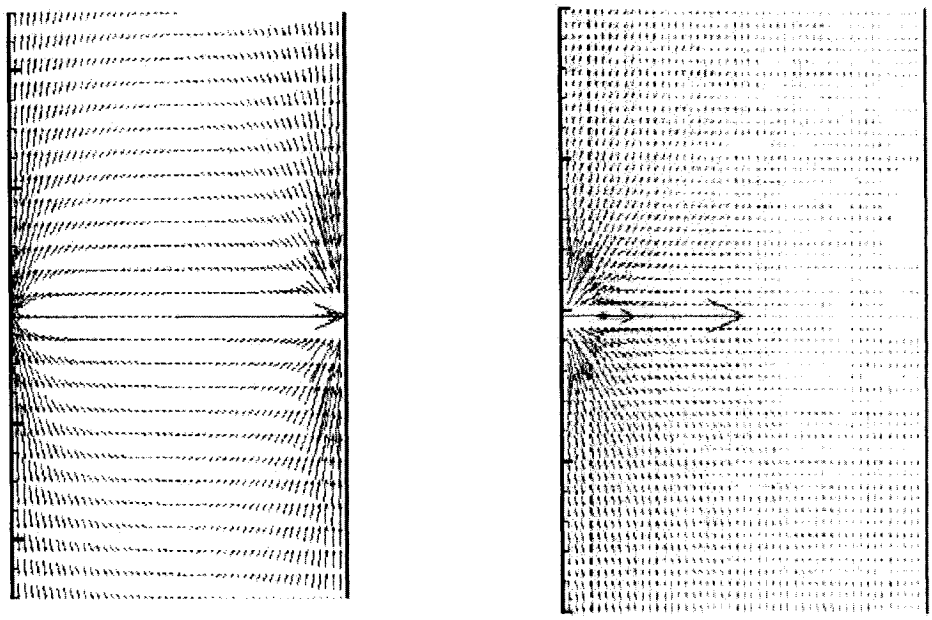

(a) Configuration A (b) Configuration D

Fig 4.4: Velocity vector at inlet locations

Fig 4.5 is the change of average temperature on the interior surface with the increase of inlet velocity. We can see that the interior surface temperature decreases as air velocity

increases. This will definitely mean a higher infiltration heat loss at the condition of higher airflow rate. Thus the airflow rate should be an appropriate value if we want to use this heat exchange phenomenon in the real building design. This result, as well as the heat flux increase at the outlet position, corresponds with the experimental results of dynamic insulated wall by Baker (2003).

From this figure, it can also be seen that the inlet velocity has the most important effect on the result; meanwhile, the infiltration path also affects the average interior surface temperature. The straight-through configuration has the smallest heat exchange area, thus the interior surface temperature is the highest. Comparatively, the average temperature is lower in the case of high inlet-low outlet and low inlet-high outlet structure, meaning that more heat exchange occurs inside the wall.

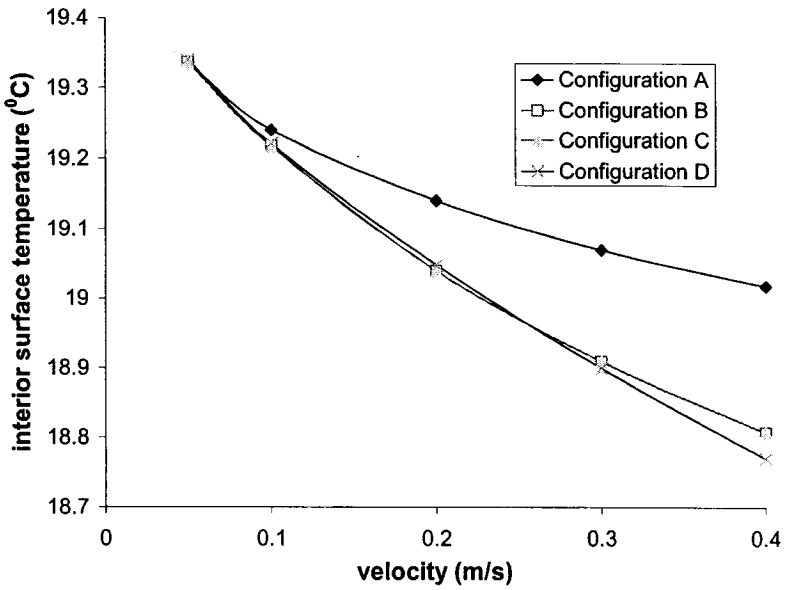

Fig 4.5: Change of average interior surface temperature with inlet velocity

4.2.2 Energy consumption

Fig 4.6 illustrates the *U*-value in the exterior surface. The simulation shows that at the exterior surface, the conductive heat loss decreases with the air velocity, influenced by the inward air flow. This comes from the fact that the temperature near the inlet approaches the outdoor temperature because of the air flow, and this tendency is the same with the theory of dynamic *U*-value (equation (2.12)) of dynamic insulation. However, this does not mean that the total heat loss decreases with the air flow rate. In fact, the higher air flow rate, the higher convective heat loss. As a matter of fact, influenced by the air infiltration, the *U*-value along the thickness of the wall is not constant. This can be found from the temperature profile in the wall (Fig 4.2, 4.3).

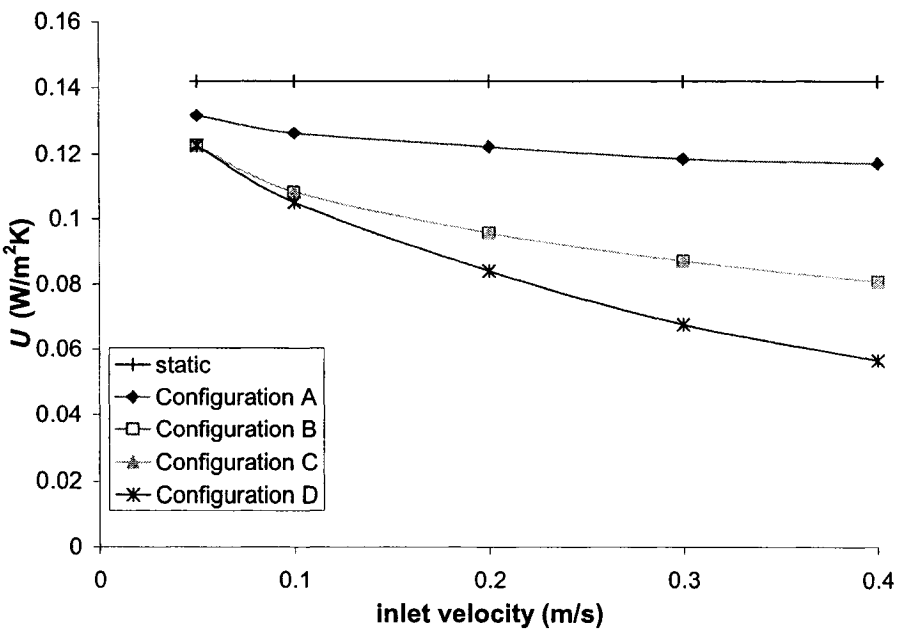

Fig 4.6: Conductive heat loss with velocity at exterior surface

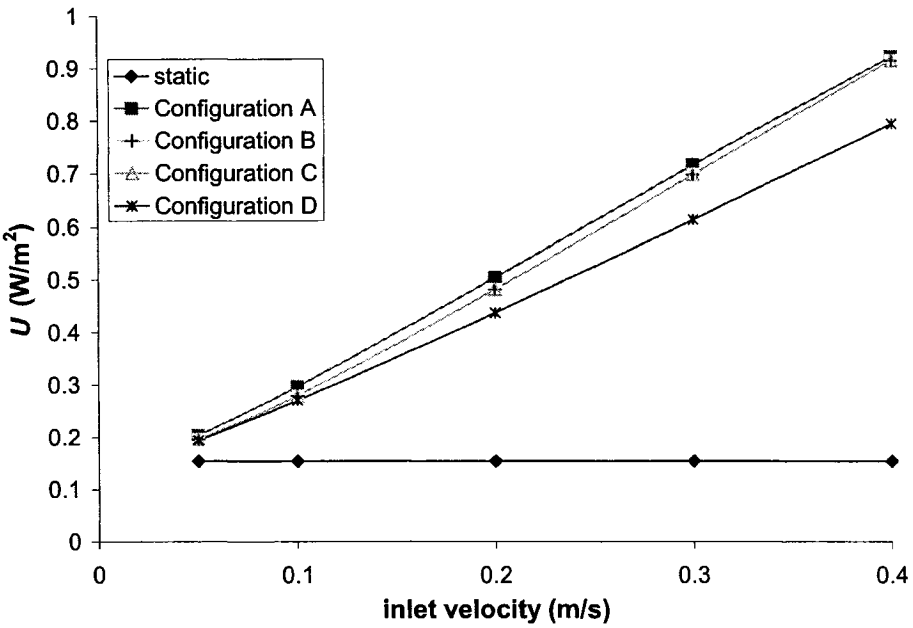

Fig 4.7: Relation of interior surface heat flux with inlet velocity

Fig 4.7 is the relation of *U*-value with the inlet velocity, in the interior surface of the wall. The results show that with the increase of inlet velocity, heat flux increases almost linearly, however, the increase rate is lower for the case of low inlet-high outlet and high inlet-low outlet configuration, especially case D, which has the longest infiltration path length.

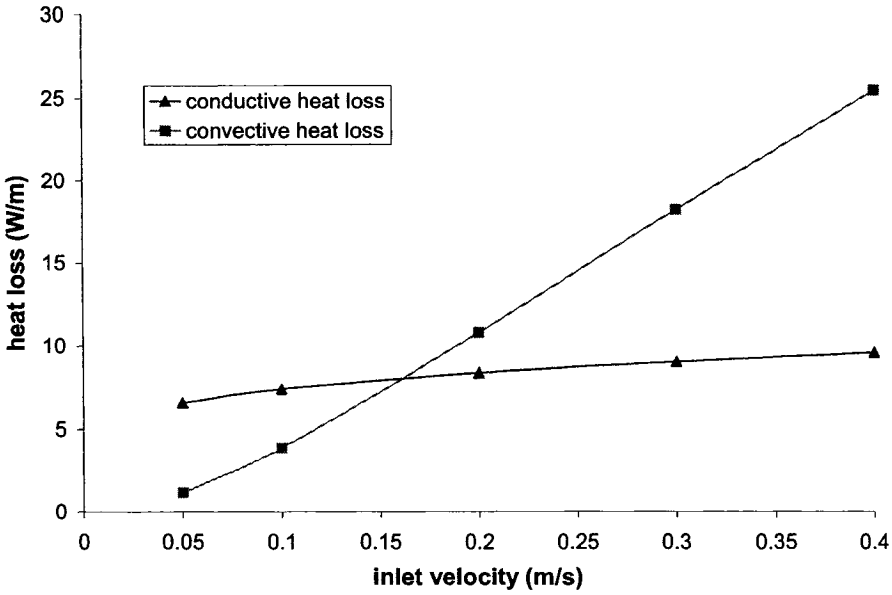

(a) Configuration A

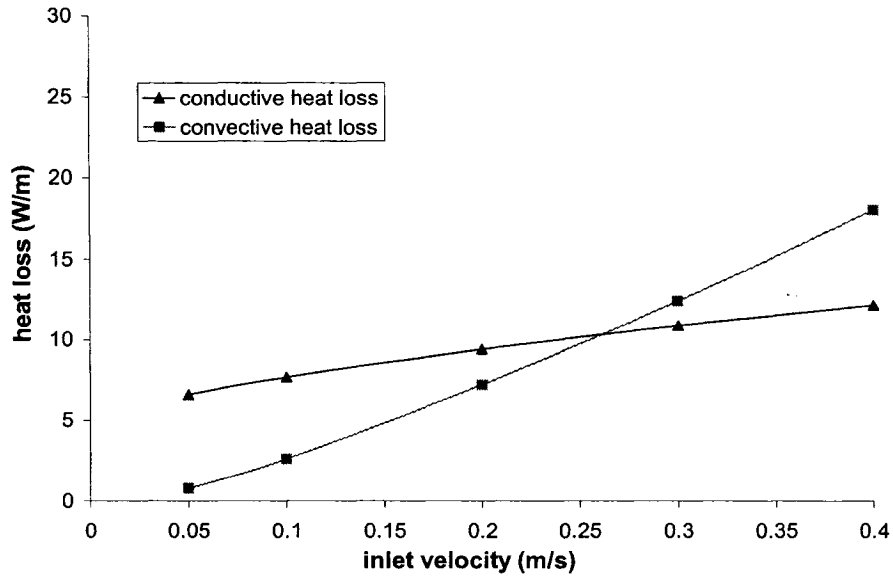

(b) Configuration D

Fig 4.8: Conductive and convective heat loss in the interior surface

Fig 4.8 illustrates the relation of interior surface conductive heat loss and convective heat loss with the inlet velocity, for configuration A and configuration D separately. It is shown that for the former case, the line representing the variation of conductive heat loss is almost flat, meaning that considering the heat transfer at interior surface, the air infiltration has little influence to the conductive heat loss for configuration A. Moreover, the convective heat loss increases dramatically with the air flow rate, as it is estimated by the conventional method. For the latter case, though the variation tendency is the same, the extent of variation is quite different. With the increase of air flow rate, the conductive loss changes from 6.6W/m to 12.1W/m. This is about twice that in configuration A, which is from 6.6W/m to 9.5W/m. Meanwhile, taking the advantage of heat exchange inside the wall, the variation of convective heat loss is not as dramatic as in the straight through configuration. At the highest air flow rate considered in the simulation, the convective heat loss under configuration D is only about 18.0 W/m, much less than that of configuration A, which is 25.4 W/m.

Fig 4.9 is the relationship of total energy reduction for the four wall configurations. From it, we can see that influenced by air infiltration, the total energy reduction reaches maximum value at an appropriate inlet velocity. At low velocity, though heat exchange efficiency is high, the amount of total heat reduction is low because of the absolute low value of the infiltration heat loss calculated by conventional approach. The curves in this figure also demonstrate that potential of energy reduction is the lowest for the configuration A.

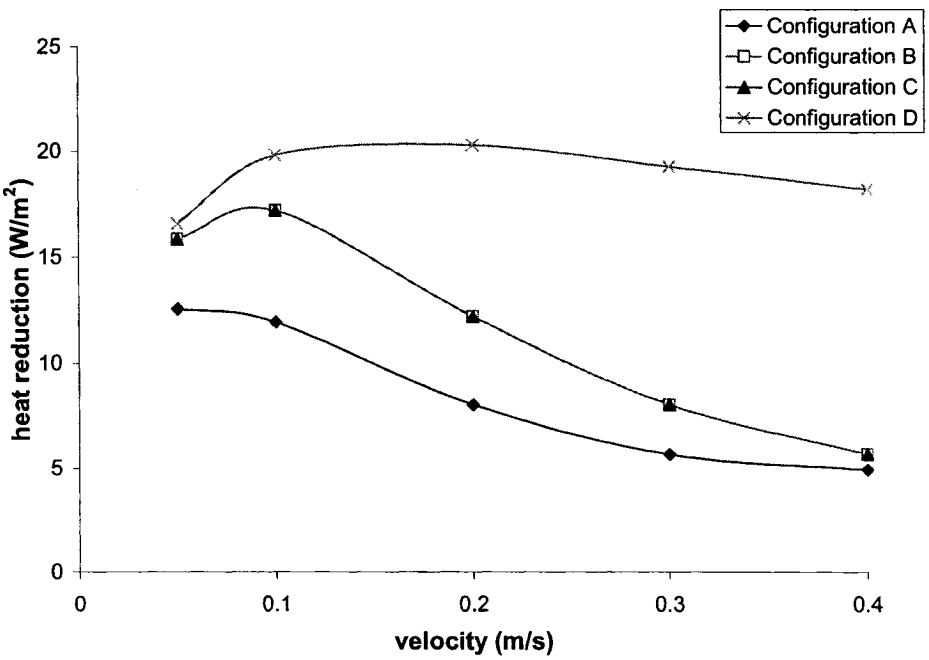

Fig 4.9: Total heat loss reduction with the inlet velocity

The infiltration heat exchange efficiency is calculated following the method by Buchanan and Sherman (2000). That is

$$\eta = 1 - \frac{Q_T - Q_0}{\dot{m} c_p \Delta T} \tag{4.1}$$

Q_T - The overall heat load (W)

Q_0 - The conduction heat load without infiltration (W)

Fig 4.10 illustrates the change of infiltration heat exchange efficiency (IHEE) with inlet velocity for the four configurations in the study. From the figure, we can also see that the

influence of heat exchange is significant when the infiltration rate is low and this effect decreases as infiltration rate increases. At a very low infiltration rate, the infiltration air is warmed almost to the room temperature in the exterior wall by the heat exchange phenomenon. The temperature distribution inside the wall is almost the same as that without infiltration. Thus the influence of infiltration to the energy consumption is very low. As inlet velocity increases, the influence of heat exchange decreases. At the higher infiltration rate, though the infiltration air can also be warmed, the temperature upon its entering the room decreases. Affected by the increased air flow rate and decreased incoming temperature to the room, the infiltration heat loss increases, and the infiltration heat exchange efficiency decreases.

From the figure, we can also find that the influence of energy consumption in the wall in infiltration path is significant. Comparatively, the configuration A has the least influence because the infiltration path is the shortest. In this case, IHEE is in the range of 0.05 to 0.3. Under most part of the inlet velocity range, IHEE value is below 0.1, thus the influence of heat exchange in the wall is limited for this kind of structure. However, if a low inlet-high outlet or high inlet-low outlet structure is adopted with a longer infiltration path, heat exchange inside the wall may have a significant influence to the thermal performance of the wall. For example, under configuration D, the influence is more significant as the infiltration path is much longer. The results in this figure once again show that the condition of low inlet/high outlet (LH) and high inlet/low outlet (HL) does not have significant influence as the curves of heat exchange coefficient for configuration B and configuration C are almost overlap.

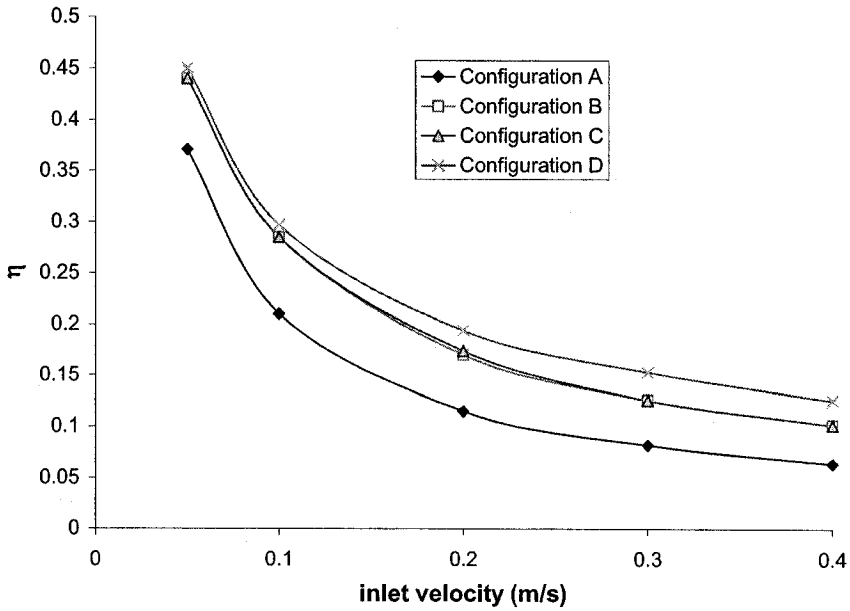

Fig 4.10: Change of IHEE with inlet velocity

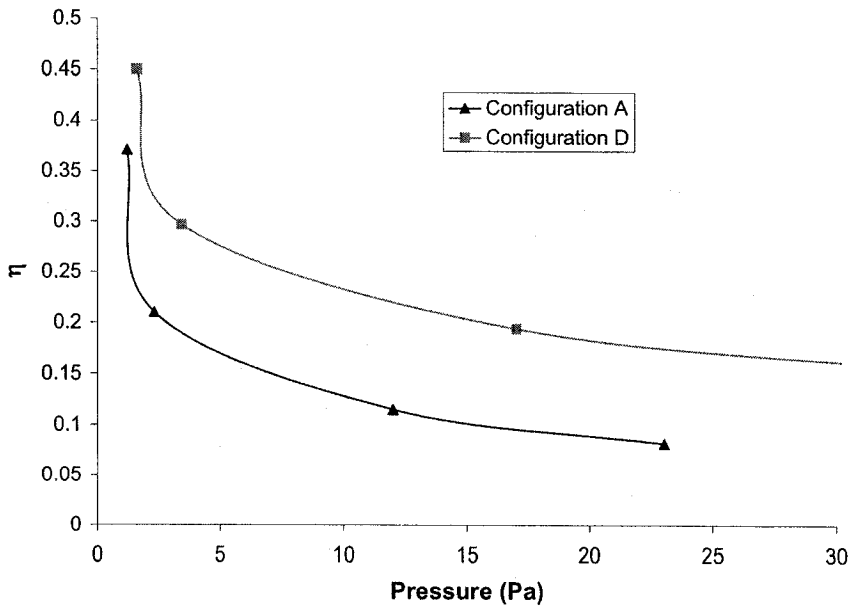

Fig 4.11: IHEE with pressure difference

Fig 4.11 is the relation of IHEE with the change of pressure difference between inlet and outlet position, for configuration A and D, respectively. It can be seen that IHEE decreases dramatically with the pressure gradient. Generally the pressure difference for residential building is less than 10Pa -15Pa. The results in this figure show that IHEE η changes obviously within this range. When pressure difference is greater than 15Pa, the variation of η is very small.

4.3 Parametric study of other influencing factors

From the above discussion, it is clear that the heat exchange performance in the building envelope is largely determined by the air flow rate through it, and the infiltration path length and configuration have secondary influences. In order to have a deeper and comprehensive understanding of this phenomenon, a parametric study is performed to consider the influence of other factors. Specific parameter variations in consideration include:

1. Variation of indoor and outdoor temperature;
2. Variation of porosity;
3. Variation of convective boundary condition.

4.3.1 Influence of indoor and outdoor temperature gradient

In the study, corresponding with the air conditioned room under typical weather conditions in winter and summer, two kinds of temperature differences between indoor

and outdoor are considered in the simulation, i.e. indoor temperature equaling 20°C, while the outdoor temperature being either 0°C or 30°C.

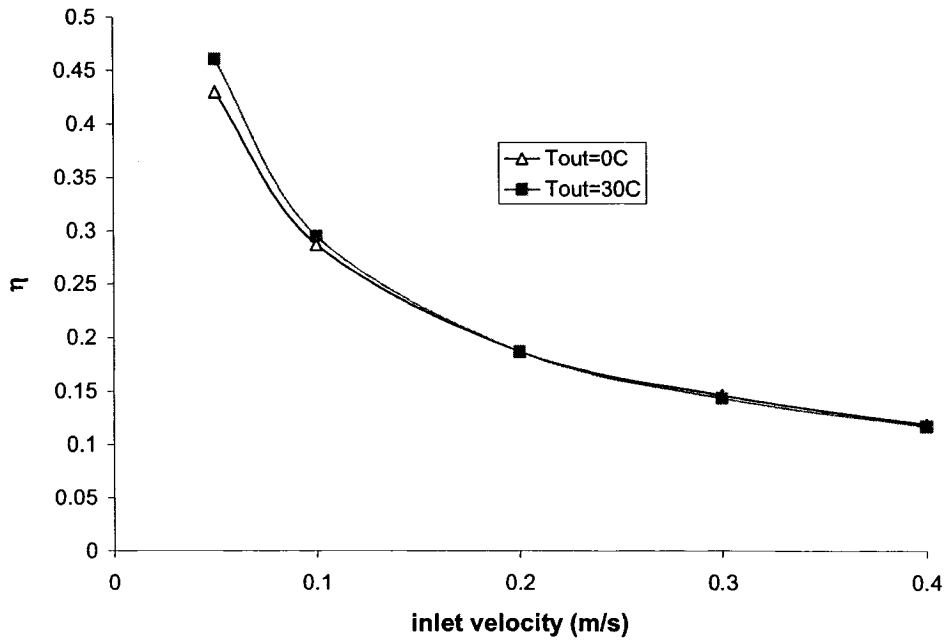

Fig 4.12: Change of infiltration heat exchange efficiency with infiltration rate under different indoor and outdoor temperature conditions

Fig 4.12 shows the relation of IHEE with air flow rate under these two conditions. From the result, we can see that the influence of the room and outside temperature difference to heat exchange performance is negligible. For the condition of the room temperature being 20°C, the heat exchange efficiency at the two conditions considered here is about the same. This means that the buoyancy does not have an obvious impact to the heat exchange performance for the structure here. This comes from two aspects. First, as the height of wall is only 2m, the air flow induced by the buoyancy is very slow. Second,

direction of air velocity induced by buoyancy is perpendicular to the heat flux direction in the wall; hence decreases its effect on the temperature distribution in the wall.

4.3.2 Influence of porosity

The second in the parameter study is to study the variation of porosity to the heat exchange performance in the wall. Three porosity values: 0.5, 0.8, and 0.9 have been applied in the simulation.

Fig 4.13 shows the relation of IHEE with air flow rate under three levels of material porosity. It can be seen that the porosity value has a limited influence on the heat exchange performance in the wall. For each configuration, under a certain air flow rate, the difference of IHEE under three porosities is less than 0.1.

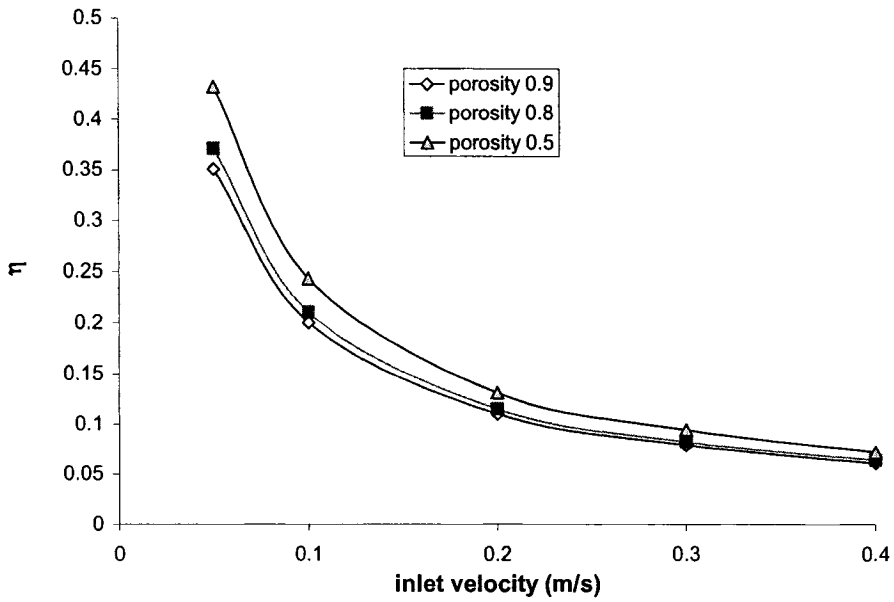

(a) Configuration A

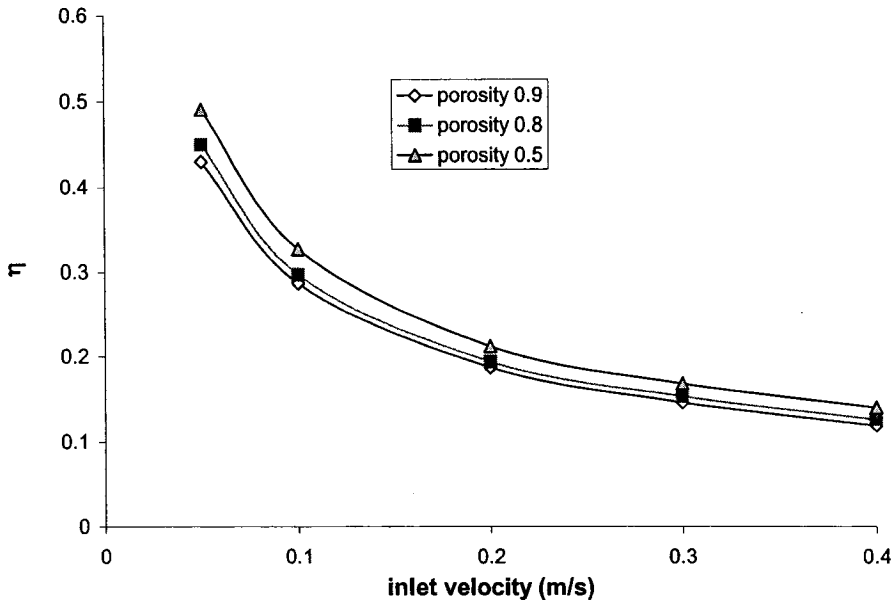

(b) Configuration D

Fig 4.13: Influence of porosity

The results demonstrate that for the condition of lower porosity, more solid matrix takes part in the heat exchange inside the wall, thus IHEE is higher. With the increase of porosity value, IHEE decreases because of the less amount of solid matrix in the material.

4.3.3 Influence of convective boundary condition coefficient

As the heat transfer in the wall is dominated by conduction, convective boundary condition at the interior and exterior surface will influence the temperature distribution in the wall. In the simulation, the exterior convective boundary coefficient condition is assumed a constant. To check the influence of the variation of this coefficient, three

values have been adopted in the parameter study: 6, 10, and 15 W/m^2K, respectively (Jayamaha et al, 1996).

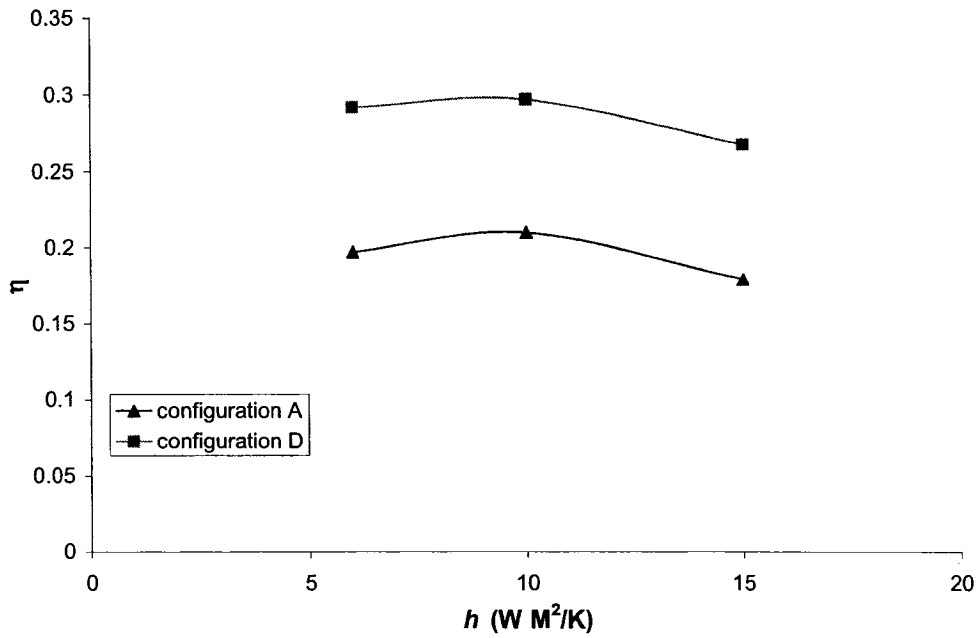

Fig 4.14: Influence of convective boundary condition coefficient

Fig 4.14 shows the relation of IHEE with different value of convective boundary condition. The results clearly show that within the given range, the variation of IHEE is less than 0.02, thus influence of convective boundary coefficient is negligible. This means that the exterior convective heat transfer coefficient has limited influence on the heat exchange efficiency. This corresponds with the investigations results concerning the influence of air film to the thermal performance of dynamic insulation by Taylor and Imbabi (1997), which states that in the assessment of heat loss through dynamic

insulation over the static equivalent, the influence of both inner and outer surface air film can be neglected.

4.4 Model verification

In this study, the verification of the numerical model is conducted concerning the following aspects:

1. Infiltration heat exchange efficiency (IHEE);
2. Temperature profile in the wall.

4.4.1 Verification on infiltration heat exchange efficiency

The impact of infiltration on the thermal performance of the wall has been measured by Claridge and Battacharyya (1989). One case in their study is the diffuse inlet and outlet configuration, which arranges the air entering and exiting the wall at different horizontal levels and "diffusing" through a large part of the wall. This corresponds to the configuration D in this study. The measured infiltration heat exchange efficiency has been compared by Buchanan and Sherman (2000) with their simulation results.

Therefore, comparison has been performed between the result obtained in this study and both experimental data and simulation result of Buchanan and Sherman (2000). This is illustrated in Fig 4.15. We can see these results agree well as follows:

- Under an air flow rate of 0.004m/s, the measured infiltration heat exchange efficiency is about 0.80, and it is about 0.65 when air flow rate is 0.02m/s. In this

study, the results under these two air flow rates are 0.87 and 0.62, respectively. While the simulation results by Buchanan and Sherman (2000) under these conditions are 0.90 and 0.75;

- Over the whole range of air flow rate in consideration, the variation of infiltration heat exchange efficiency obtained in this study and that by Buchanan and Sherman follows the same tendency: the difference is less than 0.1.

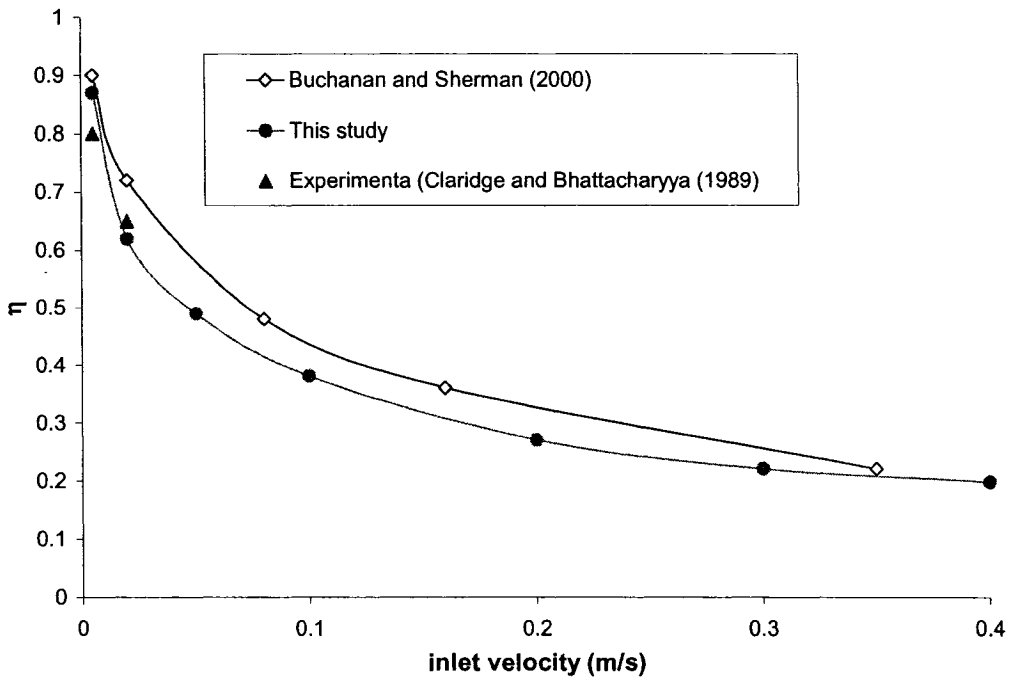

Fig 4.15: Comparison of infiltration heat exchange efficiency

4.4.2 Verification of temperature distribution in the wall

To further verify the model, the simulation results are compared with the measured temperature distribution in the wall. The experiment was carried out in the environmental

chamber (Fazio et al, 1997) in Concordia University. Being designed to meet the requirements for the guarded hot box standard test method (ASTM C 236-89), the chamber is composed of a cold box and a hot box. The two boxes have a dimension of 7.5m×3.6m×4.4m, and 7.5m×3.6m×6.0m, separately. This makes it capable for full scale measurement. An experimental investigation was performed to study the impact of air leakage to the temperature of the exterior building wall, under exfiltration condition. In the experiment, air is intensively driven through the wall through either so called "long exfiltration path" or "direct exfiltration path" (illustrated in Fig 4.16), which corresponds with low inlet-high outlet configuration and straight through configuration in study, respectively. In the direct exfiltration path, the air flows into the wall through a 20 mm diameter opening in the interior finish, centered between the studs and 300 mm above the floor. Whereas in the long path exfiltration path, the air flows into the wall through a 2 mm horizontal crack at the bottom of the interior finish and out through a 5 mm horizontal crack at the top of the exterior sheathing.

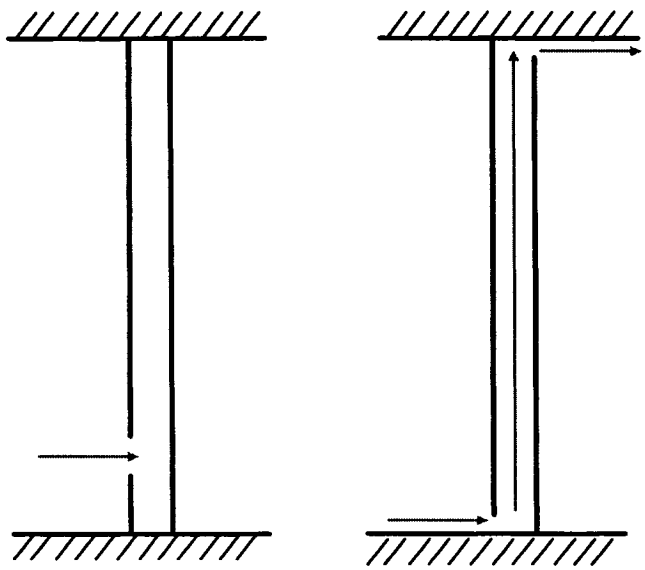

(a) direct exfiltration (b) long exfiltration

Fig 4.16: Air leakage path in the experiment

The wall is 2.4m high, and from outside to inside is composed of spun bonded polyolefin membrane weather barrier, 10 mm asphalt impregnated fiberboard, 89 mm fiberglass batt insulation between the studs, and 13 mm gypsum board.

In the experiment, the mean temperature in the hot box and cold box was maintained at 22°C and -8.5 °C, to represent the indoor and outdoor temperature in winter.

Temperature distribution was measured on the exterior surface and interior surface of insulation. The location of the thermocouples is shown in Fig 4.17, and the detail locations of the thermocouples in this figure are shown in Table 4.2.

.

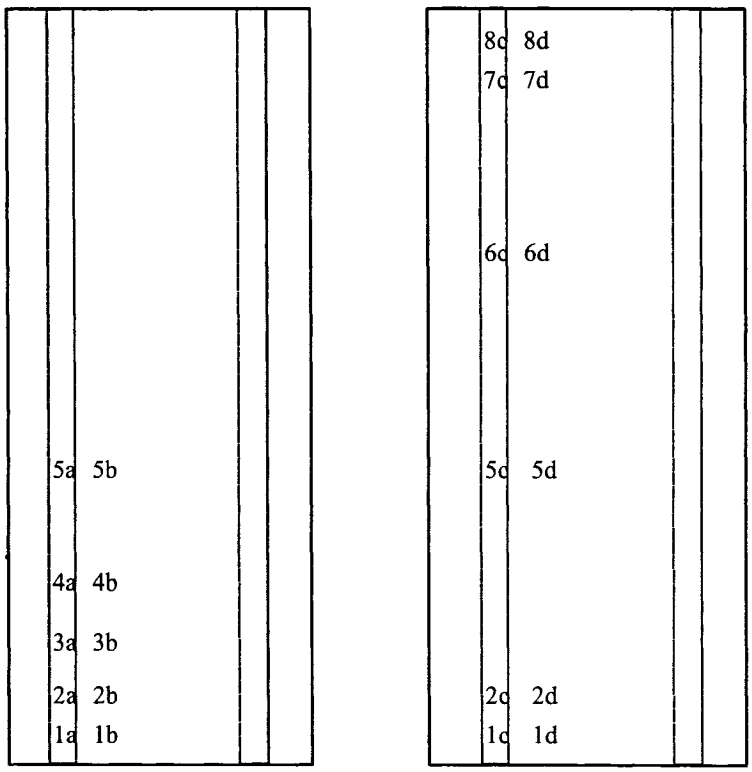

(a) direct exfiltration path (b) long exfiltration path

Legend

a, b, c, d Thermo couples

. ▯ : Wood studs location.

Fig 4.17: Profile of thermocouples

Table 4.2 Locations of thermocouples

Thermocouple ID (direct path)		Thermocouple ID (long exfiltration path)		Distance from the floor (mm)
1a	1b	1c	1d	150
2a	2b	2c	2d	300
3a	3b			450
4a	4b			600
5a	5b	5c	5d	900
		6c	6d	1500
		7c	7d	2100
		8c	8d	2250

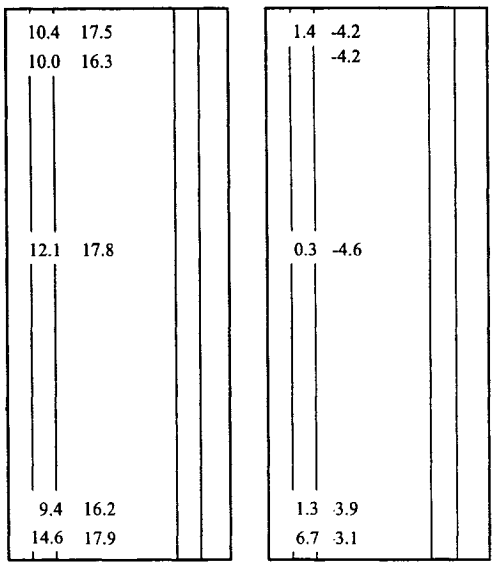

(a) Measured temperature data in insulation and wood stud

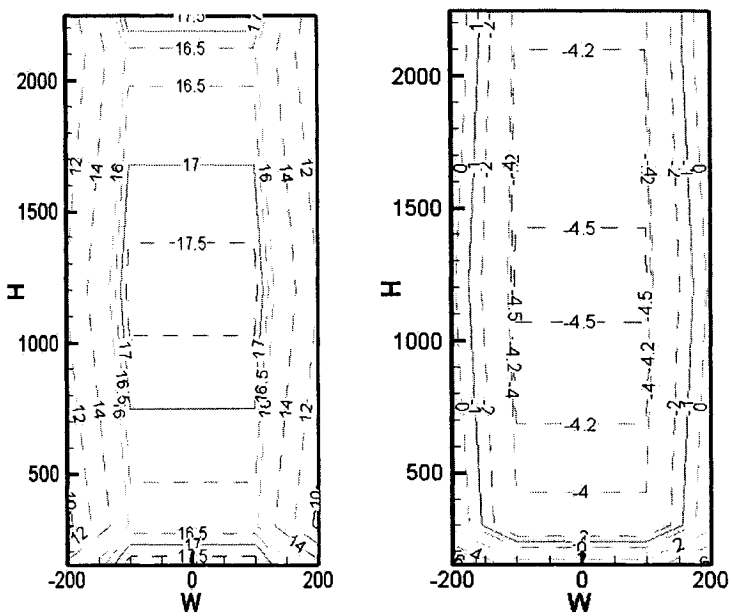

(b) Temperature contour

Fig 4.18 Experimental data of temperature profile for air tight condition

The test was carried out in the insulation and stud, and it was assumed that the temperature distribution is asymmetric. The measured temperature data and the temperature contour based on the data for air tight condition, i.e., no air flow through the wall, are illustrated in Fig 4.18. From it, we can see that in the insulation, the temperature is almost the same in the same horizontal plane, thus the measured temperature in the insulation is used to represent the temperature of the wall and compared with the simulation results.

In the simulation, convective boundary conditions for exterior and interior surfaces are first determined to be consistent with the experimental data for air tight condition. A 17.0°C and -4.2°C is adopted for the warm plane and cold plane as the initial condition, respectively, as there is fluctuation in the measured data. Meanwhile, unlike the treatment in the previous simulation, in this simulation the top and bottom boundary are not adiabatic, but a constant temperature with a convective heat transfer coefficient. On the other hand, the inlet velocity was determined according to the condition of 4Pa pressure difference between inlet and outlet, which was applied in the experiment to drive the air flow through the wall.

The experimental and simulation results with the straight-through path are shown in Fig 4.19. The calculated temperature profiles, as well as the measured date, in the warm plane and cold plane, are illustrated in Fig 4.20. We can see that the simulation results generally agree well with the experimental data. In the warm plane, the temperature increases at 300mm position because of the warm air exfiltration. On other points, the measured

temperature is very similar to the simulation result. At the 150mm and 450mm positions, there is around 1°C error between measured data and simulation result. This may come from the assumption in the simulation that the temperature in hot chamber is uniform, which is not exactly the same as the real temperature distribution of air film near the wall. In the cold plane, the temperature also increases at 300mm position, and the simulation results reflect the variation tendency at most of the measurement points, except in the 450mm position. At this point, the measured data is even higher than that in 300mm position. This may come from the design of the experiment, in which the air outlet is not specified. Thus the air may leak from the wall through several places around the 300mm height point in the cold plane, and the positions the sensors might be the potential leakage path because of the installation of these sensors.

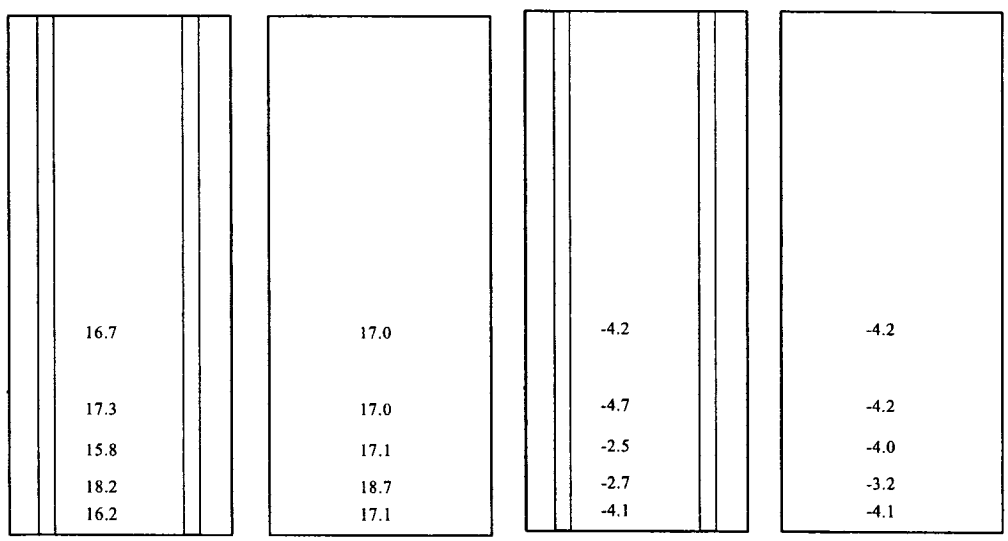

(a) Warm plane temperature (b) Cold plane temperature

Fig 4.19: Comparison of experiment and simulation results for straight through configuration

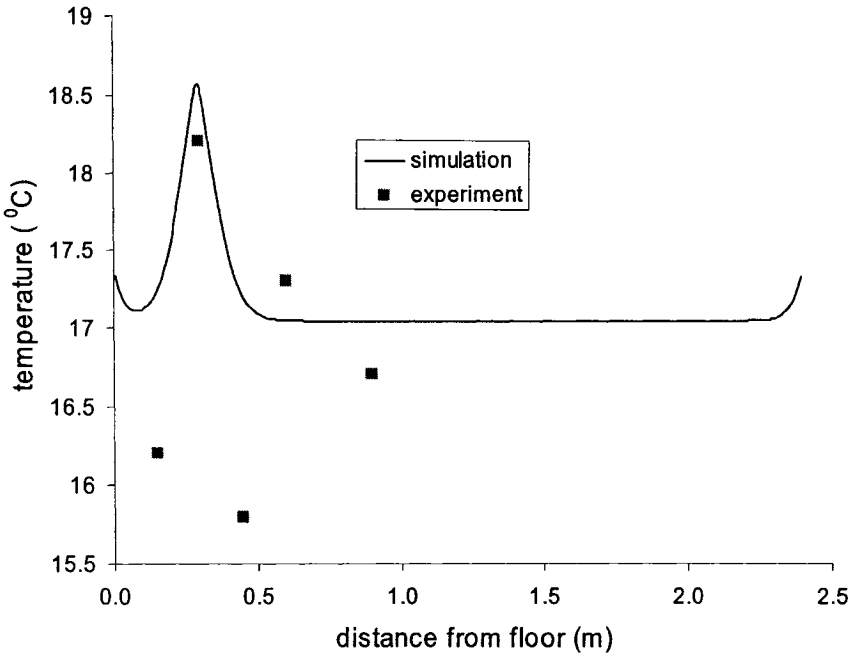

(a) Warm plane

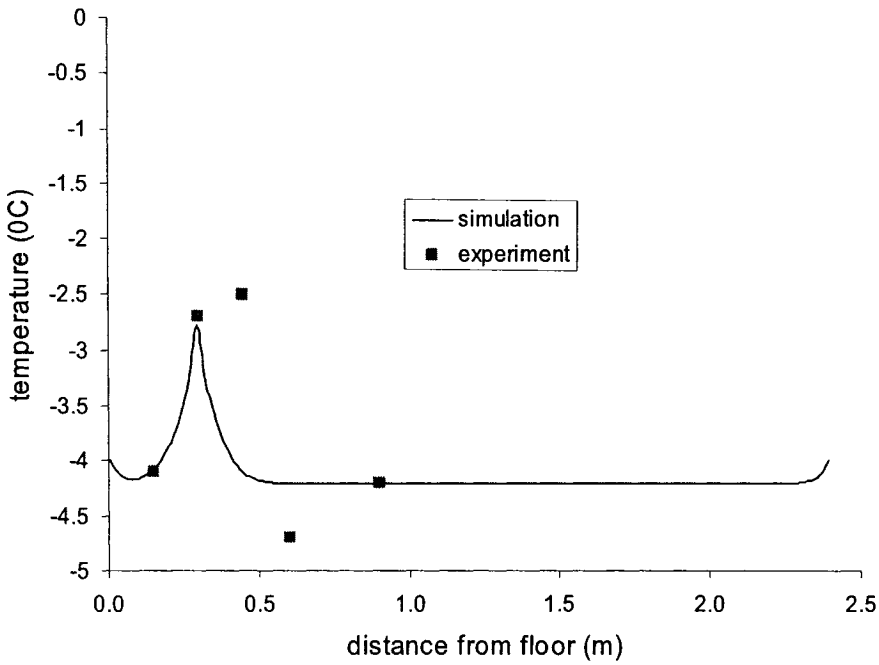

(b) Cold plane

Fig 4.20: Temperature profile of straight through configuration

The experimental and simulation results of long exfiltration path are shown in Fig 4.21. The corresponding temperature profile is illustrated in Fig 4.22. In the warm plane, the simulation results show that the temperature is higher at bottom and top of the wall, while in the area between 300mm to 2100mm, the temperature is about the same. This agrees well with most of the experimental data. The most obvious difference between simulation results and experiment data is at 2100mm position. This may also from the assumption of uniform temperature distribution in the hot chamber, as the temperature in the air film near the wall may increase with the height of the wall in the real situation. In the cold plane, the variation of measured temperature follows the same tendency as that obtained by simulation. At 150mm position, the measured temperature is obviously higher than the simulated result, and it is close to the simulated temperature near the bottom of the wall. This might because there is air leakage in this area. At the same time, the measured data for air tight condition shows that the temperature near the floor might be much higher than upper parts of the wall, even without the air flow, though this is not the situation for the straight through condition. Besides this, the measure temperature at 300mm position is about 1.5°C lower that the simulated result. The reason for the error at this point may come from the arrangement of wall samples in the experiment, as the sample with the long exfiltration path is near the door of the chamber. In fact, the measured temperature at this point is even much lower than that in the same position in the airtight configuration.

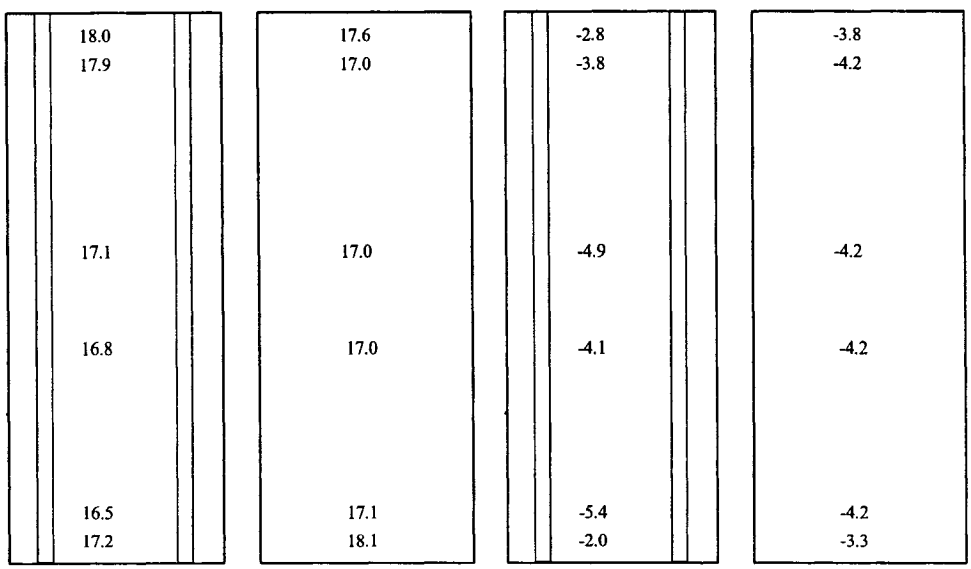

(a) Warm plane temperature

b. Cold plane temperature

Fig 4.21: Comparison of experiment and simulation results for low inlet-high outlet configuration

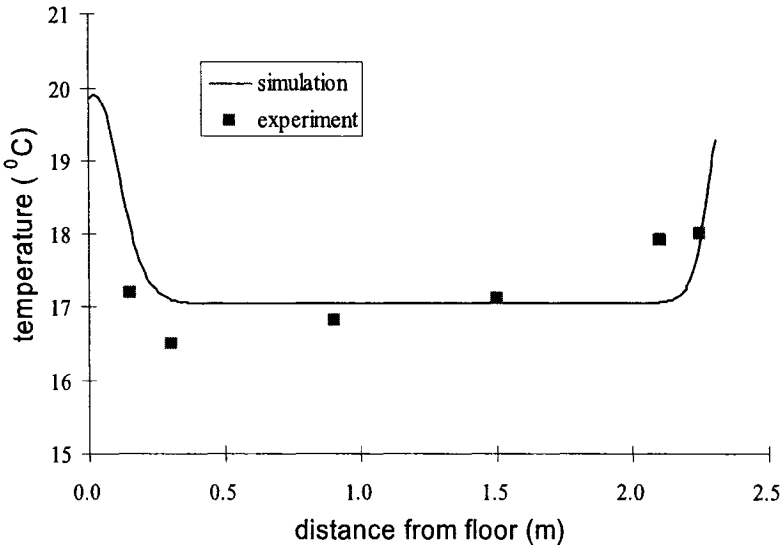

(a) Warm plane

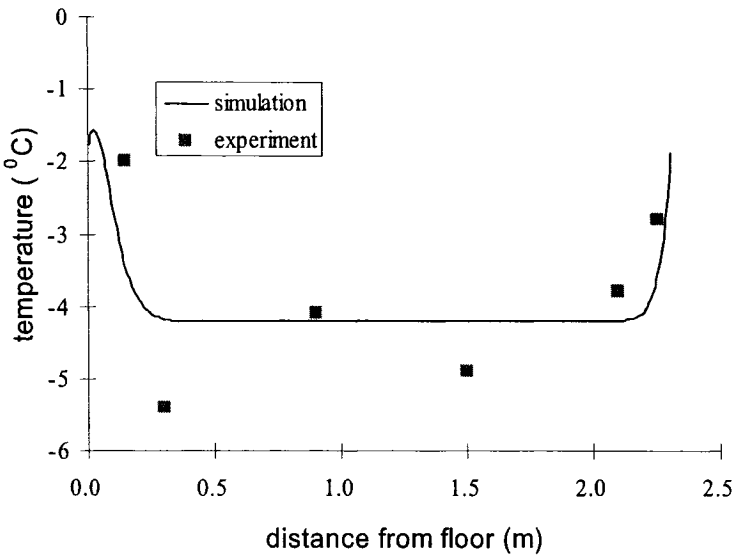

(b) Cold plane

Fig 4.22: Temperature profile of long exfiltration path configuration

4.5 Summary

CFD simulation was performed in the study and the results are presented and analyzed. Specific works in this chapter include:

1. The temperature and air velocity profile in the wall are illustrated to show the influence of air infiltration to the heat transfer in the exterior wall. The coupled conduction-infiltration heat loss is also obtained, under the variation of air flow rate and infiltration path. The impact of heat exchange to the energy consumption of the building is discussed based on the calculated infiltration heat exchange efficiency (IHEE).
2. Parameter studies have been carried out to study the influence of porosity, indoor and outdoor temperature gradient as well as convective boundary coefficient on the heat exchange efficiency.
3. The model verification has been performed by comparing the simulation results with other numerical simulation results in the literature, as well as the experiment data.

Chapter 5 Dynamic Insulation: Theory and Application

5.1 Dynamic insulation

5.1.1 Concept of dynamic insulation

The study in the previous chapters shows that impacted by the heat exchange process in the building envelope, the energy consumption is less than that is estimated by the conventional method. However, the impact of heat exchange by air infiltration in the conventional wall is limited, as only one part in the wall works for ventilation purposes. The heat exchange efficiency will be higher if most of the wall can be used in the ventilation. Inspired by this idea, the technology of dynamic insulation has been developed.

The concept of dynamic insulation (DI) is to effectively use the combination of conventional insulation and heat exchange characteristics of a wall to pre-heat fresh air for ventilation. It is regarded as one possible method for reducing building envelope heat losses while achieving better indoor air quality. The existing technology of dynamic insulation can be divided into two catalogues:

1. The design using cavities to circulate the fluid (mostly air) in the wall. The air flow direction in the cavities is generally parallel to the wall – wall acting as a heat exchanger.

2. Breathing wall design which let the gas (mostly air) transfer through the permeable insulation. The interaction of gas phase and solid phase can also act as a contra-flux mode heat exchanger (Baker, 2003).

Though ventilated walls which use a combination of air cavities have been presented, such as Baily (1987) and Chebil et al (2003), currently most of the structures of dynamic insulation system adopt the latter concept because of its easy implementation.

Besides the advantage of energy saving, the fibrous structure in dynamic insulation may also offer an effective, low energy solution to the air pollution problem in the surrounding environment. This is because the dynamic insulation can act as an air filter.

The polluted particles can be trapped by a filter through three mechanisms (Taylor et al, 1999):

1. Impaction, in which the momentum of the particle causes it to deviate its stream line around the fiber and is captured by the fiber media;
2. Interception, in which the particle follows its streamline and is captured when it comes into contact with the fiber;
3. Diffusion, in which the Brownian motion causes the particle to move independently of the air stream onto the filter media.

For the conventional air filter, the air velocity is up to 1.0 to 1.5m/s, so the particle is only filtered by impaction and interception. As the air velocity in the dynamic insulation is

relatively slow, generally 0.0005m/s to 0.005m/s, all three mechanisms are prompted, so the dynamic insulation is very effective for capturing particles less than 0.5μm or larger than 5μm in diameter. It is pointed out that dynamic insulation is also efficient at capturing particles ranging from 0.5μm to 5μm, if its thickness is greater than 60mm (Taylor and Imbibi, 1999). At this thickness of filter media, the dynamic insulation has the potential to become a high efficiency particle air filter due to the nearly zero particle penetration for all particle sizes.

5.1.2 Structure of dynamic insulation

The dynamic insulated wall component usually consists of the following main sub-layers:

1. The external envelope sub-layer. This could be a prefabricated reinforced concrete slab (Dimoudi et al, 2004), or a perforated metal sheet (Baker, 2003). The ventilation air can be introduced from the bottom or top of the external envelope sub-layer.
2. The dynamic insulation sub-layer, which may consist of layers of breathing materials, including materials such as compressed straw board, mineral wool and thin paperboard, or cellulose fiber insulation. These breathing materials let the air enter the room due to a pressure difference between interior and exterior.
3. An air gap is generally used to separate these two sub-layers.

In most of the dynamic insulation design, an air permeable internal surface construction is adopted. However, Baker (2003) pointed out that problems might exist with the use of a permeable wall liner. To solve this drawback, plasterboard, which is impermeable to

air, is chosen for the inner face of the construction. Air is drawn through the dynamic insulation sub-layer into a cavity behind the plasterboard. From there it is distributed into the room through vents.

Besides configuration of these sub-layers, other considerations in the real dynamic insulation system design include:

1. To assure the uniform air-flow and hence one-dimensional heat transfer through the wall, for the design that air comes into the wall from the bottom of the external layer, the lower 1.0m of the wall is constructed of having a higher air resistance (Dimoudi et al, 2004).
2. Pressure difference between indoor and outdoor for inward air flow can be normally achieved by means of a fan.
3. Solar energy has also been considered to increase the performance of dynamic insulation component. For example, a layer of outer glazing could raise the temperature of incoming air (Gan, 2000).
4. A heat pump or heat pipe unit has also been suggested to be inserted in the exhaust air duct to pre-heat the incoming air (Gan, 2000).

For the implementation, the material used needs to be determined based on its property, especially air permeability and thermal conductivity. In the dynamic insulation, a negative pressure gradient is needed for the inward flow, and the maximum pressure gradient should be less than 30~50Pa. Table 5.1 illustrates the measured air permeability of several typical building materials. Adopting these values to the Darcy's law, it is found

that for the air transfer velocity ranging from 0.0005m/s to 0.005m/s. The range of air permeability should be in the range of $10^{-9}m^2$ to $10^{-7}m^2$. Therefore the most suitable material for dynamic insulation will be cellulose, fiberglass or mineral wool.

Table 5.1 Measured air permeability of building materials (Taylor et al, 1999)

Material	Permeability (m^2)
Plasterboard	5.3×10^{-12}
Thermal block	8.0×10^{-12}
Fiberboard	1.8×10^{-9}
Mineral wool	3.3×10^{-9}
Cellulose	1.42×10^{-8}
Fiberglass	1.43×10^{-8}
Sheep's wool	9.0×10^{-8}

5.1.3 Heat transfer model of dynamic insulation

In the current application of dynamic insulation, efforts have been made to assure a one dimensional air flow and heat transfer. This can be illustrated by Fig 5.1, which is the structure presented by Baker (2003). Therefore heat transfer process in the dynamic can be modeled using one dimensional model as follows:

$$(\varepsilon\rho_a C_{pa} + (1-\varepsilon)\rho_s C_{ps})\frac{dT}{dt} + u\rho_a C_{pa}\frac{dT}{dx} = k_{eff}\frac{d^2T}{dx^2} \qquad (5.1)$$

Thermal performance of the dynamic insulation can be assessed based on the solution of

this equation. To make the solution process and parameter study easier, the following non-dimensional form of equation is used:

$$\sigma\frac{d\theta}{d\tau}+\frac{d\theta}{dX}=\frac{1}{Pe}\frac{d^2\theta}{dX^2} \qquad (5.2)$$

where $\theta=\frac{T-T_o}{T_i-T_o}$ $\qquad X=\frac{x}{L}$

$$\tau=\frac{tu}{L}$$

T_i - Indoor temperature (K)

T_o - Outdoor temperature (K)

L – Thickness of the dynamic insulation (m)

$$Pe=\frac{u\rho_a C_p L}{k}$$

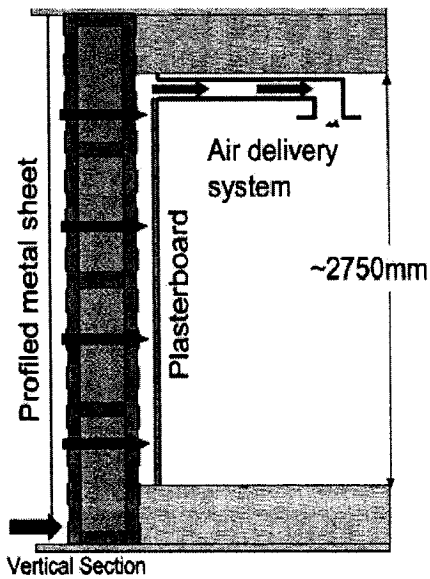

Fig 5.1: Structure by Baker (2003)

Equation (5.2) is solved by a numerical approach using finite difference method. A fully implicit scheme is used so that large time step can be adopted to correspond with the hourly change environment temperature in building simulation. TDMA algorithm is adopted to solve the algebraic equations.

First, the simulation is carried out under a steady state condition, i.e., constant temperature boundary condition:

$$X=0 \qquad \theta=0$$

$$X=1 \qquad \theta=1$$

The change of interior surface temperature with time under two porosity values and air velocities is illustrated in Fig 5.2. We can see under high porosity condition (ε=0.9), the temperature profile will reach a steady state almost within one hour. Under medium porosity condition (ε=0.5), the temperature can still reach the steady state in one hour if velocity is high. Under the condition that porosity being 0.5 and the air velocity is 0.0005m/s, it will take more than one hour for the temperature profile to reach the steady state. However, the absolute variation of temperature is not significant.

The simulation is also performed under varying ambient temperature, which follows a sinusoidal function, with a mean temperature of 5°C and the amplitude of 6°C. The change of interior surface temperature within one day is illustrated in Fig 5.3. It can be seen under the same indoor temperature as that in the steady state condition, the interior surface temperature is not the same. It is also shown that the extent of variation of the interior surface temperature is mainly influenced by the air flow rate, and the influence of porosity can be neglected.

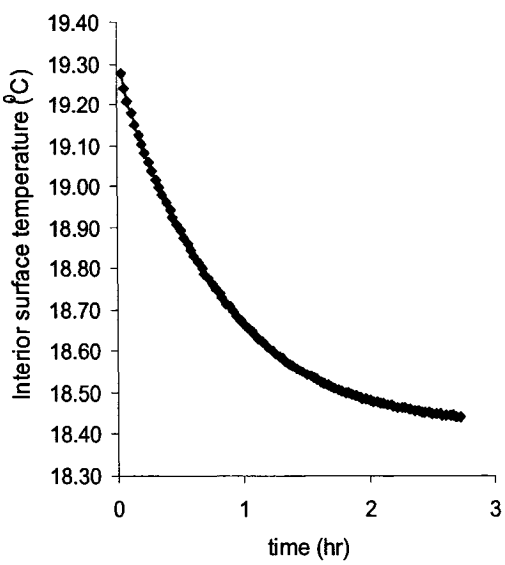

(a) ε=0.5, u=0.0005m/s

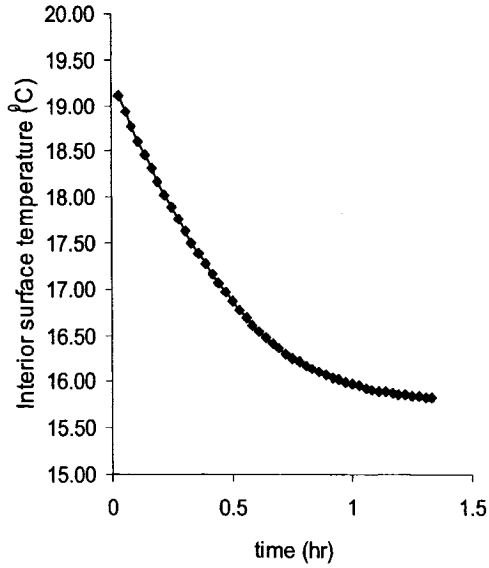

(b) ε=0.5, u=0.002m/s

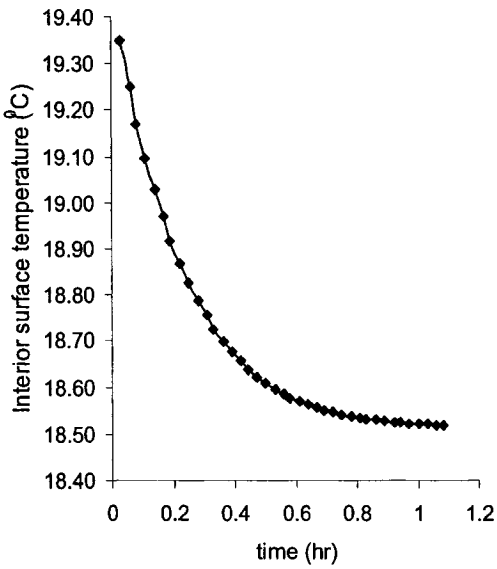

(c) ε=0.9, u=0.0005m/s

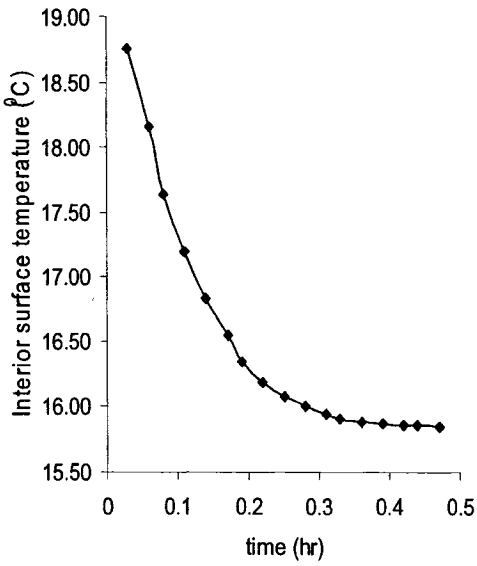

(d) ε=0.9, u=0.002m/s

Fig 5.2: Change of interior surface temperature with time

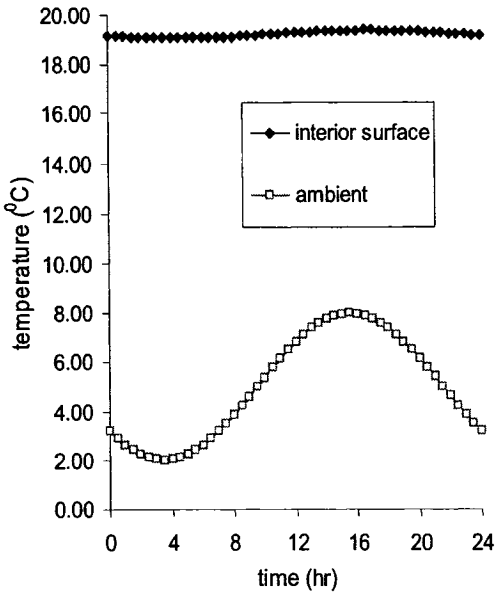

(a) ε=0.5, u=0.0005m/s

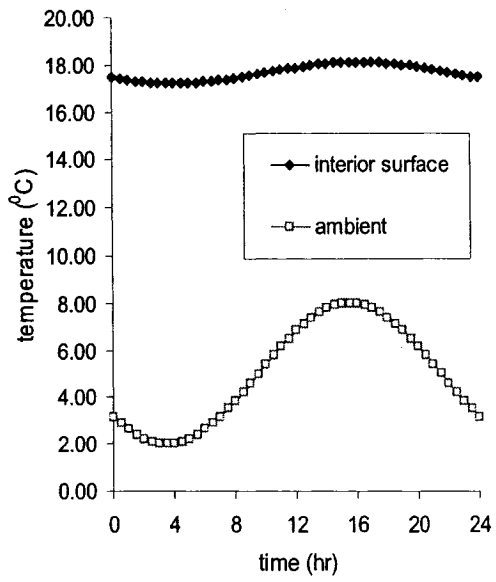

(b) ε=0.5, u=0.002m/s

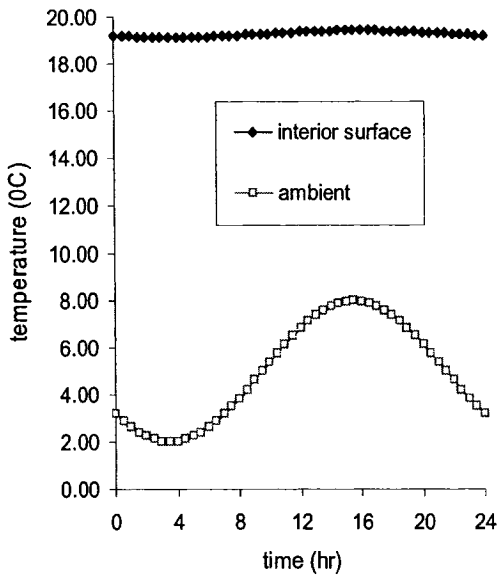

(c) ε=0.9, u=0.0005m/s

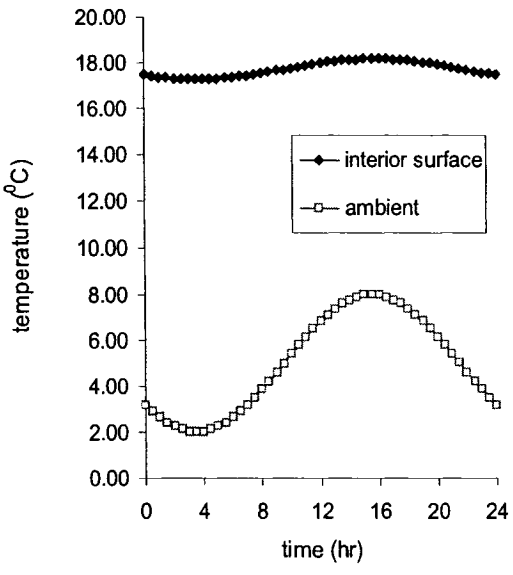

(d) ε=0.9, u=0.002m/s

Fig 5.3: Change of interior surface temperature in one day

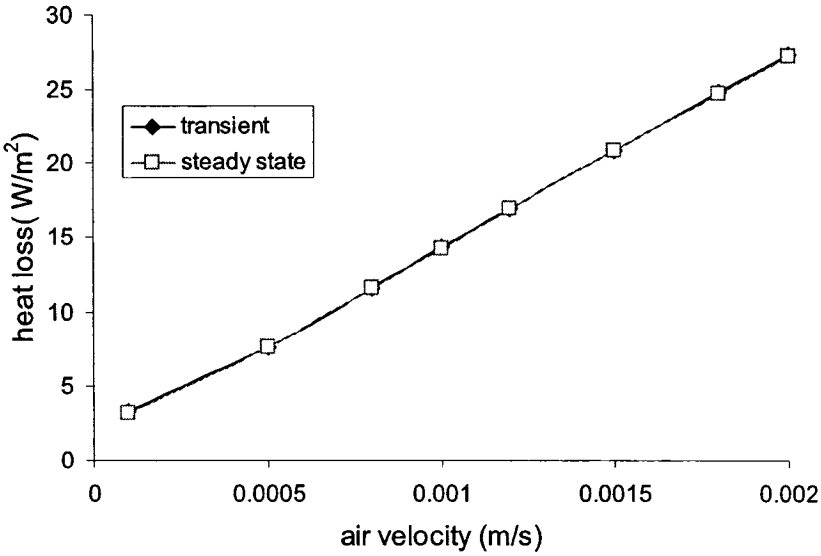

(a) ε=0.9, ρ_s=70kg/m^3, Cp_s=1000J/kg

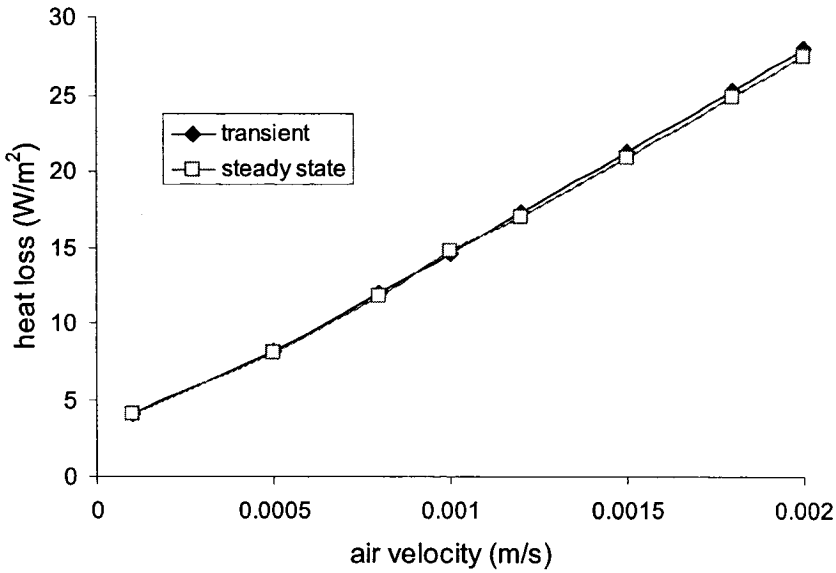

(b) ε=0.5, ρ_s=70kg/m^3, Cp_s=1000J/kg

Fig 5.4: Heat loss obtained under steady state and transient condition

Fig 5.4 shows the heat flux obtained under the steady state and transient boundary condition, for the two porosity conditions. It can be seen that in each case, there is no significant difference between the results obtained by the steady state and transient boundary condition.

By analysis the variation of parameters in equation (5.2), it is easy to find that the parameter σ will influence the time for the temperature to reach the steady state. Thus the heat capacity of the solid matrix will affect the transient thermal performance of the dynamic insulation. Parameter study has been performed concerning the influence of this factor. Fig 5.5 illustrates the change of interior surface temperature under the condition that ρ_s and Cp_s increase to 200kg/m^3 and 1500J/kg, respectively. Compared with the previous result, it is easy to find that the time lag increases, while the variation of the surface temperature during a day is about the same.

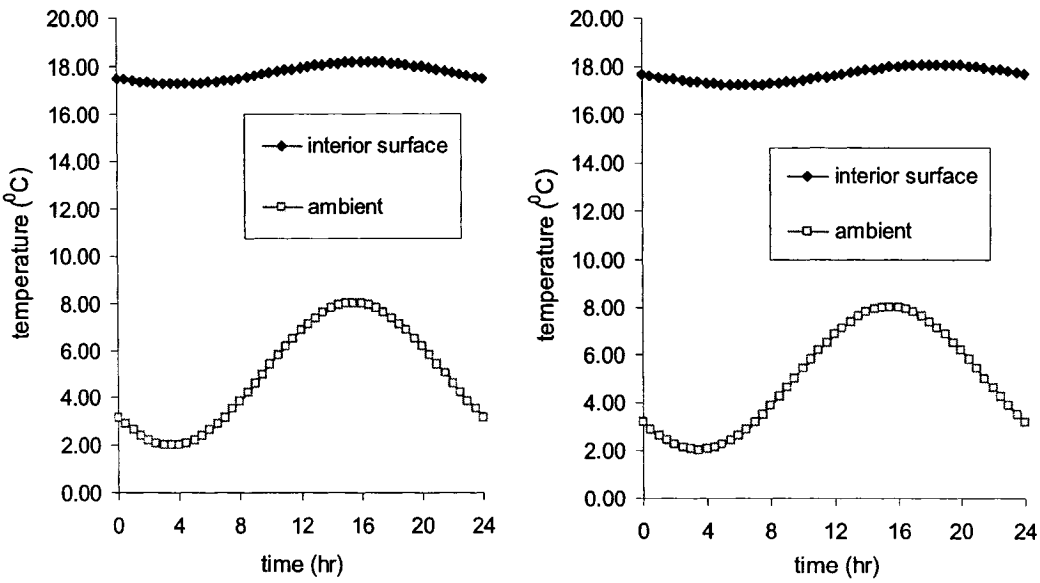

(a) ε=0.9 (b) ε=0.5

Fig 5.5: Change of interior surface temperature under $\rho_s = 200kg/m^3$, $Cp_s = 1500J/kg$

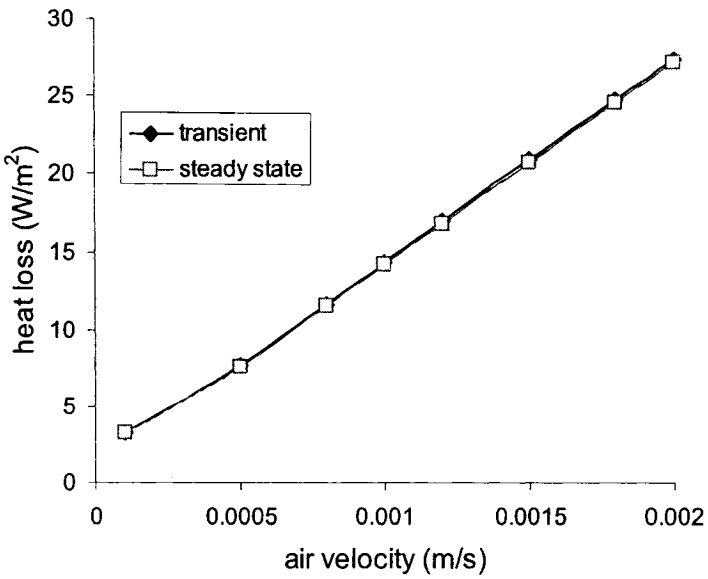

(a) ε=0.9, ρ_s=120kg/m^3, Cp_s=1500J/kg

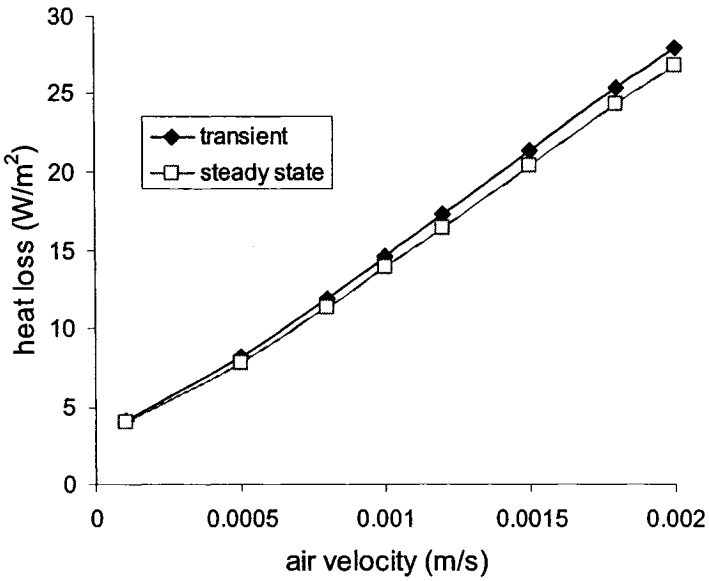

(b) ε=0.5, ρ_s=120kg/m^3, Cp_s=1500J/kg

Fig 5.6: Heat loss under different heat capacity condition

As we concern more about the property of the material to the energy consumption, the total heat loss is calculated and illustrated in Fig 5.6. It can be found the difference increase, however, is very limited. Detailed analysis finds that even at the highest air velocity, the total heat flux obtained under two conditions is within 10% of the total heat flux. Therefore concerning the energy consumption, the unsteady item in the left side of equation (5.2) has little influence to the results, and can be neglected. The steady state is a good approximation to the transient model. This is good as though the model of equation (5.2) is simple; it is not suitable for engineering implementation because of the numerical method needed in the solution process.

Under the steady condition, an analytical solution can be obtained. By deriving the heat flux in the exterior surface of the dynamic insulation, the following dynamic *U*-value expression can be obtained to represent the conductive heat loss:

$$U_{dyn} = \frac{Pe}{R(e^{Pe} - 1)} \tag{5.3}$$

$R = \frac{L}{k_{eff}}$ The effective thermal resistance of insulation material in the static condition (m^2/W)

The expression in this equation is different with the generally adopted equation in the literature, which is actually the non-dimensional ratio compared with the steady state *U*-value. Furthermore, this expression stresses more clearly the mechanism of heat exchange process in dynamic insulation, as the *Peclet* number (*Pe*) represents the ratio of convective heat transfer with the conductive heat transfer.

It is easy to obtain the analytical solution of equation (5.2) on the condition of a constant boundary convective heat transfer coefficient on the exterior and interior surface. This convective heat transfer coefficient mainly affects the interior surface temperature, which can be determined by equation (2.15). However, it has little influence on the energy consumption of the building, which has been demonstrated by the results of numerical model in the previous chapter.

As there is no heat source inside the wall, the total heat flux at any surface across the wall will be conservative. Considering the combined effect of conductive and convective heat transfer, then the overall heat transfer rate at the exterior surface of dynamic insulation is:

$$\begin{aligned} Q_T &= Q_{cond} + Q_{conv} \\ &= U_{dyn} A\Delta T + \dot{m} C_p \Delta T \\ &= U_{dyn} A\Delta T + \rho_a u A C_p \Delta T \end{aligned} \tag{5.4}$$

$\dot{m}$ - Air mass flow rate through dynamic insulation (kg/s)

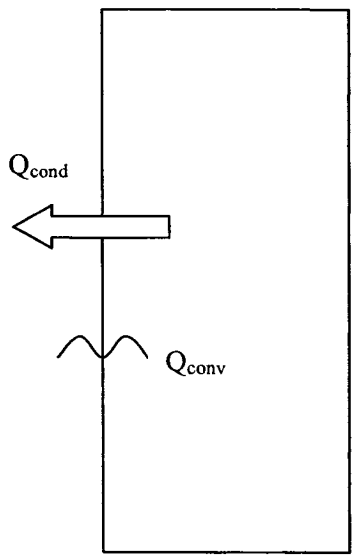

Fig 5.7: heat flux in the exterior surface of dynamic insulation

This result reflects that the heat loss through the dynamic insulated wall is greater than the 'conduction heat loss' calculated by the dynamic *U*-value, but it is less than the sum of the conduction heat loss and the ventilation heat loss for the conventional wall.

The overall heat loss coefficient for a dynamic insulation is:

$$\begin{aligned} U_T &= Q_T / (A\Delta T) \\ &= \frac{Pe}{R(e^{Pe} - 1)} + \rho_a u C_p \\ &= \frac{Pe}{R(e^{pe} - 1)} + \frac{Pe}{R} \end{aligned} \tag{5.5}$$

The heat exchange efficiency of dynamic insulation is:

$$\eta = 1 - \frac{Q_T - Q_0}{Q_{conv}} = \frac{Q_0 - Q_{cond}}{Q_{conv}}$$
$$= \frac{\frac{1}{R} - \frac{Pe}{R(e^{Pe}-1)}}{\rho u C_p} \tag{5.6}$$

This physically means the efficiency of reduction of conductive heat loss, acted by the convective air flow in the dynamic insulation.

If only part of the wall is incorporated with dynamic insulation, i.e., the ratio of the dynamic insulation area to the total area of the wall is γ, then the overall heat loss rate through the wall is:

$$Q_T = (Q_{cond} + Q_{conv}) * \gamma + Q_{conds} * (1-\gamma)$$
$$= (U_{dyn} A\Delta T + \rho_a u A C_p \Delta T) * \gamma + U_{static} A\Delta T * (1-\gamma) \tag{5.7}$$

The overall heat loss coefficient corresponding to this is

$$U_T = Q_T / (A\Delta T)$$
$$= \frac{Pe}{R(e^{pe}-1)} + \frac{\gamma Pe}{R} + \frac{1-\gamma}{R} \tag{5.8}$$

In this case, the heat exchange efficiency can also be represented by equation (5.6) because heat exchange process only occurs at the dynamic insulation part.

Fig 5.8 shows the dynamic *U*-value and corresponding heat exchange efficiency as a function of the air flow rate, for two length of the dynamic insulation: 0.1m and 0.2m. The effective conductivity of the insulation is 0.035W/m K. It can be seen that the static condition has the highest heat transfer rate, and this heat transfer rate decreases with the air flow rate. At very low air velocity, i.e., below 0.002m/s, the dynamic insulation with a

thickness of 0.2m has a lower heat transfer rate, than the dynamic insulation of 0.1m. However, when the air velocity is greater than 0.002m/s, the conductive heat loss at the exterior surface of the wall tends to be zero, for a wall with a thickness either 0.1m or 0.2m.

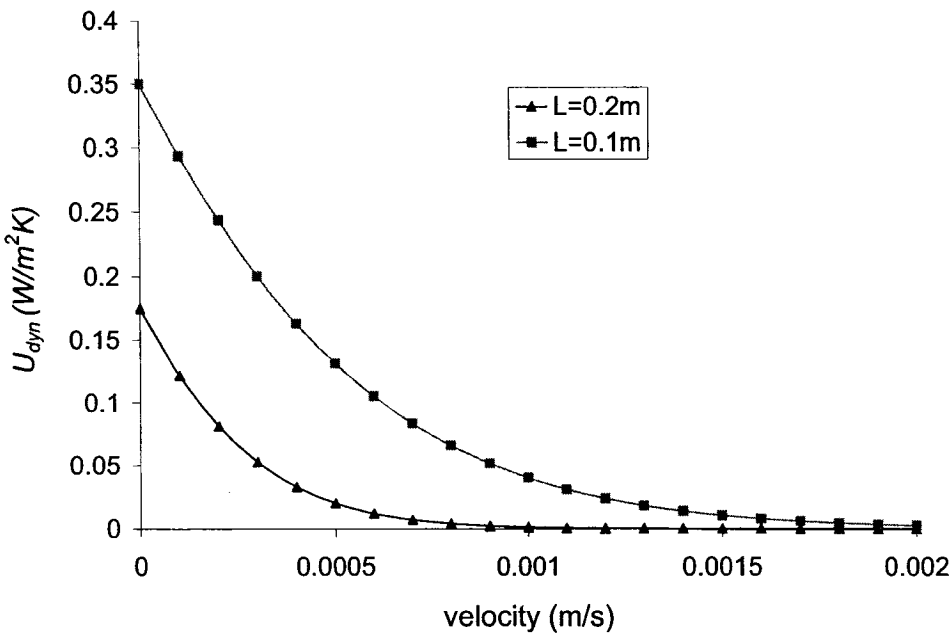

Fig 5.8: Dynamic *U*-value with velocity

Fig 5.9 shows the relation of the overall heat loss coefficient with the velocity. It can be seen the overall heat transfer coefficient is determined by the air flow rate, and the result on the condition of wall thickness 0.1m or 0.2m almost overlap.

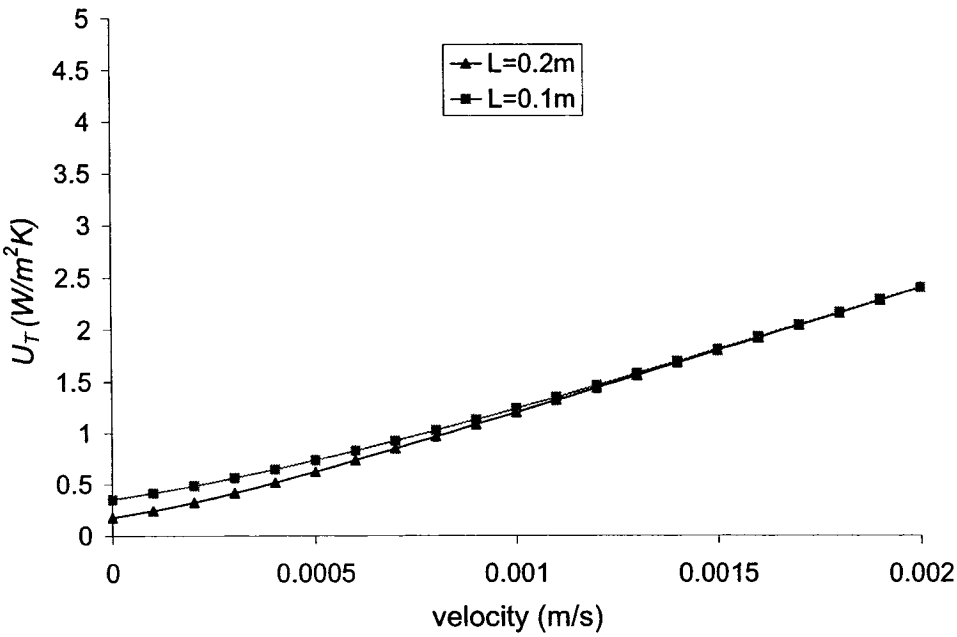

Fig 5.9: Overall heat loss coefficient

The results of overall heat transfer coefficient obtained by equation (5.6) are compared with the experiment data Baker (2003). In the measurement, a 0.17m cellulose fibre insulation breathing wall construction is adopted. To correspond with the analytical model, the overall heat transfer coefficient including both conduction and ventilation heat loss is used. The conductive heat flux is measured on internal surface of the dynamic insulation, and the ventilation heat loss is determined by the average in-coming temperature of interior surface of the wall. The results from the analytical model and experiment are illustrated in Fig 5.10. We can see that these results agree very well. Thus the analytical model can predict the energy consumption of the dynamic insulated wall with a good precision.

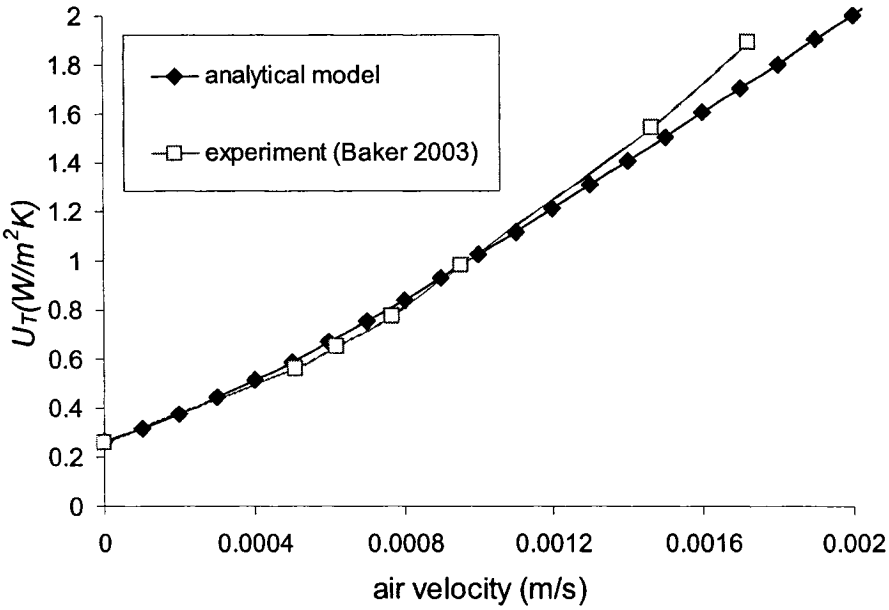

Fig 5.10: Comparison of results by analytical model and experiment data

Fig 5.11 illustrates the change of heat exchange efficiency in the insulation, corresponding with the situations in Fig 5.2 and Fig 5.3. As the heat transfer in the dynamic insulation is dominated by convective heat loss, the structure with a thickness of 0.1m has higher heat exchange efficiency than the 0.2m structure does. The reason is that the conductive heat loss in the steady state of 0.1m structure is higher than that of the 0.2m structure, and this conductive heat loss can be totally recovered because of air transfer in the dynamic insulation.

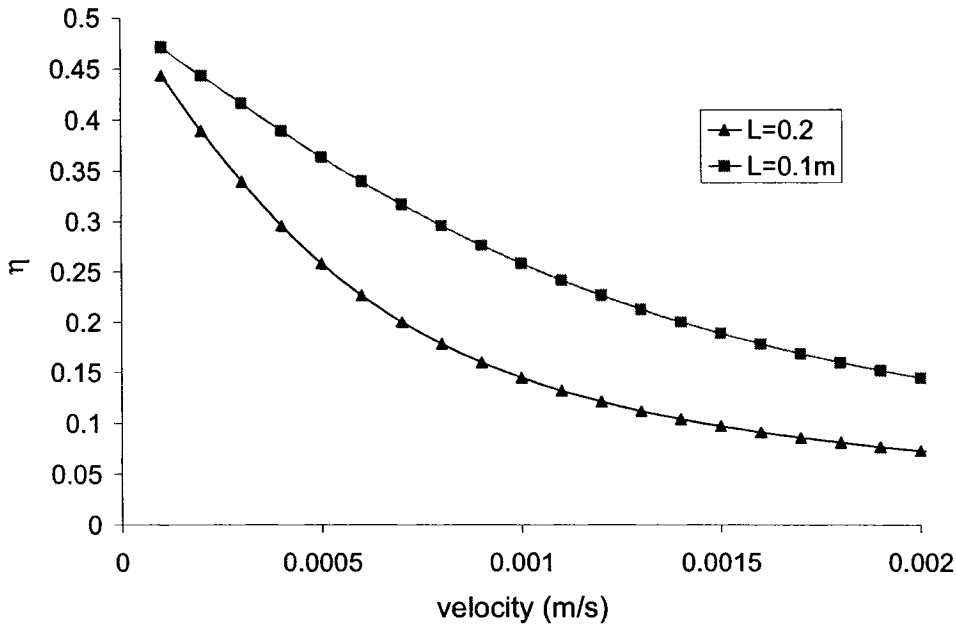

Fig 5.11: Heat exchange efficiency of dynamic insulation

5.1.4 Simulation of thermal performance of building integrated with dynamic insulated wall using TRNSYS

Though the concept of dynamic insulation was developed decades ago, the implementation of this technology is still in the early stages. Until now, no special design tools for the dynamic insulated wall have been reported. However, concerning the thermal performance, some commonly available building energy analysis tools, such as TRNSYS, can be modified to incorporate dynamic insulation elements.

Using the total heat loss coefficient expressed by equation (5.5), it is easy to determine the heat loss through the exterior wall with a dynamic insulated wall. However, in the real building design process, the designer is concerned about the overall energy consumption of the building. For this purpose, it is very helpful to simulate the thermal performance of the building which installs dynamic insulated wall, by commonly used building simulation tools, such as DOE2, EnergyPlus, Eps-r or TRNSYS. In this study, attempts have been made to carry out the simulation of a single room with dynamic insulated wall, using TRNSYS.

TRNSYS is a transient simulation program for building HVAC system thermal analysis. It has a user friendly interface, thus is easy to learn and use. It also has a modular structure, and this supplies flexibilities to the users: they can modify the existing models in the standard TRNSYS library, or add new mathematical models. One important advantage related to this study is that for the simulation of thermal performance of building envelope, it not only allows the user to select the material of the envelope, from its standard library, but also allows the users to specify the thermal resistance of the envelope. Therefore, the thermal resistance of the dynamic insulation according to the heat loss coefficient obtained can be adopted to define the thermal performance of a dynamic insulated wall. In this way, the simulation can be performed for a building incorporating dynamic insulated wall.

A simple room model is constructed for demonstration using the Type 56 (Detailed Multi-Zone Building) module in TRNSYS. It represents a single-room building, 4.5m

square by 2.5 m high. A $0.6m^2$ single glass window is inserted on the south wall. It is also assumed there is one person in the room. Two variations of this model are used – one composed entirely of standard wall constructions, and the other with a dynamic insulated wall on the west façade. A breathing wall structure is adopted for the dynamic insulated wall, because of its easy implementation, and consistence with the theory of dynamic insulation discussed earlier in this Chapter.

It is assumed that both buildings are air tight construction, so only a small amount of air could infiltrate or exfiltrate through cracks (the infiltration rate in the Type 56 model is set to 0.1 ACH in both models). In the model without a dynamic insulated wall, ventilation air is brought in through a duct and heated or cooled within the space (the ventilation rate in the Type 56 model is set according to the desired air-change rate being tested for, and the ventilation temperature is set to the outdoor air temperature). The conductive heat transfer for each wall is determined by using a standard wall type, including 0.2m brick, 0.1m or 0.2m insulation layer, and 0.01m plasterboard as interior surface.

In the model with a dynamic insulated wall, it is assumed that there would still be some air flow through direct cracks at the wall joints, so the infiltration rate (which assumes no heat transfer between the wall and the air passing through it) is kept the same as in the other model. However, in considering the slower air passage through the porous matrix of the dynamic insulated wall, the model uses the 'dynamic *U*-value' discussed above to account for the conductive heat losses through the dynamic insulated wall. The

ventilation air temperature in the Type 56 model is also set to the outdoor air temperature, thus the ventilation heat loss is the same as the other model. The wall type for the west façade is changed to a wall whose dynamic *U*-value is determined by the equation (5.3).

The simulations are carried out for different air change rates for the building. Modifying the air change rate in the normal-wall building model is simply done by changing the ventilation rate. For the dynamic insulated wall model, an increase in the air change rate requires an increase in the air velocity through the wall, which alters the 'dynamic *U*-value'.

The requirement of ventilation for this simple building is considered to be in the range of 0.2 ACH to 1.0 ACH. This corresponds with the range of the air velocity through the wall being 0.00025m/s to 0.00125m/s.The corresponding dynamic *U*-values used in the simulation are illustrated in Table 5.2.

The simulation is carried for the whole year period. The indoor temperature is set constant at 22°C, while the outdoor temperature is determined by the weather data of Madison, WI, the United States.

In the simulation, it is assumed that the exterior surface temperature of the dynamic insulated wall equals to the outdoor temperature, as air is constantly transferring through it. There might be a small error of this treatment if long wave radiation is considered.

However, it is assumed that this change is small enough that it can be ignored in the first-pass model.

In the current simulation, the energy consumption of fan is not included. However, it needs to be noticed that as pressure gradient increases in buildings incorporating dynamic insulations, the fan power used for will also increases.

Table 5.2 Situations in TRNSYS simulation

air velocity (m/s)	ACH (1/h)	0.1m insulation U_{dyn} (W/m^2)	0.2m insulation U_{dyn} (W/m^2)
0.00025	0.2	0.20	0.056
0.0005	0.4	0.112	0.015
0.00075	0.6	0.060	0.0035
0.0001	0.8	0.031	7.4E-4
0.00125	1.0	0.015	1.5e-4

By performing the simulation using TRNSYS, the energy consumption of the building under each condition can be obtained. Results are analyzed concerning the following aspects:

- Annual energy consumption of building with or without dynamic insulated wall
- Ability of energy saving by using of dynamic insulation elements
- Advantages of the implementation of dynamic insulation

Fig 5.12 illustrates the annual energy consumption of the building with normal walls only, and that of building whose west wall is the dynamic insulated wall, with the insulation being 0.1m or 0.2m thick, separately. Results in these two figures show that similar with the result of the building with normal walls only, the energy consumption of the building incorporating dynamic insulation elements increases almost linearly with the air flow rate. It can also be noticed that under each air flow rate, energy can be saved by using dynamic insulated wall in the buildings. With the increase of air flow rate, the difference of energy consumption for the building with only normal walls and the building with dynamic insulated wall increases, especially for the condition that the insulation is 0.1m.

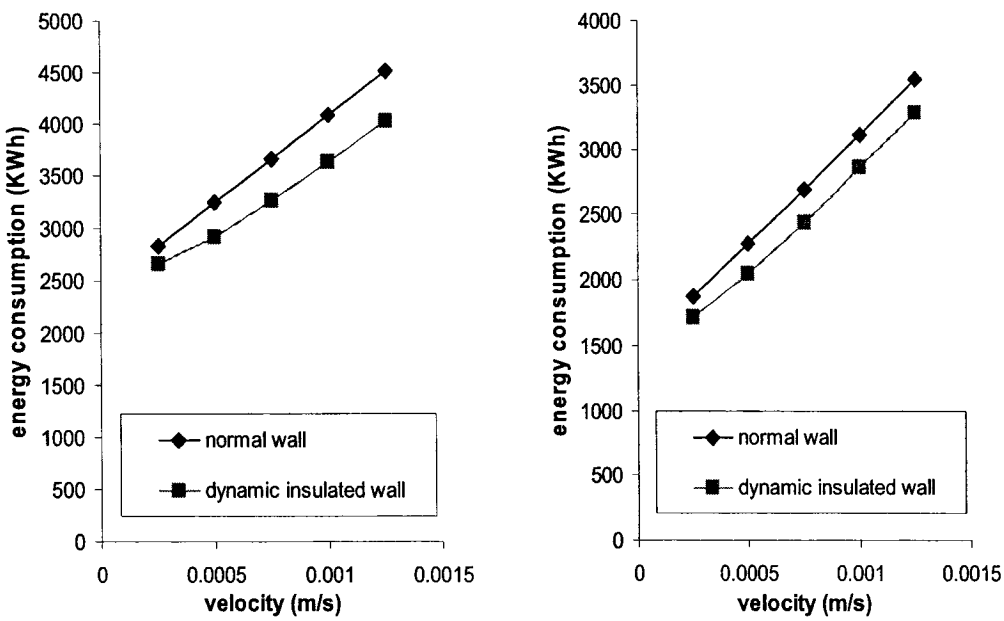

(a) Walls with 0.1m insulation

(b) Walls with 0.2m insulation

Fig 5.12 Energy consumption

Fig 5.13 illustrates the energy reduction rate of the dynamic insulated wall with an insulation thickness of 0.1m or 0.2m, obtained by analytical model, and TRNSYS simulation, respectively. The results show that the energy reduction rate is higher if 0.1m insulation is adopted in the normal wall and in the dynamic insulated wall. The energy saving extent under this condition is about 10% at most for the air flow rates. Comparatively, if the 0.2m insulation is used in the normal wall and in the dynamic insulated wall, then the energy reduction extent is lower, being 6%-8% for the velocities higher than 0.00025m/s. Meanwhile, under each insulation thickness, there is a range of the velocity that has the highest energy reduction rate. For example, for the 0.1m insulation condition, the optimum velocity for energy saving is about 0.001m/s, while for the 0.2m insulation condition this velocity value is about 0.0005m/s. However, besides the results of very low velocities, the difference of energy reducing extent is within 5% over a wild range of velocities.

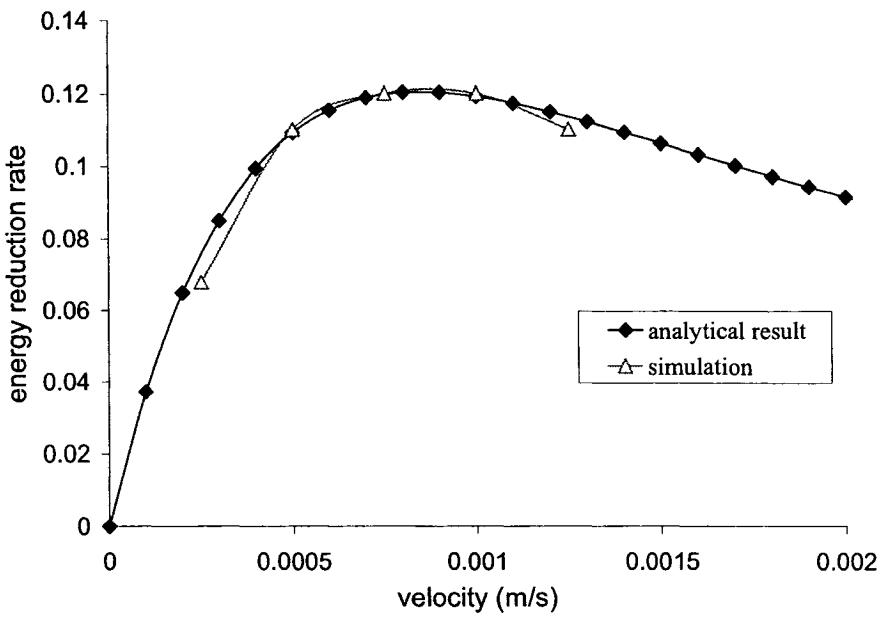

(a) Wall with 0.1m insulation

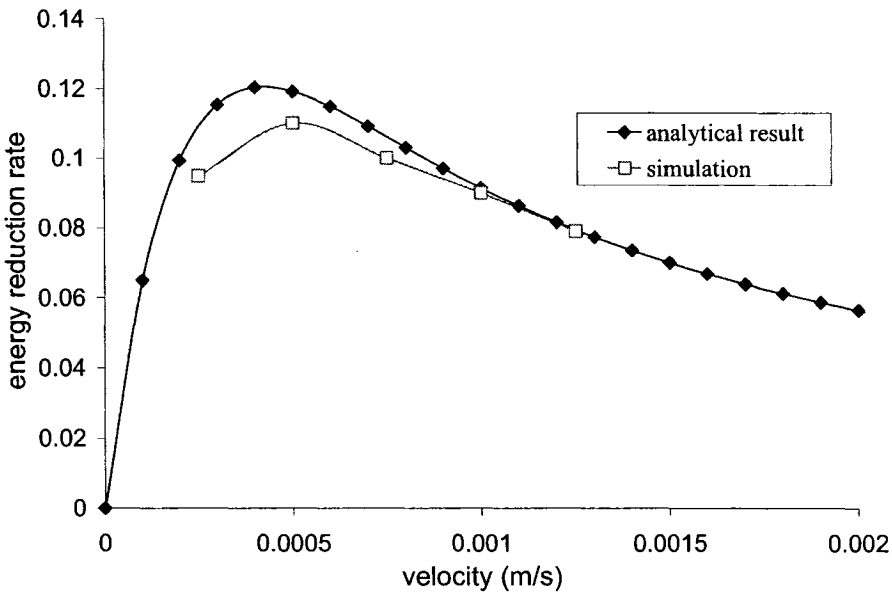

(b) Wall with 0.2m insulation

Fig 5.13 Energy reduction rate

The figures also demonstrate that the results of analytical model agree well with the TRNSYS simulation results. In the range of velocity in the investigation, the difference of energy reduction rate obtained by TRNSYS simulation and the analytical result based on overall heat transfer coefficient expressed by equation (5.5) is within 5%.

When it comes to the application of breathing wall elements, there might be problems to have the wall completely use breathing wall elements, due to other restrictions, such as the structural requirement. Parts of the wall may still be the normal wall. This will affect the efficiency of the breathing wall. Fig 5.14 shows the energy reduction rate of building under the following two conditions: (1) the west wall completely uses breathing wall elements, (2) 50% area of the west wall is breathing wall elements. It can be seen that if the breathing wall only accounts for 50% of the west wall, then the energy saving capability reduces to only one half of it is under the condition that the west wall completely incorporating the breathing wall elements.

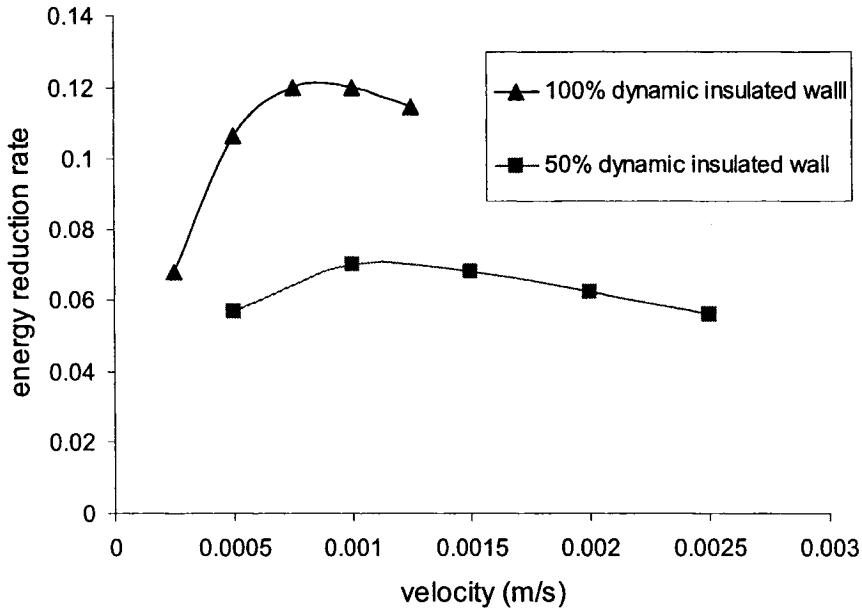

Fig 5.14 Influence of ratio of dynamic insulated wall to normal wall

5.1.5 Application field of dynamic insulation and barriers to application

The concept of dynamic insulation is well known in Scandinavian countries and was first implemented in Norway in agricultural buildings. However, it can have a wide application field due to the mechanism of its working principle.

First, the temperature difference between indoor and outdoor does not influence the performance of dynamic insulation itself, because:

1. Temperature is not included in dynamic *U*-value expressed of equation (5.3) and total heat loss coefficient expression (equation 5.5).

2. Numerical simulation on the heat exchange performance of the exterior building wall by Buchanan and Sherman (2000) and in this study demonstrates that the influence of temperature gradient is insignificant.

This suggests that dynamic insulation has the potential to be implemented in most climate conditions. As a matter of fact, besides cold weather condition such as Scandinavian countries, experimental set-ups for dynamic insulation have been developed in mild climate countries such as United Kingdom (Baker, 2003), Greece (Dimoudi et al, 2004), and Japan (Dalehaug 1993).

However, as dynamic insulation needs de-pressurization of the building, the actual implementation may be different. For the mild and variable climate countries such as UK, the only way to be reliably de-pressurized the building is by using fans, while in Canada and Scandinavian countries where the indoor and outdoor temperature difference in winter reaches 40K, it could provide the needed de-pressurization by stack effect.

The ideal type of building for implementation of dynamic insulation is the place that more fresh air is preferred, for example, swimming pools and hospitals. Concerning the energy consumption, it can be used in both business and residential buildings (Baily, 1987). However, the results in this study show that it may be more appropriate for small detached buildings, as the heat loss through it is directly related with the ventilation rate.

Though theoretical analysis and experimental tests have been conducted to evaluate the performance of dynamic insulation, and the possibility of its implementation has been

discussed, there are still problems in the application of dynamic insulation. Specific barriers are as follows:

1. Technical problems exist concerning moisture transport in the insulation. Taking advantage of appropriate air flowing through the wall, dynamic insulation will have better performance in reducing the risk of condensation, compared with the conventional wall. However, it is pointed out that under some conditions, such as the solar radiation on wet timber cladding, condensation may occur in the dynamic insulated wall (Taylor and Imbabi, 1998). As air needs to be driven through the wall, it lacks the effective way to avoid possible condensation in the insulation under those conditions.
2. The guideline for dynamic insulated wall design is not well developed. Suggestions should be made concerning the aspects such as: what is the suitable thickness for each sub-layer, what kind of material is more appropriate, and how to determine the dimension of an inlet crack.
3. There is a conflict between the minimization of heat loss by reducing air flow rate, and the removal of water vapor and other indoor pollutants by increasing air flow rate. Thus the air flow rate should be optimized.
4. The dynamic insulation has not been integrated in the commonly used building design tools such as DOE2, EnergyPlus, Esp-r, and TRNSYS. In this study, TRNSYS has been used to simulate the thermal performance of a simple building with dynamic insulated walls. However, the approach needs the designer to have a thorough knowledge of heat transfer in dynamic insulation, hence is still not convenient for the engineering implementation.

5. The impacts of dynamic insulation on the requirements of building regulations and standards have not been investigated.
6. For the application of dynamic insulation, other parts of the building need to be well insulated, this may bring difficulties in construction process and increase the construction cost.
7. The property of materials concerning the air permeability and water vapor permeability is not accessible to some designers.
8. Building designers are still unfamiliar with the concept of dynamic insulation. It may take a long time for them to recognize the advantage of this technique and implementing it in their designs.

5.1.6 Advantages and limitations of dynamic insulation

Concerning energy consumption, the following benefits are claimed for the application of dynamic insulation:

1. Less energy is required to maintain an indoor air temperature, thus the operating costs for space heating and cooling are reduced.
    - According to the results of this study, the energy saving by using dynamic insulation in a building is about 10%. Simulation by Krarti (1994) of a room with a dynamic insulated wall showed that the overall energy saving may reach 20%, while the simulation results by Baily (1987) point out the energy saving during a heating period vary from 7% to 14%, without any additional equipment such as a heat pump.
    - The product Energy*flo*^{TM} cell developed by The Environmental Building Partnership Limited, United Kingdom is also claimed to reduce the

required heating and cooling load by 10%, compared to the Scotland building regulation standard (Environmental Building Partnership Limited, 2005).

2. As low heat loss can be achieved by using a thin dynamic insulated wall, it is possible to avoid the need to use thick wall construction to meet the building regulations to reduce construction cost.
3. By using dynamic insulation, the wall becomes the air supplying ventilator, thus saving the cost of supplying and installing ventilation ducts.
4. As dynamic insulation is generally working in contra-flux mode, it will also prevent the water vapor getting into the wall from the interior, therefore reducing the risk of condensation in the wall.

Meanwhile, working as an air filter, dynamic insulation can remove airborne particulate pollution from the ventilation air. Therefore better indoor air quality could be provided for the building occupant.

Though dynamic insulation is a possible approach to supply a good indoor environment with less energy consumption, and has the above advantages. Limitations exist concerning its performances, and this serious affects the implementation of this technique. The specific limitations are follows:

1. Though it is claimed that the dynamic insulation can reduce the conductive heat loss, convective heat loss increases with the air flow rate, and additional electrical energy may be required to drive fans. Thus the overall energy saving is not very

significant (generally is less than 10%). This might make this technique less attractive.

2. Dynamic insulation can work as an air filter. However, dust and other particles trapped in the insulation may prompt the growth of bacteria. This might bring potential problem to the occupants' health. Meanwhile, it is pointed that dynamic insulation may not be effective to remove chemical pollutants (Taylor and Imbabi, 1998).

5.1.7 Future perspectives of dynamic insulation

Research on the dynamic insulation until now focuses on the heat transfer process and focuses have been on its ability to reduce energy consumption. For the purpose of having this technique implemented in the real buildings, future work needs to be performed at least on the following aspects:

1. Moisture exists in the real environment and will affect the performance of dynamic insulated walls. Comprehensive research is needed to evaluate the thermal performance of the dynamic insulation by using a coupled heat and moisture transfer model, and to find out the appropriate method to avoid the occurrence of condensation.
2. So far, the influence of long wave radiation has not been considered in the simulation. Therefore a comprehensive heat transfer analysis combining conduction, convection, as well as radiation is needed, especially considering the radiation between different layers.

3. To assure that the dynamic insulation operating in contra-flux mode, de-pressurization of the building is needed. The pressure drop must be no higher than 5-10Pa, otherwise the occupants will find it difficult to open doors and windows. Therefore the control strategy for air supply needs to be studied and optimized to minimize the electricity consumption. Dimoudi et al (2004) concluded that to keep the indoor environment under adequate de-pressurization, the fan should be operated with variable speed. Thus a control strategy for the fan operating is needed for the application of dynamic insulation in real environmental situations.
4. As the overall energy saving by dynamic insulation is only about 10%, it is less attractive because this in only marginally better than a supply-and-exhaust ventilation system (Morrison and Karagiozis, 1992). One option for this problem is to combine the dynamic insulation with natural ventilation, or hybrid ventilation, taking the advantage of pressure gradient by wind and stack effect. For example, Etheridge and Zhang (1998) pointed out that a strong synergy exists between dynamic insulation and wind energy. Therefore there is a good potential to extent the application of dynamic insulation to a natural ventilated system. For this purpose, investigation needs to be carried concerning the following two aspects:
    a. Investigating the property of building materials which might be implemented in the dynamic insulation. As air flow in the porous insulation is in the Darcy's regime, the air flow rate under a certain pressure gradient between indoor and outdoor environment is determined by the permeability of the material. Permeability of some materials has

been shown in Table 5.1. However, if we want to combine dynamic insulation with natural ventilation in places with different weather conditions, these materials are not enough. Therefore permeability of more building materials needs to be supplied.

b. Investigating the control strategy of the dynamic insulation system. This is more important as the simulation in this study demonstrate that the thermal performance of the dynamic insulation is directly related to the air flow rate through it. As energy consumption of the building integrated with dynamic insulated walls is almost proportional to the pressure gradient, which is related to the square of the wind speed, the heat loss of dynamic insulation may increase dramatically due to an increase of wind speed. Therefore the control system needs to be carefully designed to assure the dynamic insulation work in certain weather conditions.

5. With air transferring through the dynamic insulated wall, the temperature distribution changes. One important aspect is that the interior surface temperature will deviate from that without ventilation. In heating season, the interior surface temperature decreases with the air flow rate. A CFD simulation shows that this may affect the thermal comfort of occupants in the room (Gan, 2000). However, there is no further report on this topic. For the application of dynamic insulation, investigation should be preceded on this aspect, adopting the approach of:

   a. Numerical simulation, especially for the configuration that air does not enter the room uniformly through vast area of the internal surface of the wall, but through vents on some part of the wall (such as the prototype

dynamic insulated wall by Baker, 2003, and the recommended design by Morrison et al, 1992);

b. Experiment work to find its influence on thermal comfort, for example, the perceived experiment.

5.2 Analytical model for heat exchange performance in conventional walls

By analyzing the velocity profile in the wall (Fig 4.4), it is noticed that for straight through configuration, air velocity is very small except in the area near inlet and outlet. Besides these inlet and outlet vicinity areas, in a certain area near the direct line connecting the inlet and outlet, the horizontal velocity (u) is much greater than the vertical velocity (v). However, in most parts of the wall, the velocity in two directions is near to zero. This means that besides the inlet and outlet area, the air flow in the wall is almost along a one dimensional path in a certain area. The similar condition is observed in the low inlet/high outlet or high inlet/low outlet configuration, except that in most of the area between inlet and outlet, the air flow is mainly in the vertical direction (a nearly uniform with a velocity v).

The above observation suggests that it is possible to develop an analytical model for the estimation of coupled conduction and infiltration heat loss, based on the one dimensional air flow and heat transfer analysis, following the same approach with that in the study of the dynamic insulation, i.e., treating parts of the conventional wall as dynamic insulated wall.

5.2.1 Determination of ventilated area

Fig 5.15 illustrates the typical non-dimensional air velocity profile in several vertical planes, which are away from the exterior surface with different distances (e.g., 1/10L means the distance from the exterior surface is 1/10 thickness of the wall). It can be seen that the air velocity distribution area in these planes are almost the same, though in the middle of the area, the air velocity decreases significantly with the increase of the distance from the exterior surface.

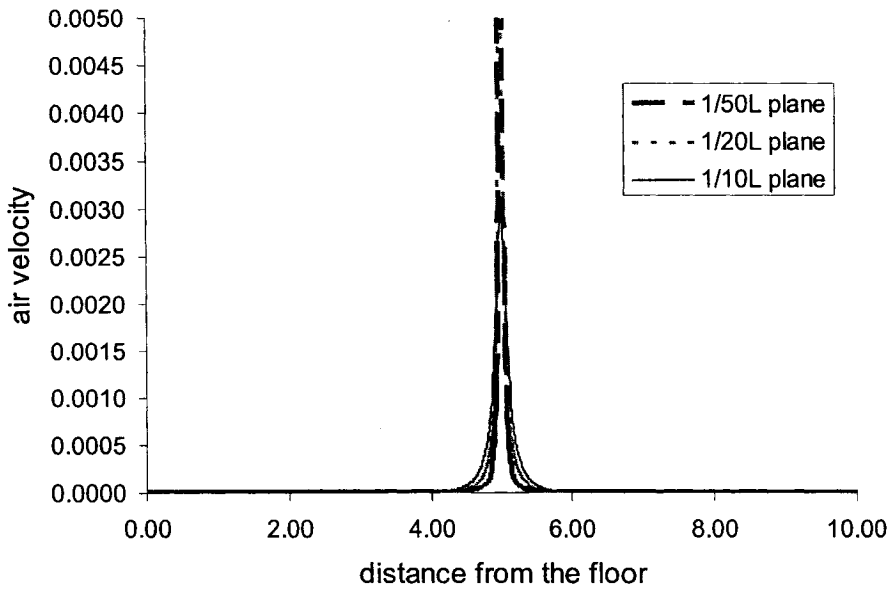

Fig 5.15: Typical air velocity profiles in several planes along the wall thickness

Therefore, as discussed in Chapter 4, the whole wall can be divided into infiltration affected area and infiltration not-affected area, as shown in Fig 5.16. From the point view of air flow, they can be named ventilated area and non-ventilated area, respectively. In the ventilated area, both conductive heat loss and infiltration heat loss will be considered

in the determination of energy consumption of the building, while in the non-ventilated area, only conduction is included. The air flow in the ventilated area is assumed to be one dimensional and uniform, as that in the dynamic insulated wall. Adopted the same method discussed in previous sections, the overall heat flux at the exterior surface of the wall is as follows:

$$\begin{aligned} Q_T &= U_{dyn} A_{\inf} \Delta T + \dot{m} C_{pa} \Delta T + U_{static} A_{nf} \Delta T \\ &= U_{dyn} hw\Delta T + uhw\rho C_{pa} \Delta T + U_{static} (H-h) w \Delta T \end{aligned} \tag{5.9}$$

A_{inf} – Ventilated area (m^2)

A_{nf} – Non-ventilated area (m^2)

w – The width of the wall (m)

u – The uniform velocity through the ventilated area (m/s), which is related to the average velocity through the crack as follows:

$$u = \frac{u_{in} h_{crack}}{h} \tag{5.10}$$

u_{in}- Average velocity in the crack area (m/s)

h_{crack} – The width of the crack (m)

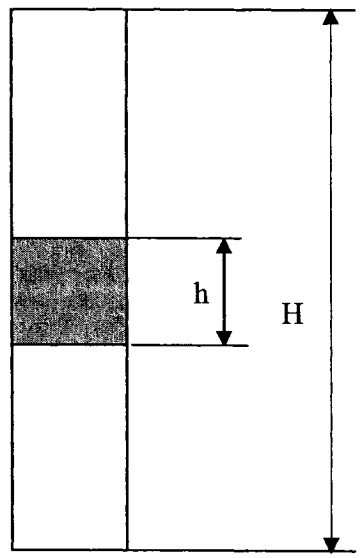

Fig 5.16: Ventilated area

The infiltration heat exchange efficiency is hence derived as:

$$\eta = 1 - \frac{Q_t - Q_0}{\dot{m} C_{pa} \Delta T} = \frac{U_{static} - U_{dyn}}{u \rho C_{pa}} \tag{5.11}$$

where U_{dyn} is also determined by u according to equation (5.3).

It can be found from the above analysis that the key point for this analytical model is to determine the range of the ventilated area. For this purpose, parameter study is performed according to the numerical simulation, with the variation of crack width, air inlet velocity and ratio of thickness to the height of the wall.

Fig 5.17 illustrates the temperature profile of several vertical planes with different distances from the exterior surface of the wall, with the variation of crack width. The ratio of thickness to the height of the wall here is 0.1, and air inlet velocity is 0.1m/s. It can be seen that though there is a variation of ventilated area range in different planes, this variation is not significant. Therefore, the influence of variation of crack width can be ignored. This means that as the material in the simulation is assumed to be homogeneous, when the air comes into the wall, its flow is similar to that from a jet. After a short distance from it, it flows mainly along the infiltration path, which is induced by the pressure gradient between inlet and outlet.

Fig 5.18 illustrates the temperature profile of several planes with the variation of inlet air velocity, under the condition that ratio of thickness to the height of the wall is 0.1 and crack width is 1/1000H. It can be found that when air velocity decreases to 0.01m/s, the influence of infiltration becomes less significant, and the ventilated area decreases, compared with the result obtained under velocity being 0.1m/s. The influence of air infiltration is even less obvious when air inlet velocity becomes 0.001m/s. However, it also can be noticed that though ventilated area decreases under the condition inlet

velocity 0.01m/s or 0.001m/s, it only decreases about one half compared with that of air velocity being 0.1m/s. This is not proportional to the variation of inlet velocity, which from 0.1m/s to 0.01m/s, or even 0.001m/s.

Fig 5.19 illustrates the variation of temperature profile when the ratio of thickness and height of the wall becomes 0.05. Compared to Fig 5.18, it can be found the ventilated area decreases about half. This means that the ventilated area is almost determined by the ratio of thickness to the height of the wall.

From the above analysis, it is shown that the ventilated area is first related with the wall thickness. It is also related to the inlet air velocity. However, the variation of the ventilated area is much smaller than the variation of the velocity. On this observation, the following relation is suggested to estimate the ventilated area:

$$\begin{aligned} h &= nL_{eff} \\ n &= 3 \sim 4 L_{eff} \qquad \textit{for ST Path} \\ n &= 5 \sim 7 L_{eff} \qquad \textit{for LH or HL path} \end{aligned} \tag{5.12}$$

L_{eff}- The effective thickness of the ventilated area (m)

The coefficient n is also influenced by the porosity of the material. For high porosity condition, as the effective thermal conductivity is relatively lower, the higher coefficient is used. However, if the porosity is lower, the effective thermal conductivity increases, hence the lower coefficient will be used.

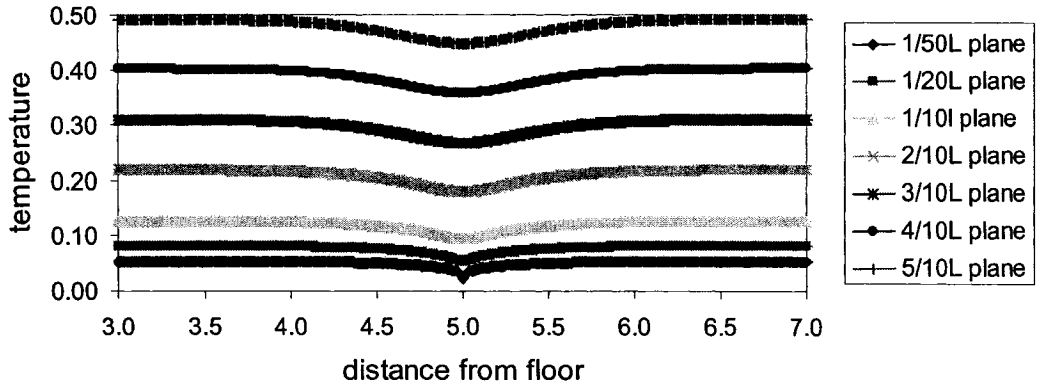

(a) h_{crack} =1/1000 H

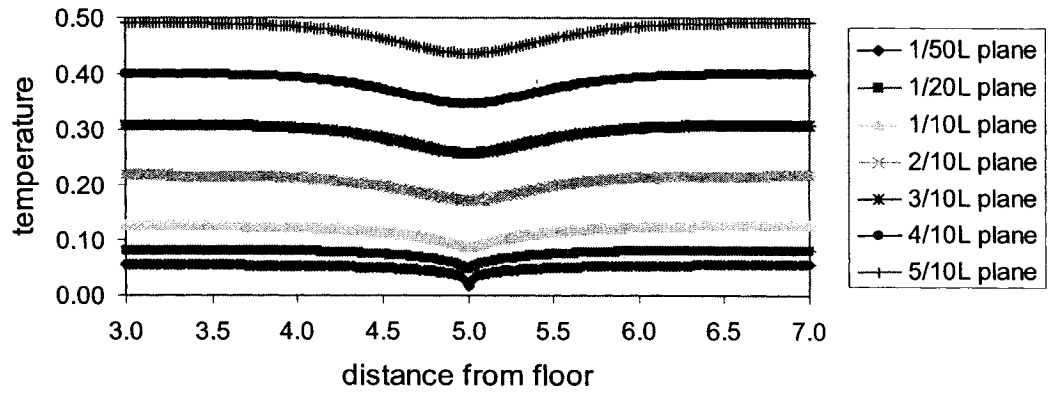

(b) h_{crack} =1/500 H

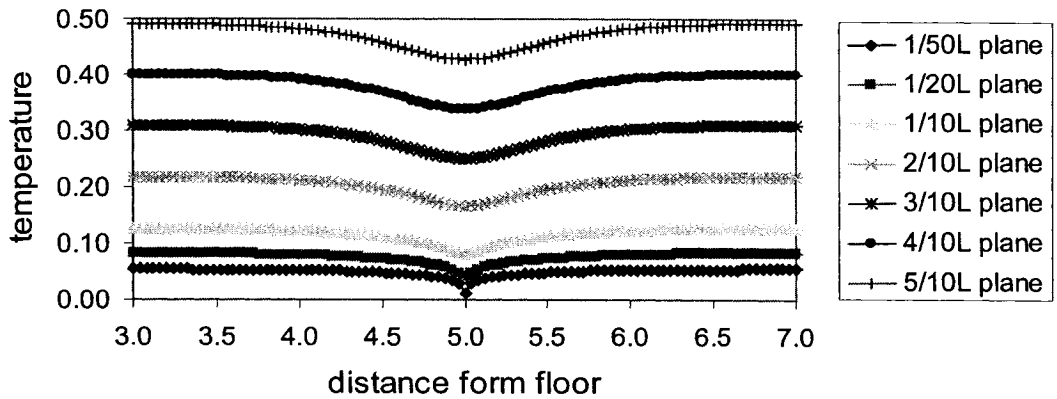

(c) h_{crack} =1/250 H

Fig 5.17: Temperature profile with the variation of crack width

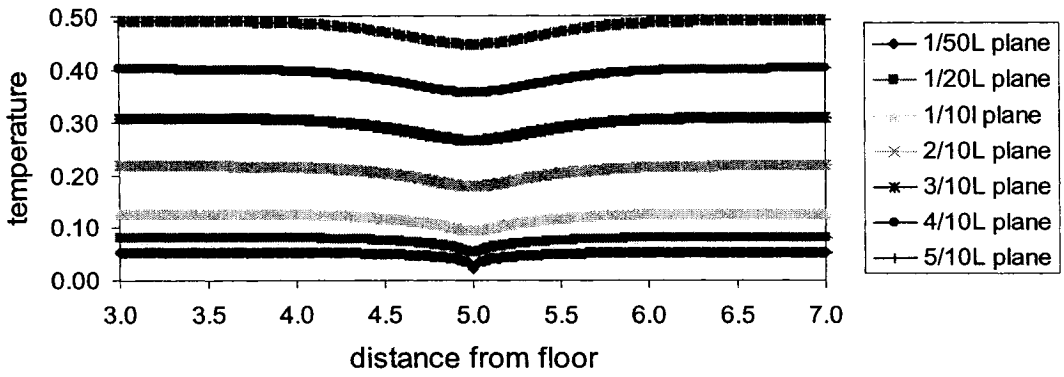

(a) Inlet velocity 0.1m/s

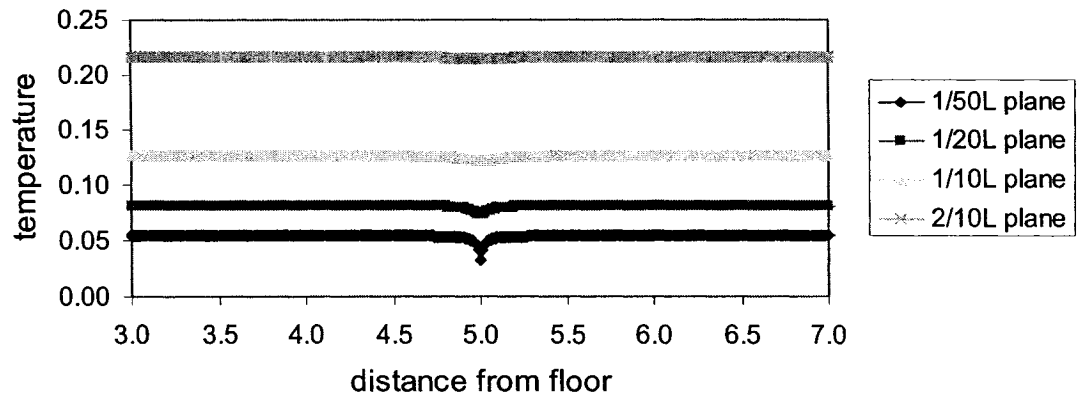

(b) Inlet velocity 0.01m/s

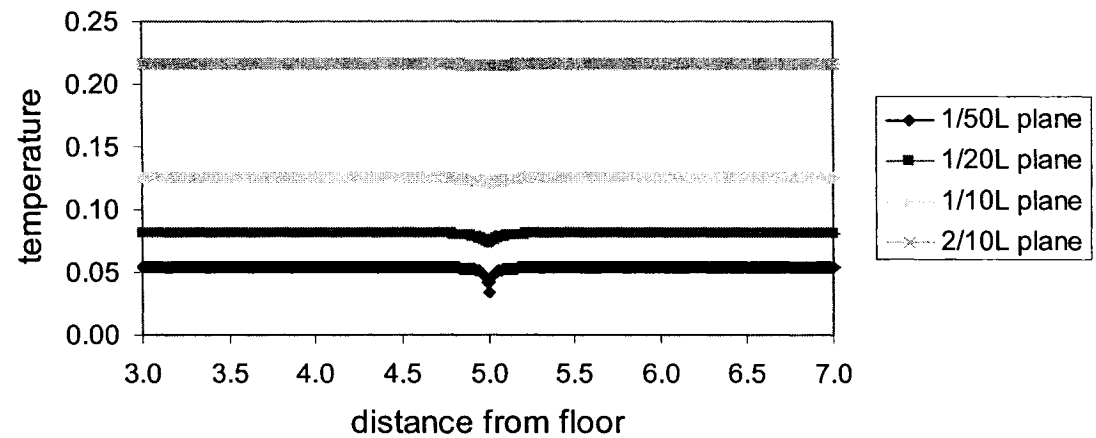

(c) Inlet velocity 0.001m/s

Fig 5.18: Variation of temperature with the inlet air velocity

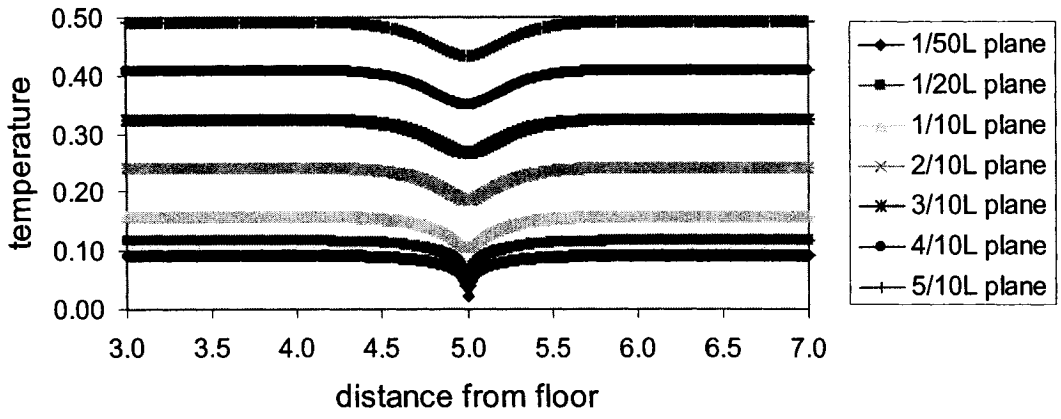

(a) h_{crack} =1/1000 H

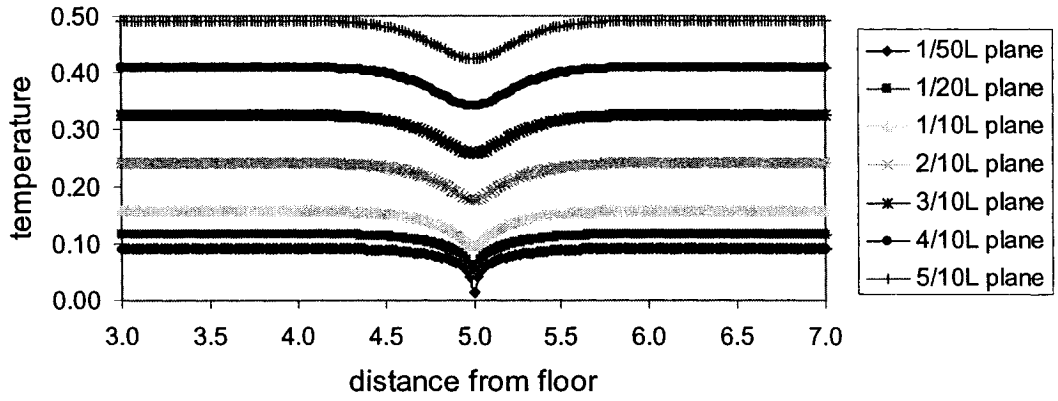

(b) h_{crack} =1/500 H

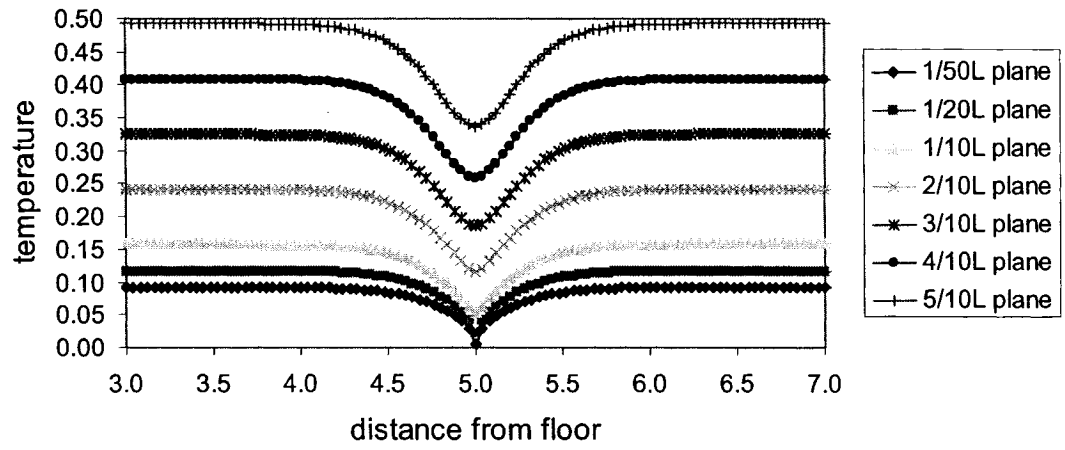

(c) h_{crack} =1/250 H

Fig 5.19: Variation of temperature profile when *L=0.05H*

5.2.2 Determination of the effective thickness of ventilated area

For the straight through configuration, the effective thickness of the ventilated area equals to the thickness of the wall. However, as pressure gradient between outlet and outlet increase under the condition of low inlet/high outlet (LH) or high inlet/low outlet (HL) configuration, the effective thickness of the ventilated area needs to be modified to include the influence of this pressure gradient increase.

As the thickness of the wall is much less than the height of the it, if the infiltration air enters the wall through a lower position inlet and exits from a higher position outlet, or vise versa, it will transfer along a vertical path between inlet and outlet. From the results of the numerical simulation in Chapter 4, it is found that the vertical velocity (v) is very small and almost uniform along most part of this infiltration path. Therefore, the vertical velocity is estimated according to the mass conservation as follows:

$$v = \frac{u_{in} h_{crack}}{L} \tag{5.13}$$

Adopting this velocity, the increased pressure gradient between outlet and inlet can be calculated according to the Darcy's law, i.e.:

$$\nabla p_{\inf} = \frac{\mu}{K} v H_{\inf} \tag{5.14}$$

$H_{\inf}$- Vertical distance between inlet and outlet (m)

Thus the effective thickness of the ventilated area is estimated as:

$$L_{eff} = L + \frac{\nabla p_{\inf}}{u_{in}\mu / K} \tag{5.15}$$

5.2.3 Analytical model results

Using the above analytical model, results have been obtained to compare with the numerical simulation results. Fig 5.20 shows the results of 0.2m thickness wall, for different porosity conditions. For the condition of porosity being 0.9 or 0.8, the coefficient n=4 is used for straight through configuration, while for the porosity of 0.5, the coefficient n is 3.5. It can be seen that under each condition, the results of the analytical model agree very well with that obtained by numerical simulation, with a maximum error less than 10%.

Fig 5.21 shows the results for configuration B, both by using analytical model and numerical simulation. In the simulation, coefficient n is 5, to represent the relative shorter vertical distance between inlet and outlet. It can be seen from the figure that the analytical model can be used to estimate the heat exchange efficiency for this kind of shorter LH infiltration path configuration.

Fig 5.22 is the comparison for the 0.1m wall. It can be seen that the error increases in this case. This is because the air velocity is close to a uniform distribution after a short distance from the inlet. In this short distance, the air velocity distribution is not uniform. As the thickness decreases, the ratio of this distance to the wall thickness increase, thus the error of the uniform velocity treatment increases. However, the maximum error in this case is still within 10%.

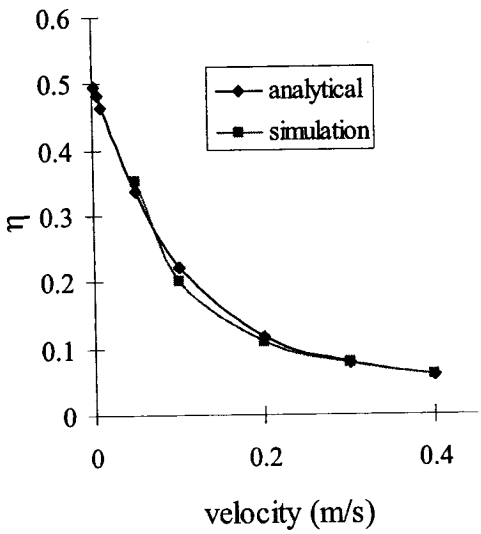

(a) ST configuration $h=4L_{eff}$

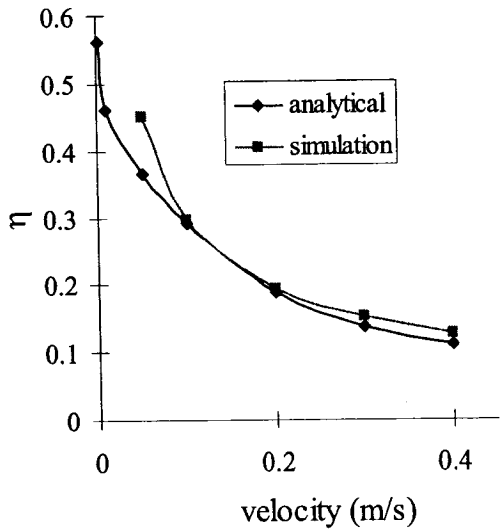

(b) LH configuration $h=6L_{eff}$

(a) Porosity 0.9

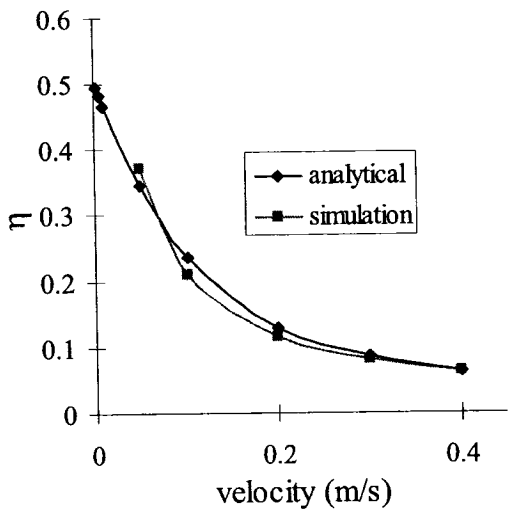

(a) ST configuration $h=4L_{eff}$

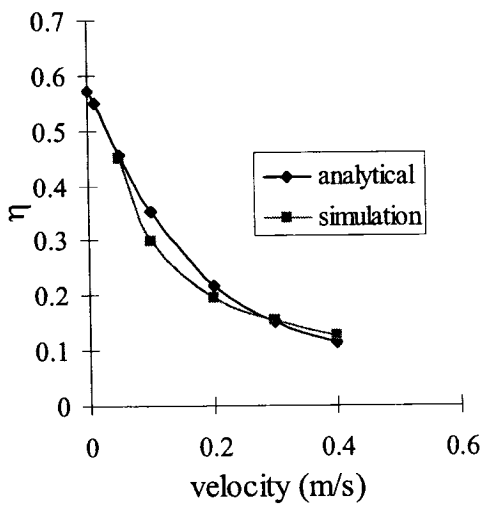

(b) LH configuration $h=6L_{eff}$

(b) Porosity 0.8

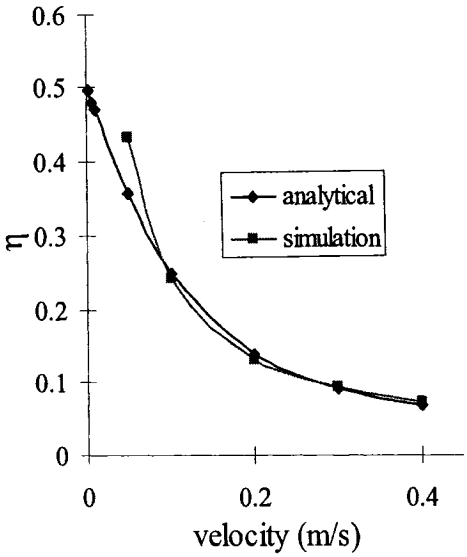

(a) ST configuration $h=3.5L_{eff}$

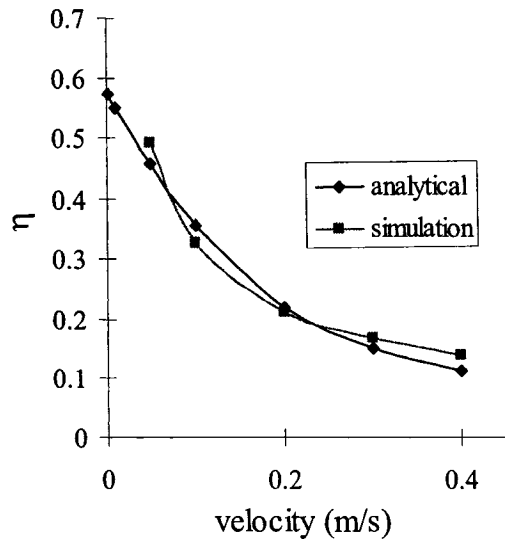

(b) LH configuration $h=5L_{eff}$

(c) Porosity 0.5

Fig 5.20 Comparison of results by analytical model and numerical simulation for 0.2m wall

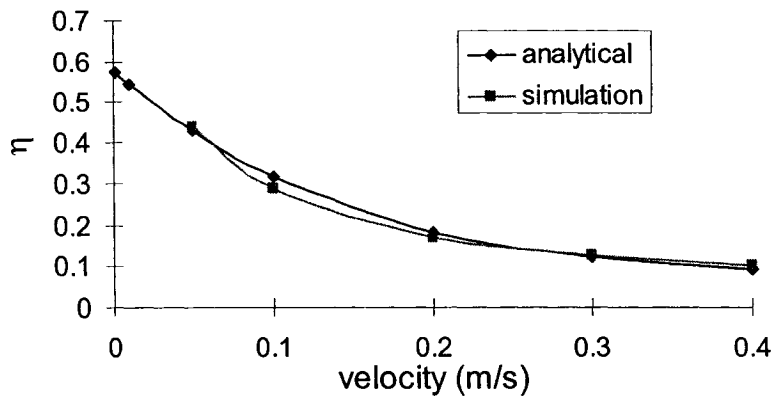

$h=5L_{eff}$

Fig 5.21 Results for configuration B

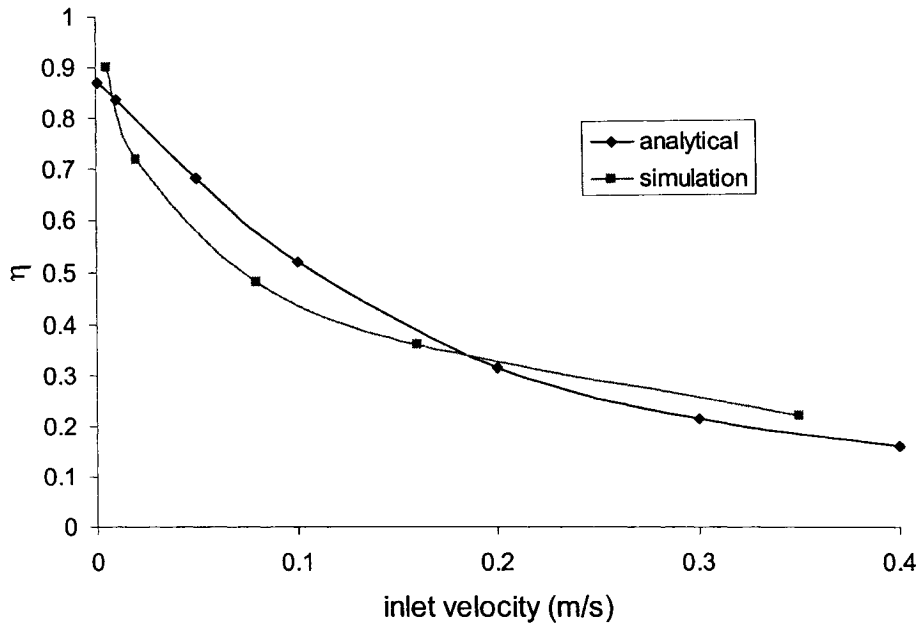

$h=7L_{eff}$

Fig 5.22: Comparison of results by analytical model and numerical simulation for 0.1m wall

5.2.4 Discussion

In the above model, the ventilated area is only determined by the thickness of the wall and the infiltration path, and the influence of air velocity to the ventilated area is ignored. However, as it is shown before, when inlet velocity is 0.01m/s, the ventilated area becomes to only about half of that when inlet velocity is 0.1m/s, according to the numerical simulation. Therefore, it is necessary to verify if the treatment of neglecting the influence of inlet velocity to ventilated area is reasonable.

Fig 5.23 and Fig 5.24 illustrate the comparison of results neglecting and including the influence of air inlet velocity, straight through air path and low inlet/high outlet infiltration path, separately. For the case of variable ventilated area, under the straight through condition, corresponding to the air velocity of 0.001m/s, 0.01m/s, 0.1m/s, 0.4m/s, n is 1, 2, 3, and 4, respectively (see equation (5.11)), according to the temperature profile obtained by numerical simulation, as illustrated in Fig 5. 18. The similar treatment is made for the variable n in the HL configuration.

From these two figures, it can be seen that if considering the influence of inlet velocity, the infiltration heat exchange efficiency decreases at the very low inlet velocity condition. However, the figures also demonstrate the influence of inlet velocity is very limited. The difference of η with or without the influence of air velocity is less than 10% for both ST and LH infiltration path, and is within 5% in the high infiltration loss condition. Therefore, the presented analytical model, which uses a constant ventilated area over the whole range of inlet air velocity for the convenience in the engineering implementation, is a good approximation.

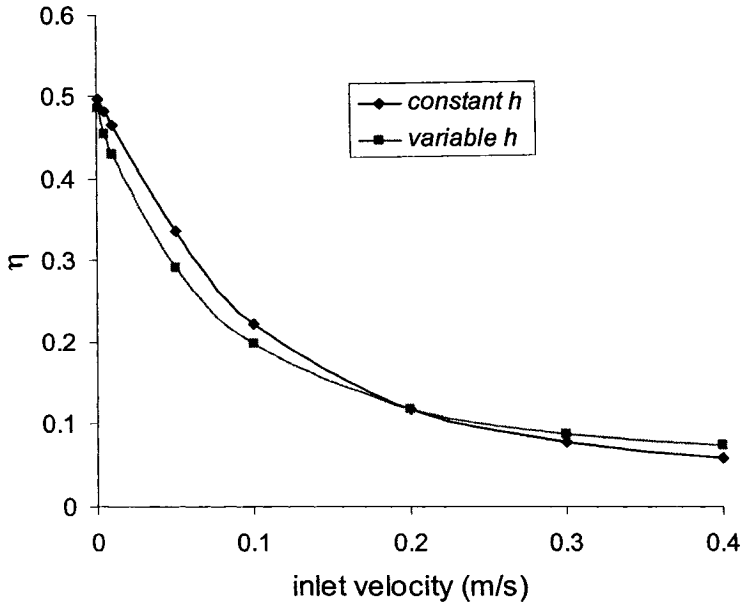

Fig 5.23: Comparison of results with or without the influence of inlet velocity for straight through infiltration path

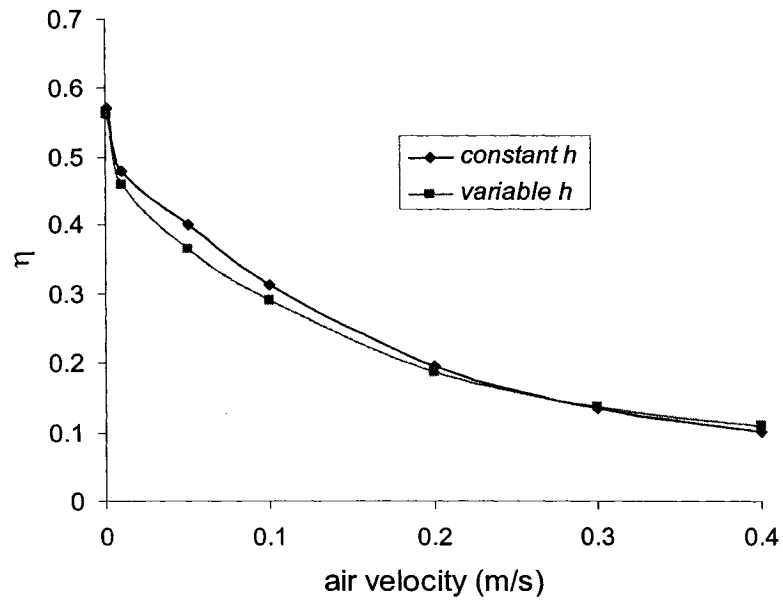

Fig 5.24: Comparison of results with or without the influence of inlet velocity for low inlet-high outlet infiltration path

To further assess the model, a sensitivity analysis is performed considering the variation of coefficient n. Fig 5.25 illustrates the results for ST configuration, under a series of n values. From the figure, it can be seen the variation under these n values is not significant. Even when n=6 or n=2 is used, the maximum error of η value is less than 0.15, compared with the results under n=3 or n=4. The difference is within 0.1 under most of the air flow conditions. This also means that variation of n under different air flow rates will not significantly influence the results of η.

Therefore the model using a constant n value under different air flow rates has an acceptable accuracy for the engineering implementation. Of course, the relationship expressed in equation (5.12) is suggested. As it is the result of a numerical parameter study for flow rates which are related with an obvious infiltration heat loss.

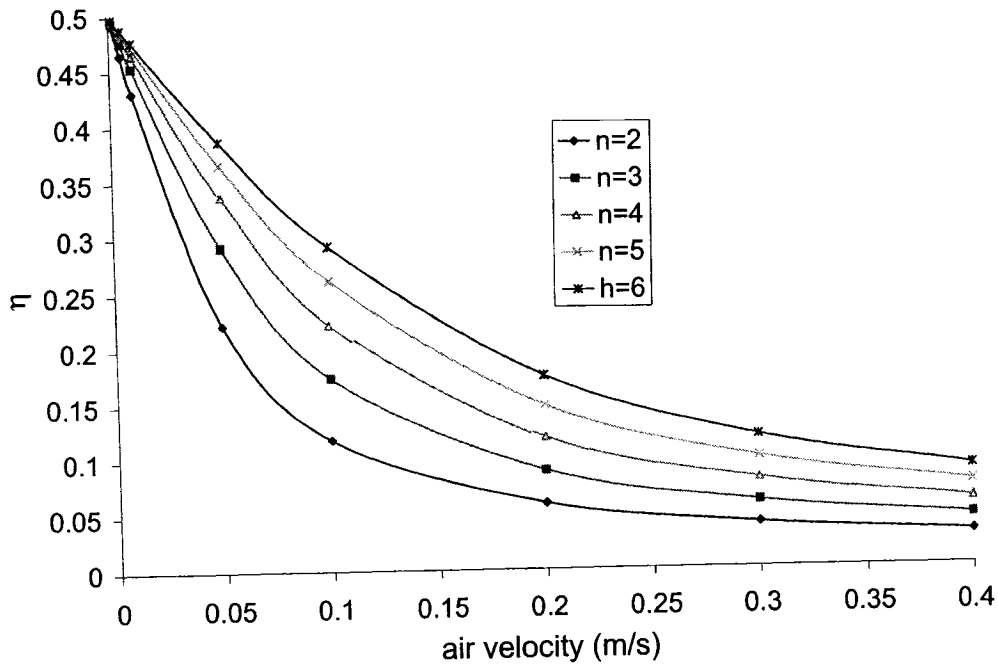

Fig 5.25 Results under a series of n values

5.3 Summary

This chapter discusses the potential implementation of heat exchange performance in the exterior walls, concerning the following aspects:

1. The performance of dynamic insulation is analyzed, considering both the transient and the steady-state boundary condition, and the influence of material properties. The results show that difference of the heat flux obtained by the steady-state analysis and transient simulation is not significant. Therefore the heat transfer coefficients obtained by the steady-state analysis is a convenient tool with an acceptable precision for engineering;

2. The analytical model based on steady-state analysis and the heat coefficients from it are applied using TRNSYS to simulate the thermal performance of building with dynamic insulated walls, to overcome the problem that the theory on heat transfer in dynamic insulation is not integrated in the generally used building simulation tools;
3. Adopting the same approach with the analytical model for dynamic insulation, an analytical model for heat exchange performance in the normal walls is developed. The results of the analytical model agree well with the results by numerical simulation, demonstrating that the model is suitable for engineering implementation.

Chapter 6 Conclusion and future work

6.1 Conclusion

Infiltration/exfiltration heat loss is an important component in the estimation of total heat loss through building envelope. As the air transfers through the building envelope, it exchanges heat with solid matrix of the building material. The coupled heat loss through the building envelope is hence less than the summation of conduction heat loss and infiltration heat loss calculated by the conventional method. This thesis performed a comprehensive research on heat exchange performance of the building envelope, to investigate the impact of this process to the energy consumption of the building, and its potential implementation. Detailed work in the thesis is described as follows.

A CFD model based on combined heat and mass transfer in porous media is presented in Chapter 3. Compared with the numerical model by Buchanan and Sherman (2000), in which the simulation is carried out for the whole building, model in this study focuses on the heat exchange phenomenon inside the envelope component and needs less computer resources. The model is developed based on the volume average method, and microscopic effects in the porous building material are taken into account. Meanwhile, a modified pressure correction method is presented to simplify the simulation process.

According to the simulation results obtained and parameter study performed in Chapter 4, the flowing conclusions have been derived:

1. The air flow rate is the most important factor for the heat exchange performance in the building envelope;
2. Heat exchange phenomenon in the building envelope mainly occurs at the area near the inlet and outlet. The whole envelope can be divided into infiltrated affected and non-affected areas. Thus it is a local phenomenon and its effect is limited if we only consider the influence of infiltration in the conventional wall;
3. In the infiltrated affected area, the heat flux varies significantly throughout the envelope, being smaller at the outside near the inlet position than the inside. Meanwhile, the interior surface temperature drops because of the heat exchange in the envelope;
4. The infiltration path length and configuration also have an obvious impact on the heat exchange performance. This means that the relative position of inlet and outlet influence the heat exchange performance, however, the arrangement of low inlet/high outlet (LH) and high inlet/low outlet (HL) does not have obvious difference;
5. The temperature difference between indoor and outdoor does not have a significant influence to the heat exchange phenomenon inside the envelope;
6. Influence of the porosity is limited, thus high porosity material might be used in the building design if more fresh air is preferred;
7. Influence of convective boundary coefficient is insignificant;

The simulation results have been compared with that in the literature and the temperature profiles obtained from the experiment in the environmental chamber, and have shown good agreement.

Chapter 5 discussed the potential implementation of this heat exchange performance in the building envelope. The following results are derived from the analysis:

1. In the design of dynamic insulation, one dimensional air flow and heat transfer is assured. According to the velocity profile obtained by numerical simulation, air flow in the conventional wall because of infiltration is also mainly one dimensional. Therefore it is possible to describe the heat exchange process in the conventional wall by an analytical approach;
2. The transient boundary condition will have an impact on heat loss through dynamic insulation; however, the heat flux obtained by this condition is not significantly different from that obtained by the steady-state analysis;
3. Building simulation tools, such as TRNSYS, can be used to simulate the thermal performance of building with dynamic insulated walls;
4. The presented analytical model for infiltration heat exchange performance in the conventional wall, which uses the ventilated area to represent the infiltration path, is suitable for engineering implementation.

6.2 Future work

Though some results have been obtained, further work is needed to analyses this heat exchange performance more comprehensively and make the potential implementation feasible in the building design. For this purpose, future work includes:

1. As actual exterior walls are multilayer systems and always contains air gaps, and air gap is needed in order to make the air transfer through most of the wall in dynamic insulation, simulation needs to be carried to consider the interaction between the air gap and porous insulation. Meanwhile, for the multilayer system, influence of radiation, especially long wave radiation, should be included in the model.
2. Including the influence of moisture in the model. As the infiltrating air is generally humid, the content of moist will affect the overall thermal performance of the wall. Its effect is especially important when the condensation occurs. A more comprehensive model needs to consider the moisture transfer as well as the heat transfer through the wall.
3. Develop a module of dynamic insulation to be integrated in TRNSYS. In the current simulation using TRNSYS, an assumed unintentional infiltration rate is used. More work is needed in the module to estimate the real infiltration rate, combining a research on building material. Meanwhile, other influence, such as the change of fan power, will be included in the simulation.

References

Abadie, M. O., Finlayson, E. U., and Gadgil, A. J. 2002. Infiltration Heat Recovery in Building Walls: Computational Fluid Dynamics Investigations Results. Lawrence Berkeley Laboratory Report, LBNL-51324

Alazmi, B., Vafai, K. 2000. Analysis of variants within the porous media transport models. Transactions ASME, Journal of Heat Transfer, v 122, n2, p303-326

ASHRAE. 1993. Handbook of Fundamentals, American Society of Heating, Refrigerating and Air Conditioning Engineering

ASTM. 1991. ASTM E 283-91 Standard Test Method for Determining the Rate of Air Leakage Through Exterior Windows, Curtain Walls, and Doors Under Specified Pressure Differences Across the Specimen. American Society for Testing and Materials Annual book of Standards, Vol. 04.07, p486-489.

Baily, N. R. 1987. Dynamic insulation systems and energy conservation in buildings. ASHRAE Transactions, n93, pt1, p447-466

Baker, P. H. 2003. The thermal performance of a prototype dynamically insulted wall. Building Services Engineering Research and Technology, v 24, n 1, p25-34

Baker, P. H., Sealens, D., Grace, M., Inoue, T. 2000. Advanced envelopes. IEA Annex 32 Final report III. Laboratorium Bouwfysica, K.U. Leuven, Belgium

Bankvall, C., Mattsson, B., Kalagasidis, A. S. 2004. Air transport in and through the building envelope. Performance of the exterior envelops of the whole buildings IX International conference, Clearwater Beach, Florida, USA

Barhoun, H., Guarracino, G. 2004. Evaluating the energy impact of air infiltration through walls with a coupled heat and mass transfer method. Proceedings of CIB conference, Toronto, Canada

Batchelor, G. K. 1954. Heat transfer by free convection across a closed cavity between vertical boundaries at different temperatures. Quarterly of Applied Mathematics, v12, p209-233

Bear, J. 1972. Dynamics of fluids in porous media. New York: American Elsevise Pub. Co.

Bejan, A. 1995. Convection heat transfer. 2nd edition. Wiley, New York

Bennacer, R., Beji, H., Mohamad, A. A. 2003. Double diffusive convection in a vertical

enclosure inserted with two saturated porous layers confining a fluid layer. International Journal of Thermal Science, v42, n2, p141-151

Bhattacharyya, S., Claridge, D. E. 1995. Energy impact of air leakage through insulated wall. Journal of Solar Engineering, v117, n3, p167-172

Buchanan, C. R., Sherman, M. H. 2000. A mathematical model for infiltration heat recovery. Lawrence Berkeley Laboratory Report, LBL-44294

Caffey, G. E. 1979. Residential air infiltration. ASHRAE Transactions, v85, p41-57

Chan, W. R., Price, P. N., Sohn, M. D., Gadgil, A. J. 2003. Analysis of U.S. residential air leakage database. Lawrence Berkeley Laboratory Report, LBNL 53367

Chang, W. J., Chang, W. L. 1996. Mixed convection in a vertical parallel-plate channel partially filled with porous media of high permeability. International Journal of Heat and Mass Transfer, v39, n7, p1331-1343

Chebil, S., Galanis, N., Zmeureanu, R. 2003. Computer simulation of thermal impact of air infiltration through multilayered exterior walls. Eighth International IBPSA Conference, Eindhoven, Netherlands

Chen, W., Liu, W. 2004. Numerical analysis of heat transfer in a composite wall solar-collector system with a porous absorber. Applied Energy, v78, n2, p 137-149

Cheng, P., Hsu, C. T. 1986. Applications of van Driest's mixing length theory to transverse thermal dispersion in forced convection flow through a packed bed. International Communications of Heat and Mass Transfer, v13, p613-625

Claridge, D. E., Bhattacharyya, S. 1989. Measured impact of infiltration to a test cell. American Society of Mechanical Engineers, Solar Energy Division (Publication) SED, p121-130

Claridge, D. E., Liu, M., Bhattacharyya, S. 1995. Impact of air infiltration in frame walls on energy loads: taking advantage of the interaction between infiltration, solar radiation, and conduction. In "Airflow Performance of Building Envelopes, Components, and Systems, ASTM STP 1255" Mark P. Modera and Andrew K. Persily Eds. American Society for Testing and Materials, Philadelphia, p178-196

Dalehaug, A. 1993. Dynamic insulation in walls. Research Report No. 53. Hokkaido Prefectural Cold Region Housing and Urban Research Institute, Japan

Dimouli, A., Androutsopoulus, A., Lykoulis, S. 2004. Experimental work on a linked, dynamic and ventilated, wall component. Energy and Buildings, v36, n5, p443-453

Du, J. H., Hu, X., Wu, W., Wang, B. W. 2003. A thermal dispersion model for single phase flow in porous media. Heat Transfer – Asian Research, v32, n6, p545-552

Environmental Building Partnership Limited. 2005. Technical Bulletin 1. Rev.1

Etheridge, D. W., Zhang, J. J. 1998. Dynamic insulation and natural ventilation: feasibility study. Building Services Engineering Research & Technology, v19, n4, p203-212

Fazio, P., Athienitis, A. K., Marsh, C., Rao, J. 1997. Environmental chamber for investigation of building envelope performance. Journal of Architectural Engineering, v3 n2, p97-102

Fu, W. S., Huang, H. C. 1999. Effects of a random porosity model on heat transfer performance of porous media. International Journal of Heat and Mass Transfer, v42, n1, p13-25

Gan, G. 2000. Numerical evaluation of thermal comfort in rooms with dynamic insulation. Building and Environment, v35, n5, p445-453

Gratia, E., De Harde, A. 2004. Natural cooling strategies efficiency in an office building with a double-skin façade. Energy and Buildings, v36, n11, p1139-1152

Hadim, A. 1994. Forced convection in a porous channel with localized heat sources. ASME Journal of Heat Transfer, v116, p465-472

Hagentoft, C. E., Blomberg, T. 1D-HAM Coupled heat, air and moisture transport in multi-layered wall structures. Accessed in May, 2006 (http://www.buildingphysics.com/manuals/1dham.pdf)

Hensen, J., Bartak, M., Drkal, F. 2002. Modeling and simulation of double-skin façade systems. ASHEA Transactions, v108, part2, p1251-1258

Hsiao, H. T., Advani, S. G. 2002. A coupled approach to predict microscopic temperature distribution inside a unit cell of nonisothermal laminar flow in periodic porous media. Journal of Porous Media, v5, n2, p69-85

Hsu, C. T. 2003. Heat and mass transfer in porous media. Environmental fluid mechanics: theories and applications, p257-295

Jayamaha, S. E. G., Wijeysundra, N. E., Chou, S. K. 1996. Measurement of the heat transfer coefficient for walls. Building and Environment, v31, n5, p399-407

Jiang, P. X., Ren, Z. P., Wang, B. W. 1999. Numerical simulation of forced convection heat transfer in porous plate channels using thermal equilibrium and nonthermal equilibrium models. Numerical Heat Transfer, Part A: Applications. v35, n1, p99-

Kaviany, M. 1995. Principles of heat transfer in porous media. Second Edition, New York: Springer-Verlag

Kaviany, M. 1999. Principles of convective heat transfer. 2nd edition, New York: Springer-Verlag

Kim, S. Y., Paek, J. W., Kang, B. H. 2000. Flow and heat transfer corrections for porous fin in a plate-fin heat exchanger. Transactions of ASME, Journal of Heat Transfer, v122, n3, p572-578

Koch, D. L., Brady, J. F. 1986. Effective diffusivity of fibrous media. AIChE Journal, v32, n4, p575-591

Kohonen, R., Virtanen, M. 1987. Thermal coupling leakage flow and heating load of buildings. ASHRAE Transactions, v93, p2302-2318

Krarti, M. 1994. Effect of airflow on heat transfer in walls. Journal of Solar Energy Engineering, v116, n1, p35-42

Lacarriere, B., Lartigue, B., Monchoux, F. 2003. Numerical study of heat transfer in a wall of vertically perforated bricks: influence of assembly method. Energy and building, v35, n3, p229-237

Lorente, S. 2002. Heat losses through building walls with closed, open and deformable cavities. International Journal of Energy Research, v26, n7, p611-632

Luikov, A. W. 1966. Heat and mass transfer in capillary-porous bodies. Pergamon Press, Oxford

Manz, H. 2003. Numerical simulation of heat transfer by natural convection in cavities of façade elements. Energy and Buildings, v35, n3, p305-311

Mercier, J. F., Weisman, G., Firdaouss, M., Le Quere, P. 2002. Heat transfer associated to natural convection flow in a partly porous cavity. Transactions of ASME, Journal of Heat Transfer, v124, p130-143

Merrikh, A. A., Mohamad, A. A. 2002. Non-Darcy effects in buoyancy driven flows in an enclosure filled with vertically layered porous media. International journal of heat and mass transfer, v45, n21, p4305-4313

Miguel, A. F., van de Braak, N. J., Silva, A. M., Bot, G. P. A. 2001. Wind-induced airflow through permeable materials. Part I: The motion equation. Journal of Wind Engineering and Industrial Aerodynimics, v89, n1, p45-57

Miguel, A. F., van de Braak, N. J., Silva, A. M., Bot, G. P. A. 2001. Wind-induced airflow through permeable materials. Part II: Air infiltration in enclosures. Journal of Wind Engineering and Industrial Aerodynimics, v89, n1, p59-72

Morrison, I. D., Karagiozis, A. N. 1992. Energy impact of dynamic wall ventilation. Proceedings of 18th Annual Energy Society of Canada, Edmonton, Alberta

Morrison, I. D., Karagiozis, A. N., Kumaran, K. 1992. Thermal performance of a residential dynamic wall. Proceedings of the ASHRAE/DOE/BTECC Conference, Clearwater Beach, Florida, USA

Moyne, C., Didierjean, S., Souto, H. P. A., da Dilveira, O. T. 2000. Thermal dispersion in porous media: One-equaiton model. International Journal of Heat and Mass Transfer, v43, n20, p3853-3867

Oesterle, E. 2001. Double-skin facades: integrated planning: building physics, construction, aerophysics, air-conditioning, economic viability. Munich, London, Prestel

Patankar, S. V. 1989. Numerical heat transfer and fluid flow. Washington: Hemisphere Pub. Corp.; New York: McGraw-Hill

Pedras, M. H. J, de Lemos, M. J. S. 2002. Macroscopic turbulence modeling for incompressible flow through undeformable porous media, International Journal of Heat and Mass Transfer, v44, n6, p1081-1093

Philip, J. R., DeVries, O. A. 1957. Moisture movement in porous materials under temperature gradients. Transactions of American Geophysics Union, v 38, p222–232

Raoche, P. J. 1998. Fundamentals of computational fluid dynamics. Albuquerque, N.M, Hermosa Publishers

Saha, A. K. 2000. Unsteady free convection in a vertical channel with a built-in heated square cylinder. Numerical Heat Transfer, Part A, v38, p795-818

Taylor, B. J., Cawthorne, D. A., Imbabi, M. S. 1996. Analytical investigation of the steady-state behaviour of dynamic and diffusive building envelopes. Building and Environment, v 31, No6, p519-525

Taylor, B. J., Imbabi, M. S. 1997. The effect of air film thermal resistance on the behavior of dynamic insulation. Building and Environment, v32, n5, p397-404

Taylor, B. J., Imbabi, M. S. 1998. Application of dynamic insulation in buildings. Renewable Energy, v15, n1-4 pt1, p377-382

Taylor, B. J., Webster, R., Imbabi, M. S. 1999. The building envelope as an air filter. Building and Environment, v34, n3, p353-361

Vafai, K., Tien, C. L. 1981. Boundary and initial on flow and heat transfer in porous media. International Journal of Heat and Mass Transfer, v24, p195-203

Vasile, C., Lorente, S., Perrin, B. 1998. Study of convective inside cavities coupled with heat and mass transfer through porous media – application to vertical hollow bricks –a first approach. Energy and Building, v28, n3, p229-235

Von Grabe, J. 2002. A prediction tool for the temperature field of double facades. Energy and Buildings, v34, n9, p891-899

Walker, L. S., Sherman, M. H. 2003. Heat recovery in building envelopes. Proceedings AIVC BETEC Conference, Washington, DC, INIVE eeig, Brussels, Belgium. LBNL-53484

Whitaker, S. 1997. Simultaneous heat, mass and momentum transfer-a theory of drying. Advanced Heat Transfer, v13, p119–203

Wirtz, R. A. 1997. A semi-empirical model for porous media heat exchanger design. Proceedings, American Society of Mechanical Engineers National Heat Transfer Conference, Baltimore, MD, USA

Wong, H. H., Rathby, G. D. 1979. Improved finite-difference methods based on a critical evaluation of the approximation errors. Numerical Heat Transfer, v2, p139-163

Zollner, A., Winter, E. R. F., Viskanta, R. 2002. Experimental studies of combined heat transfer in turbulent mixed convection fluid flows in double-skin façade. International Journal of Heat and Mass Transfer, v 45, n22, p4401-4408